AWARD NUMBER: W81XWH-16-1-0342

TITLE: 89Zr-Trastuzumab-PET, Rapid Autopsies, and Patient-Derived Xenografts to Determine the Extent of Clonal Evolution in Treatment-Refractory HER2+Gastric Cancer

PRINCIPAL INVESTIGATOR: Sohail Tavazoie

CONTRACTING ORGANIZATION: Rockefeller University

REPORT DATE: Dec 2019

TYPE OF REPORT: FINAL

PREPARED FOR: U.S. Army Medical Research and Materiel Command

Fort Detrick, Maryland 21702-5012

DISTRIBUTION STATEMENT: Approved for Public Release;

Distribution Unlimited

The views, opinions and/or findings contained in this report are those of the author(s) and should not be construed as an official Department of the Army position, policy or decision unless so designated by other documentation.

REPORT DOCUMENTATION PAGE

Form Approved
OMB No. 0704-0188

Public reporting burden for this collection of information is estimated to average 1 hour per response, including the time for reviewing instructions, searching existing data sources, gathering and maintaining the data needed, and completing and reviewing this collection of information. Send comments regarding this burden estimate or any other aspect of this collection of information, including suggestions for reducing this burden to Department of Defense, Washington Headquarters Services, Directorate for Information Operations and Reports (0704-0188), 1215 Jefferson Davis Highway, Suite 1204, Arlington, VA 22202-4302. Respondents should be aware that notwithstanding any other provision of law, no person shall be subject to any penalty for failing to comply with a collection of information if it does not display a currently valid OMB control number. **PLEASE DO NOT RETURN YOUR FORM TO THE ABOVE ADDRESS.**

1. REPORT DATE	2. REPORT TYPE	3. DATES COVERED
Dec 2019	FINAL	09/01/2016 - 08/31/2019

4. TITLE AND SUBTITLE
89Zr-Trastuzumab-PET, Rapid Autopsies, and Patient-Derived Xenografts to Determine the Extent of Clonal Evolution in Treatment-Refractory HER2+Gastric Cancer

5a. CONTRACT NUMBER

5b. GRANT NUMBER
W81XWH-16-1-0342

5c. PROGRAM ELEMENT NUMBER

6. AUTHOR(S)
CA150646 (Janjigian), CA150646P1 (Tavazoie), CA150646P2 (Lewis)

E-Mail: janjigiy@mskcc.org

5d. PROJECT NUMBER

5e. TASK NUMBER

5f. WORK UNIT NUMBER

7. PERFORMING ORGANIZATION NAME(S) AND ADDRESS(ES)

Sloan-Kettering Institute for Cancer Research, 1275 York Avenue, New York, NY 10065

8. PERFORMING ORGANIZATION REPORT NUMBER

9. SPONSORING / MONITORING AGENCY NAME(S) AND ADDRESS(ES)

U.S. Army Medical Research and Materiel Command
Fort Detrick, Maryland 21702-5012

10. SPONSOR/MONITOR'S ACRONYM(S)

11. SPONSOR/MONITOR'S REPORT NUMBER(S)

12. DISTRIBUTION / AVAILABILITY STATEMENT

Approved for Public Release; Distribution Unlimited

13. SUPPLEMENTARY NOTES

14. ABSTRACT

The short-term milestones of this project include; 1) complete accrual to Phase II afatinib/trastuzumab trial and 89Zrtrastuzumab PET trial, 2) establish a tumor and PDX bank from 8-10 autopsies, representing the diversity of gastric metastasis; 3) characterize genetic features of tumor clonal evolution, using DNA, RNAseq and miRNA analysis; 4) explore functional significance of the observed alterations in established PDX models; and 4) correlate distinct HER2+ gastric cancer signatures in order to better understand factors driving tumor progression and drug resistance.

15. SUBJECT TERMS
Trastuzumab, Rapid Autopsies, Patient Derived Xenografts, PDXs, Functional PET, HER2+ gastric cancer

16. SECURITY CLASSIFICATION OF:			17. LIMITATION OF ABSTRACT	18. NUMBER OF PAGES	19a. NAME OF RESPONSIBLE PERSON
a. REPORT	b. ABSTRACT	c. THIS PAGE			19b. TELEPHONE NUMBER *(include area code)*
Unclassified	Unclassified	Unclassified	Unclassified		USAMRMC

Table of Contents

Page

1. Introduction…….4

2. Keywords…….4

3. Overall Project Summary…….....4

4. Key Research Accomplishments……4-6

5. Conclusion……7-20

6. Publications, Abstracts, and Presentations……..…..…….22

7. Inventions, Patents and Licenses……23

8. Other Achievements…….23

9. References……..24

10. Appendices……25

INTRODUCTION

An estimated 1.5 million people were diagnosed with esophagogastric (EG) cancer worldwide in 2018, representing the third leading cause of cancer-related death.1 Moreover, the incidence of gastroesophageal junction (GEJ) cancer is increasing rapidly in Western countries, in particular among young individuals. Genomically, roughly a third of EG tumors are characterized by chromosomal instability and aberrant activation of human epidermal growth factor receptor (HER) tyrosine kinases (HER1-4). In patients whose cancers harbor ERBB2 amplification or overexpression of HER2 protein, the combination of the anti-HER2 antibody trastuzumab with cytotoxic chemotherapy (a fluoropyrimidine and platinum) is the recommended first-line therapy. Patients treated with this combination have a median overall survival (OS) of 13·8 months and an overall response rate (ORR) of 47%. While trastuzumab improves survival in patients with *ERBB2*-amplified cancer, disease progression still usually occurs within a year. Our ongoing Phase II of afatinib/trastuzumab and rapid autopsy program provided a unique opportunity to define the extent of genomic heterogeneity and tumor evolution upon pharmacological pressure in patients with trastuzumab-refractory, *ERBB2* amplified cancer.

We established an extensively characterized library of patient derived xenografts (PDX) from patients with HER2+ EG cancer. During the funding period of the award we sequenced and genomically characterized these PDXs and used en-vivo selection techniques to derive tumors with liver funded though Also, we will generate highly metastatic/aggressive derivative from the PDX. We will characterize these PDX to find out potential target pathways.

KEYWORDS
Trastuzumab, Rapid Autopsies, Patient Derived Xenografts, PDXs, Functional PET, HER2+ gastric cancer

ACCOMPLISHMENTS

What are the major goals of the project?

1. To develop molecular targeted PET scan for patients with HER2+ EG cancer
2. Collection and analysis of HER2+ tumor samples from patients enrolled in phase II trial
3. To develop hypothesis driven combination strategies to overcome trastuzumab resistance in HER2+ EG cancer
4. Accrue patients with HER2+ EG cancer to MSK phase II clinical trials
5. Continue to establish EG cancer patient derived xenograft in immune deficient mice to reflect wide variety of patients
6. In-vivo selection of metastatic PDXs to develop models with propensity to develop liver metastasis

What was accomplished under these goals?

1. Regulatory approval of MSKCC IRB 13-165 by HRPO in May 2017 (Janjigian)
2. Regulatory approval of MSKCC IRB 11-116 by HRPO in June 2017 (Janjigian)
3. Specific Aim 1

    Major Task 1-

    a. ^{89}Zr-trastuzumab radiotracer manufacturing (Lewis) - Zr-trastuzumab manufacturing is a success and ongoing.

b. Perform ^{89}Zr-trastuzumab PET/CTs pre and post HER2 directed therapy on patients enrolled on phase II afatinib/paclitaxel or trastuzumab/pembrolizumab/chemotherapy trials(Janjigian/Lewis).- We successfully performed Zr-trastuzumab PET on 11 patients treated with anti- HER2 therapy (see figures and analysis below).

c. Analysis of HER2 expression on post treatment biopsies at week 2 on afatinib (Janjigian/ Vakiani) -We have analyzed HER2 expression on 8 post treatment biopsies at week 2 on afatinib.

Major Task 2-

d. Complete accrual to phase II trial of afatinib/paclitaxel in HER2+EG tumors (Janjigian) - 11-166 protocol accrual has closed. 8 patients have been treated total with Afatanib and Paclitaxel, 4 patients were treated since 9/2017.

e. Determine clinical efficacy of afatinib/paclitaxel in HER2+ EG tumors in Phase II setting (Janjigian/Lewis)- A total of 8 patients have been treated with Afatanib and Paclitaxel. The median age was 68.5. There were 5 males enrolled and 3 females. 4 patients are currently AWD, while 4 DOD. 3 patients experienced POD, 1 patient had SD, and 3 patients had a PR, while one patient has not yet been evaluated. Patients tolerated a median of 2.5 cycles [range: 1 – 7].

f. Collect tumor samples from patients enrolled on Phase II trial (Janjigian)- We successfully collected 88 samples of HER2 patients. We collected samples from 31 patients with HER2+ EG adenocarcinoma receiving trastuzumab/pembrolizumab and 8 patients treated with afatinib/paclitaxel.

g. Proteomic analysis of tumor samples (Lewis)—Completed on 3 patients

Specific Aim 2

Major Task 1-

a. Perform targeted exon sequencing on samples obtained from serial biopsies (Janjigian)- We successfully sequenced 37 HER2+ EG cancer obtained prior to initiation of trastuzumab based therapy. Additionally, we sequenced 34 samples from from patients on first-line pembrolizumab/ trastuzumab study, and were able to biopsy 10 patient at progression with 10 matched pre/post progression paired samples analyzed. Serial samples from the 8 patients on the phase II afatinib/paclitaxel trial has been sequenced with the analysis ongoing.

b. Perform Rapid Autopsies (Janjigian/Iacobuzio) —4 rapid autopsies were performed and data analysis is completed (see figures and analysis below).

c. Perform targeted exon sequencing, RNA-seq and miRNA-Seq profiling all matched primary tumor and all sites of metastasis obtained from rapid autopsies (Janjigian/ Iacobuzio)- This analysis is ongoing.

Major Task 2-

a. Bioinformatics and Biostatistician Analysis (Janjigian/Shultz/ Capanu)- Bioinformatics and Biostatistics have completed the analysis of related HER2 experiments and studies.

Specific Aim 3

Major task 1-

a. Establish Patient Derived Xenografts (PDXs) from biopsy samples (Janjigian/ De Stanchina)- We implanted 113 PDXs . We established 67 PDXs derived from 57 patients with HER2+

tumors. PDX models were also used to image response to treatment which has increased our understanding of resistance and will allow us to design future studies.

b. Histological review, molecular characterization and comparison of established PDXs to parental tumor to confirm accurate representation of the parental tumor (Janjigian/Vakiani)- Targeted sequencing was performed using MSK-IMPACT next-generation sequcing platform. The PDXs have corresponding clinical sequencing from patient tumors allowing genomic fidelity between patient and PDX samples. We have sequenced a total of 49 PDX samples. Of these, 20 were HER2+. There are another 23 PDXs currently pending sequencing.

Major Task 2-

a. Establishment of organoids from PDX samples (Lewis)- We have successfully collected samples for organoids for 8 HER2 patients.

Specific Aim 4

Major Task 1-

a.Therapeutic experiments on established PDXs to evaluate how the genomic alterations impact sensitivity to next generation of therapies (Janjigian/ de Stanchina/Tavazoie)- Therapeutic experiments were performed to determine the sensitivity of tumor GD to afatinib or pertuzumab + Taxol combination.

b.Perform gain/loss of function studies afatinib-sensitive *ERBB2*-amplified cell lines resistant to this agent (Janjigian/ de Stanchina/Tavazoie)- This was attempted but was not successful due to failure for cell lines to grow. We are currently studying this in organoids.

c.shRNA kinase library screen (Janjigian/ de Stanchina)- This was attempted but was not successful due to failure for cell lines to grow. We are currently studying this in organoids.

Major Task 2-

a.Progression passages of PDX models of HER2+ gastric cancer for *in vivo* selection of metastasis (Tavazoie)- Progression and passages of eight PDX models of HER2 gastric cancer for in vivo selection of metastasis.

Major Task 3-

a.microRNA profiling studies (Tavazoie)- micro RNA profiling of isogenic highly or lowly metastatic HER2 amplified PDX has been completed.

b.Analysis of microRNA profile results obtained (Tavazoie)- microRNA profile results have been obtained.

Major Task 4-

a.Advise in functional testing of candidate genes (Tavazoie)- This is ongoing.

Specific Aim 1

89Zr-trastuzumab PET

We successfully performed Zr-trastuzumab PET on 11 patients since September 2016.

We hypothesized that functional imaging with 89Zr-trastuzumab PET could identify afatinib-sensitive and afatinib-resistant tumor sites prior to evidence of clinical progression. These tumor sites could then be explored post-therapy. To explore this hypothesis, we performed 89Zr-trastuzumab PET imaging before treatment and before the first CT assessment (after 3–5 weeks on therapy) in 8 patients, one treated with afatinib monotherapy and seven with afatinib/trastuzumab. All patients demonstrated 89Zr-trastuzumab tumor uptake in at least one disease site prior to therapy initiation. In the pre-treatment scans, we observed a wide range in median standardized uptake values (SUV) among patients and among lesions in individual patients (median SUVmax 15.6; range, 6.4 to 23.8; Figure 3C). Four patients (50%) had visible metastases on CT that did not exhibit 89Zr-trastuzumab uptake on PET, indicating pre-treatment intra-patient HER2 expression heterogeneity between sites. All 4 of these patients demonstrated disease progression within 6 weeks. Even when mean 89Zr-trastuzumab uptake declined 3–5 weeks post-therapy, we observed intra-patient lesion-to-lesion variability in this change (Fig. 1C). Notably, the 3 patients with tumor regression on afatinib and afatinib/trastuzumab therapy had uniformly high 89Zr-trastuzumab uptake (SUV >5) in all lesions visualized on CT (see Fig. 3C). These data suggest that homogenous pretreatment 89Zr-trastuzumab uptake may be a marker of afatinib sensitivity and that heterogeneous uptake at baseline or variable 89Zr-trastuzumab PET response may be indicators of poor response to afatinib in ERBB2-amplified EG cancer.

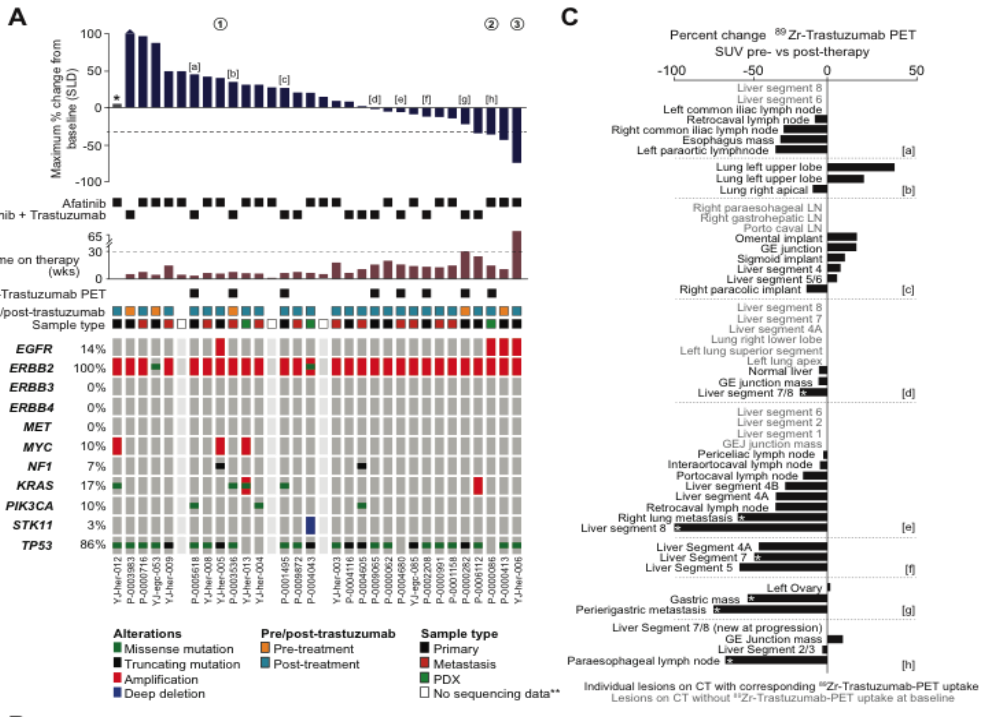


Figure 1: (A) Individual treatment outcomes. (C) Percent change 89Zr-trastuzumab SUV pre- and post-therapy.

Figure 1 shows individual treatment outcomes in 20 patients treated with afatinib and 12 patients treated with afatinib and trastuzumab. A percentage best change from baseline in the target lesion assessed by RECIST 1.1. Relevant clinical features (time on therapy, type of sequenced sample, and time point of the sequenced sample) plus key genomic alterations in sequenced samples are shown for each patient. SLD, sum of longest diameter on CT scan. *Non-evaluable. **Sample uninformative due to low tumor content. B, dual probe EGFR and ERBB2 FISH from tumor biopsy collected prior to protocol treatment demonstrated diffuse and uniform ERBB2 and EGFR co-amplification in virtually all tumor cells. There was no additional tissue on P-0000413. C, Percent change in 89Zr-trastuzumab PET standard uptake value (SUV) pre- vs post-therapy for each individual lesion on CT in 1 patient treated with afatinib monotherapy and 7 patients treated with afatinib/trastuzumab. White stars inside the bar plots denote lesions with resolution of uptake to baseline SUV.

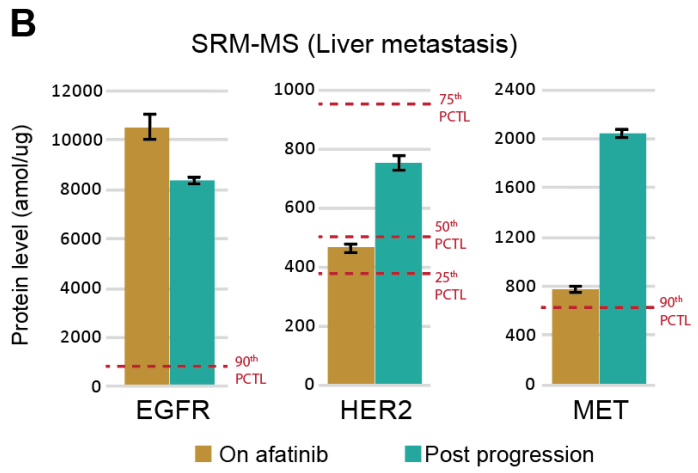


Figure 2: Proteomic analysis of HER2 samples from patient treated with afatinib therapy

As shown in figure 2, mass spectroscopy proteomic analysis of the tumor samples from patient 2 with HER2 amplified trastuzumab refractory gastric cancer and dramatic response demonstrated high level of EGFR expression on mass spectrometry. In this patient response was relative transient likely related to high level of MET expression seen in the tumor. The variation of EGFR, MET and HER2 amplification may shed light on the variation in response. This analysis is ongoing.

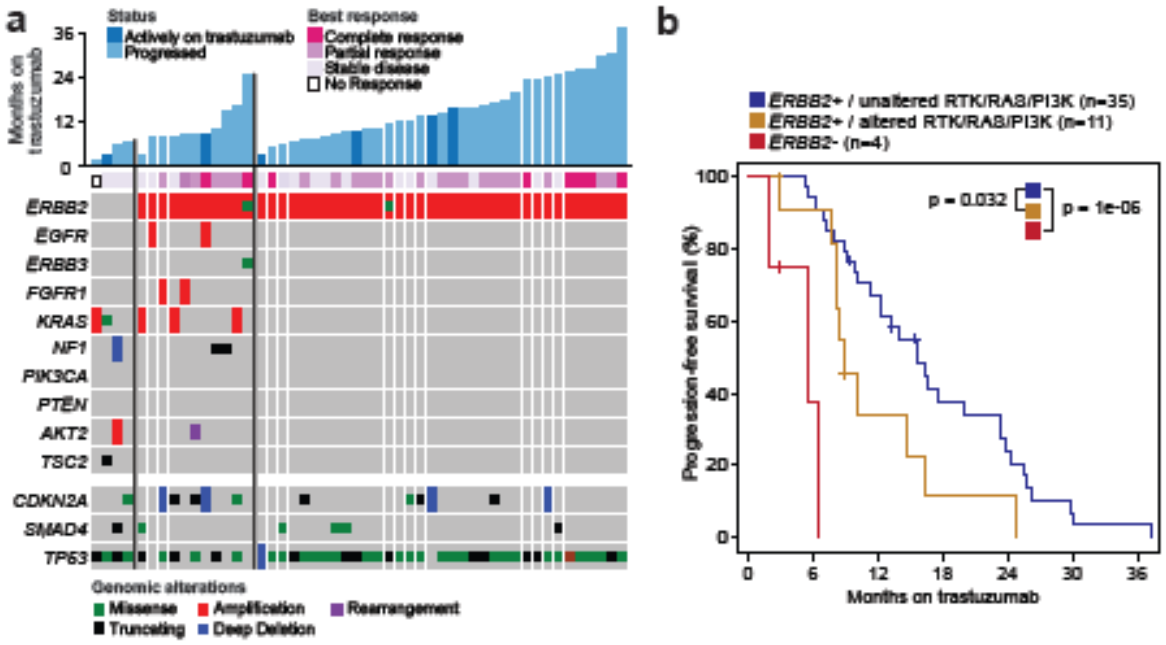


Figure 3: Genomic characterization of intrinsic and acquired trastuzumab resistance in patients with HER2+ esophagogastric cancer.

Figure 3 shows: (A) Duration and best response on first-line trastuzumab/chemotherapy for 50 patients with HER2-positive metastatic EG cancer is shown integrated with pre-treatment somatic genomics (legend, as indicated). (B) Kaplan-Meier progression free survival curves showing favorable outcome in ERBB2-amplified RTK/RAS/PI(3)K-wildtype tumors. Patients with *ERBB2*-negative by IMPACT or *ERBB2*+ and RTK/RAS/PI(3)K pathway activated tumors have significantly shorter time to progression on first-line trastuzumab therapy. (C) Analysis of somatic alterations in 23 pairs of matched pre- and post-trastuzumab samples. The oncoprint illustrates several oncogenic alterations that are shared between or private to the paired pre- and post- samples. (D) A representative case that illustrates loss of *ERBB2* in the post-treatment sample, which was validated by H&E, FISH, and IHC on the matched pre- and post-treatment specimens. (E) The anatomy of the acquired ERBB2 exon 16 deletion in the post-trastuzumab specimen.

Specific Aim 2

We successfully sequenced 37 HER2+ EG cancer obtained prior to initiation of trastuzumab based therapy. Additionally, we sequenced 34 samples from from patients on first-line pembrolizumab/ trastuzumab study, and were able to biopsy 10 patient at progression with 10 matched pre/post progression paired samples analyzed.

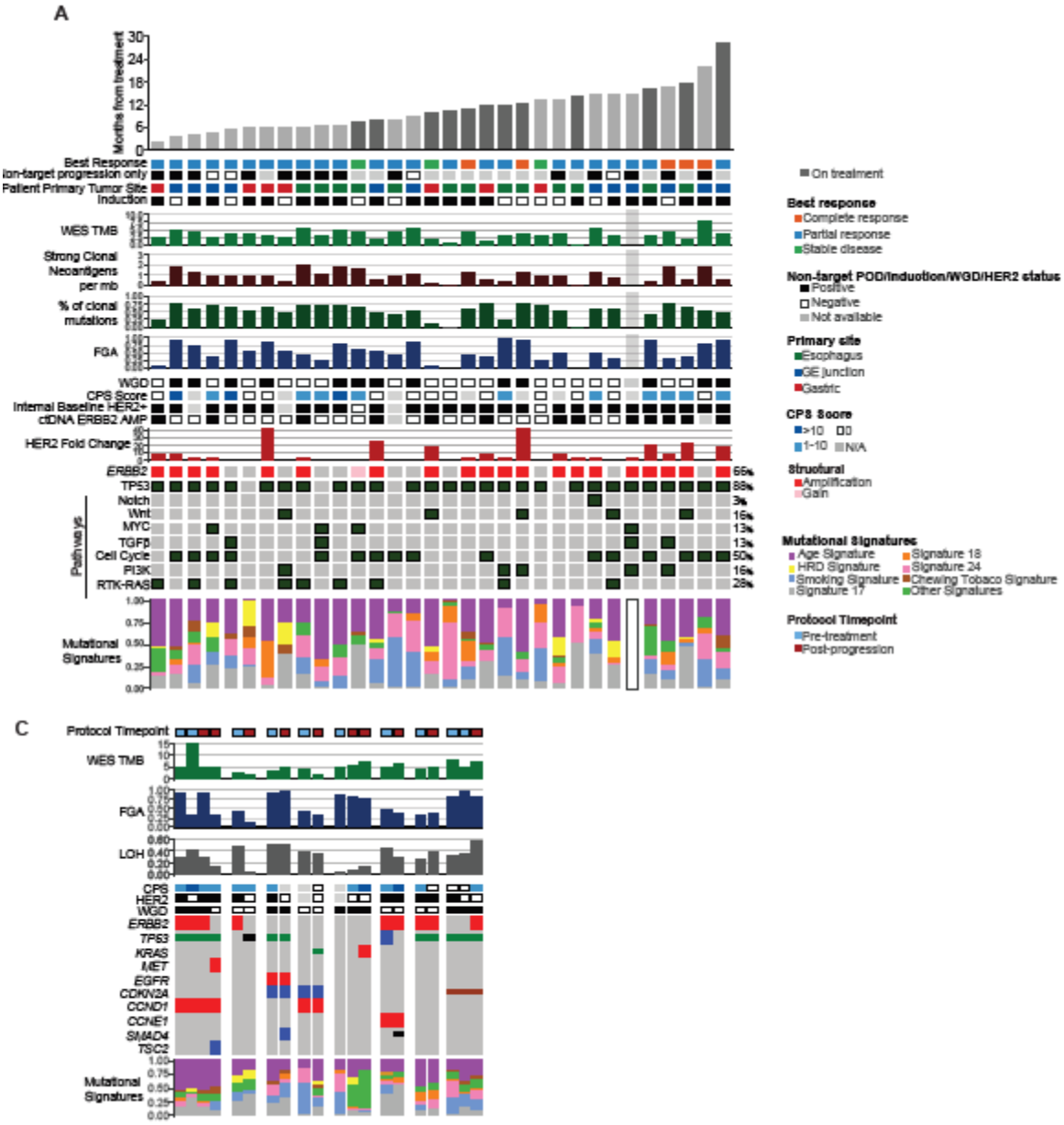


Figure 4: (a) co-occurring genomic alterations, tumor mutation burden, PDL-1, and MSK HER2 status (n=29), (c) Determinants of resistance to therapy in HER2 patients treated with trastuzumab and pembrolizumab

As shown in figure 4, of 37 HER2+ patients treated with trastuzumab in combination with pembrolizumab, 32 were sequenced using MSK-IMPACT and 31 were also analyzed by whole exome sequencing (WES). Figure 4A indicates co-occurring genomic alterations, tumor mutation burden, PDL-1

status, and HER2 status at MSK. In select patients who initially responded and later progressed on therapy, we performed research biopsies to allow for analysis to uncover determinants of resistance to therapy. Three of the 8 patients demonstrated new, activating alterations in the RTK/RAS pathway, including *KRAS* amplification, *KRAS* mutation, and *MET* amplification (Figure 4C). Two of the 8 patients (neither of whom developed an activating MAPK pathway alteration), demonstrated loss of *ERBB2* amplification at progression. Of the remaining fourthree patients, the post-progression tumors of two patients had inactivating alterations in *SMAD4*.

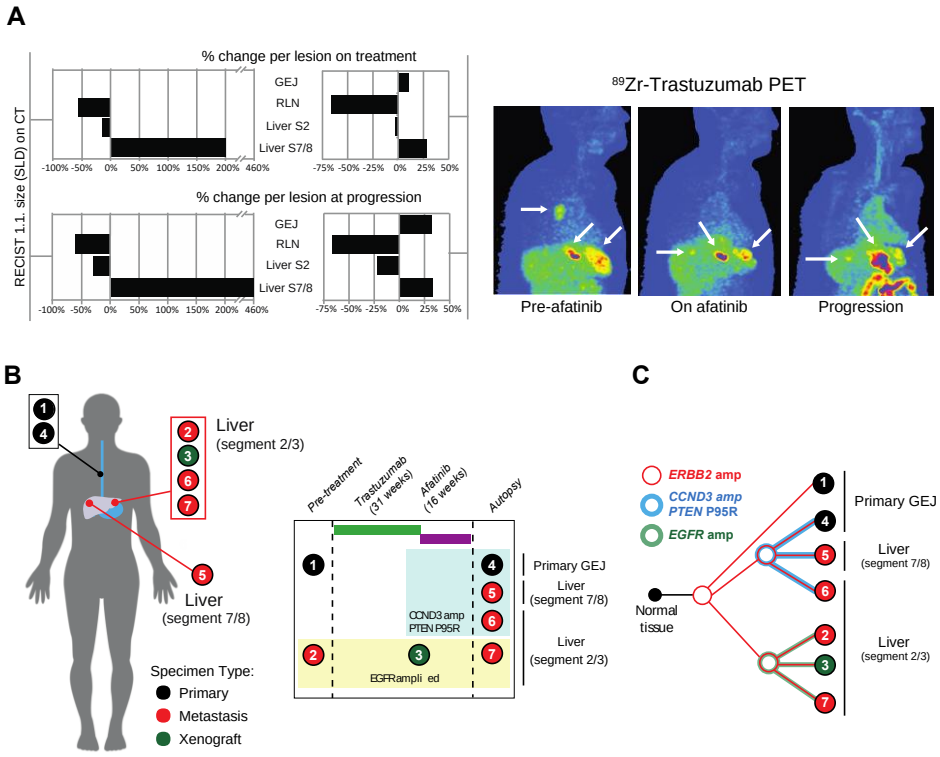


Figure 5: Intrapatient disease heterogeneity and lack of EGFR amplification as mechanism of afatinib resistance in patient P-0000086.

Figure 5 shows intrapatient disease heterogeneity and lack of EGFR amplification as mechanism of afatinib resistance in patient P-0000086. (a) Radiographic tumor assessment using 89Zr-trastuzumab PET and conventional CT scan, with corresponding bar graphs. 89Zr-trastuzumab PET values in SUV and CT measurements in mm. 89Zr-trastuzumab PET images include three panels: left panel (pre-afatinib) is a baseline pretreatment image showing uptake in segment 2/3 liver metastasis (SUV 16.4), GE junction (SUV 21.5) and retroesophageal lymph node (SUV 9.1); middle panel (on afatinib) corresponds to 3 weeks post-treatment initiation, showing resolution of retroesophageal lymph node (SUV 3.0) with decrease in size but persistent high uptake in segment 2/3 liver lesion (SUV 15.8), similar uptake in GE junction (SUV 23.7) and a new lesion in liver segment 7/8 appeared on 89Zr-trastuzumab PET (SUV 8.6); right panel (progression) shows post-progression 89Zr-trastuzumab PET uptake in GE junction (SUV 28.5) and segment 7/8 liver lesion (SUV 9.0), decreased uptake in liver segment 2/3 (SUV 12.3) and ongoing resolution of retroesophageal lymph node. (b) Genomic comparison of matched pre- and post-treatment primary and liver segment 2/3 and post-treatment progression liver segment 7/8 obtained at warm autopsy. EGFR amplification was unique to the segment 2/3 liver lesion with ongoing response. The enlarging GE junction tumor and segment 7/8 liver metastasis were not EGFR-amplified. In addition to a likely pathogenic mutation in PTEN (P95R, also present in a segment 2/3 liver lesion), the non-

responding metastases acquired an amplification of CCND3. SUV, standardized uptake value on 89Zr-trastuzumab PET; SLD, sum of longest diameter on CT scan. (c) Phylogenetic tree showing the inferred patterns of clonal evolution for the samples described in Figure 5b.

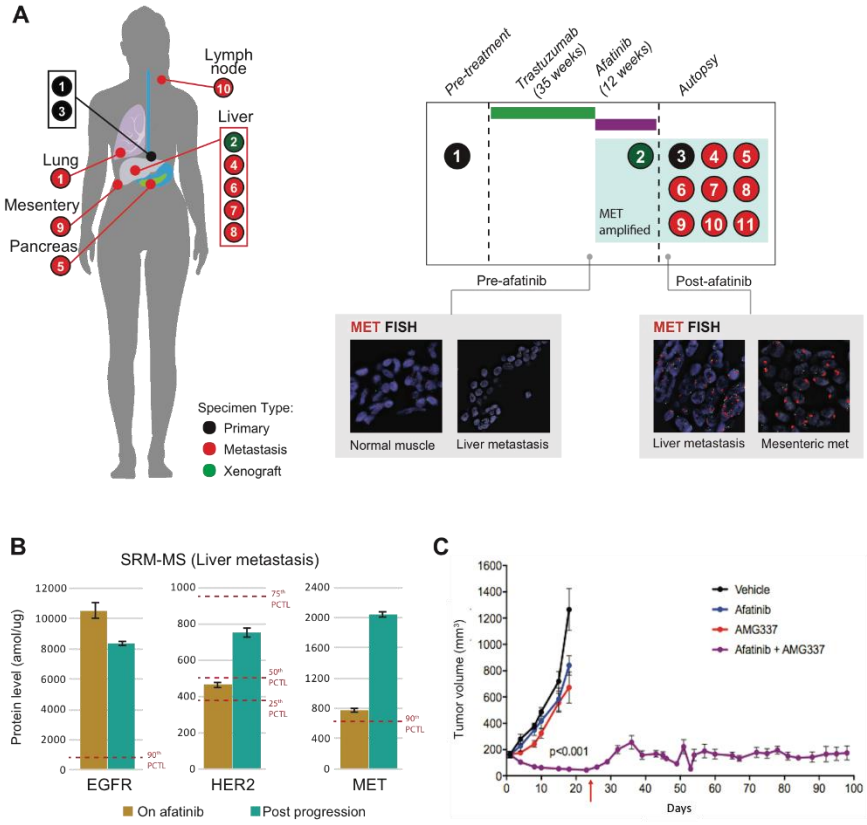


Figure 6: Acquired MET amplification as a mechanism of afatinib resistance in patient P-0000413 with EGFR- and ERBB2-amplified EG cancer

Figure 6 shows acquired MET amplification as a mechanism of afatinib resistance in patient P-0000413 with EGFR- and ERBB2-amplified EG cancer. (a) Genomic comparison of matched pretreatment biopsy with post-treatment metastases obtained at warm autopsy demonstrating acquired MET amplification. (b) SRM-MS analysis of liver metastasis sample obtained on afatinib with post-progression autopsy sample revealing increased MET and HER2 and decreased EGFR expression. (c) Efficacy of afatinib and afatinib/AMG 337 in MET/EGFR/ERBB2-amplified PDX model established from patient P-0000413. The combination of afatinib/AMG 337 resulted in complete tumor response at 21 days in MET/EGFR/ERBB2-amplified PDX. Red arrow indicates when the mice were rechallenged with the afatinib/AMG 337 combination following discontinuation of drug treatment, with durable tumor control again achieved.

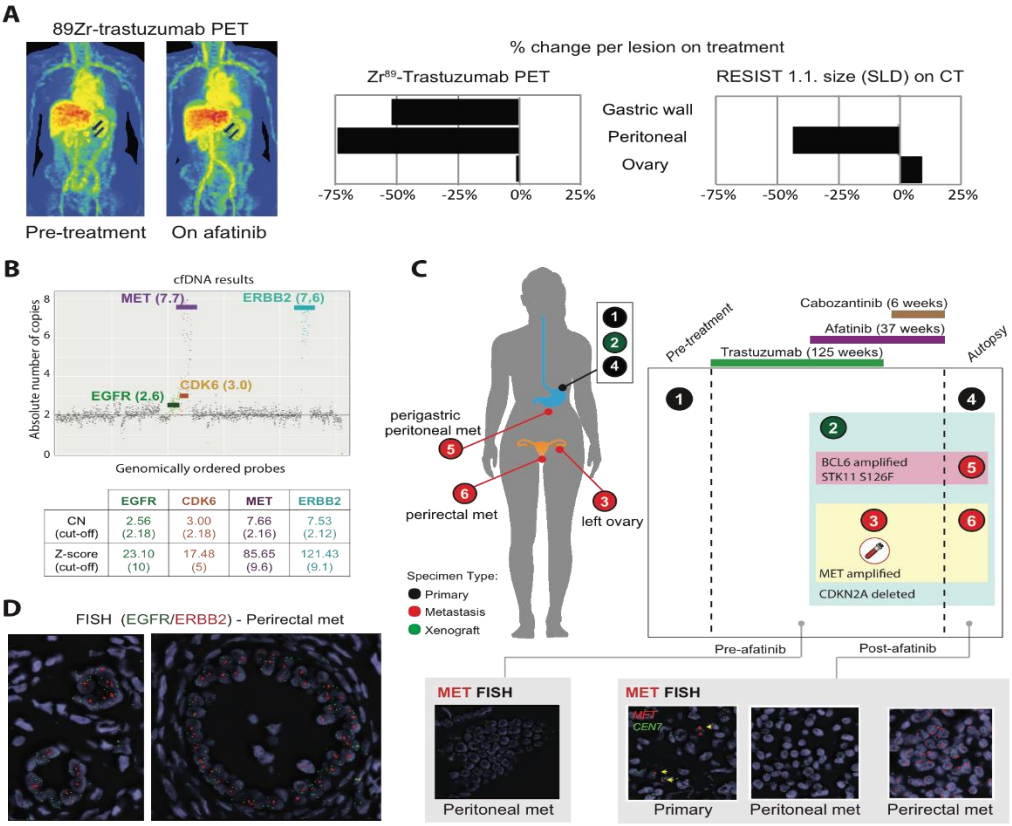


Figure 7: Acquired MET amplification as a mechanism of afatinib/trastuzumab resistance in patient P-0000282 with ERBB2-amplified EG cancer

Figure 7 shows acquired MET amplification as a mechanism of afatinib/trastuzumab resistance in patient P-0000282 with ERBB2-amplified EG cancer. (a) Radiographic tumor assessment using 89Zr-trastuzumab PET and conventional CT scan, with corresponding bar graphs. 89Zr-trastuzumab PET values in SUV and CT measurements in mm. 89Zr-trastuzumab PET, left panel, is a baseline pretreatment image showing uptake in left ovary metastasis (SUV 5.1) not visible in this projection, perigastric peritoneal metastasis (SUV 7.2, lower arrow) and gastric mass (SUV 8.2, upper arrow). Right panel is 89Zr-trastuzumab PET 5 weeks post-treatment initiation, showing resolution of uptake in perigastric peritoneal metastasis (SUV 1.8) and gastric mass (SUV 3.9) and persistently high uptake in left ovarian metastasis (SUV 5.2) not seen on MIP images. (b) cfDNA analysis at the time of disease progression on afatinib/trastuzumab, demonstrating co-occurring ERBB2 and MET amplifications. (c) Genomic comparison of matched pretreatment biopsy with post-treatment metastases obtained from left ovarian metastasis and subsequently at rapid autopsy, demonstrating acquired MET amplification unique to the progressing lesions. The perigastric metastasis and the primary tumor, both of which demonstrated ongoing response to afatinib/trastuzumab, did not harbor MET amplification. (d) Dual probe EGFR and ERBB2 FISH from perirectal tumor biopsy collected after treatment demonstrated ERBB2 amplification and low-level gain of EGFR in a subset of tumor cells.

Specific Aim 3

Patient Derived Xenografts (PDXs)

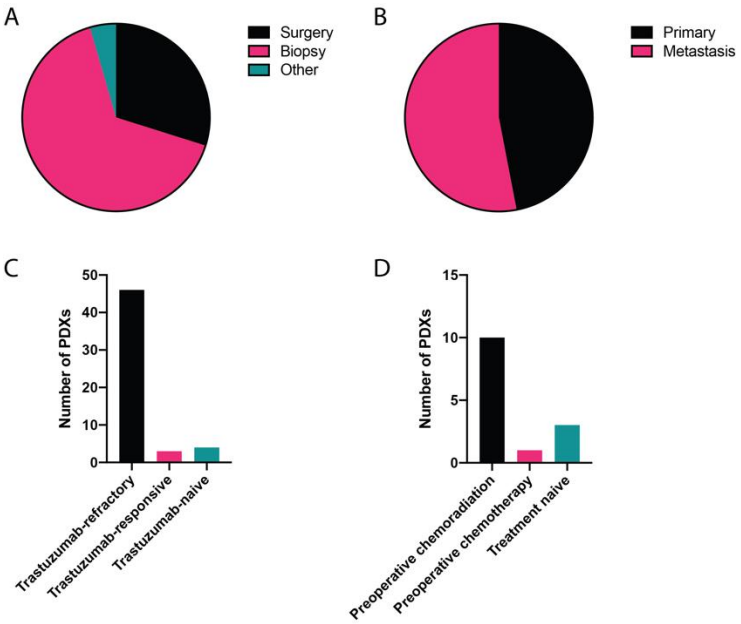


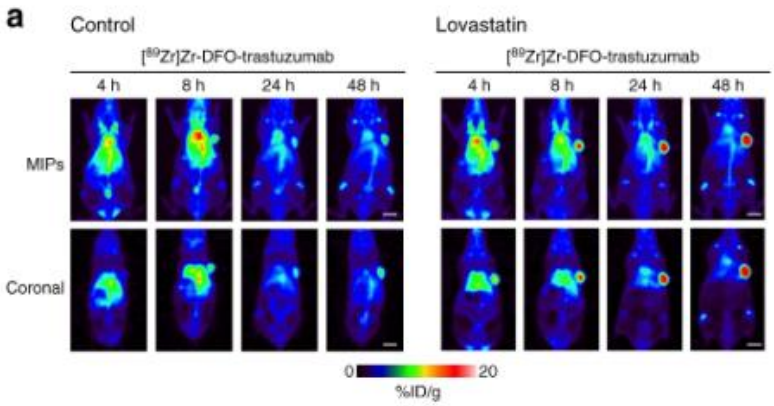
Figure 8. Overview of HER2-positive esophagogastric cancer PDXs. (a) Procedure for generation of PDXs. (b) Tissue origin (primary tumor or metastasis) for PDXs. (c) Treatment history with trastuzumab for HER2-positive PDXs derived from patients with metastatic disease. (d) Preoperative treatment history for PDXs derived from patients with localized HER2-positive tumors.

Table 1. Patient and PDX characteristics

Characteristic	N (%)
Gender (%)	
Women	11 (19)
Men	46 (81)
Anatomic tumor location (%)	
Gastroesophageal junction	18 (31)
Esophagus	18 (31)
Stomach	22 (38)
Stage at initial PDX collection (%)	
IV	43 (75)
III	8 (14)
II	5 (9)
I	1 (2)
Number of PDX per patient (%)	
1	46 (81)
2	9 (16)
3	1 (2)
Sample Type (%)	
Primary	31 (47)
Metastasis	33 (53)
Procedure Type	
Surgery	20 (30)
Biopsy	44 (66)
Other	3 (4)

As shown in figure 8 and table 1, we have generated a collection of 113 patient-derived xenograft (PDX) models from patients with gastric, esophageal and gastroesophageal junction cancers. Of these 113 PDXs, 67 PDXs were derived from 57 patients with HER2-positive tumors, including patients with metastatic (43 patients, 75%) and early stage/locally advanced (14 patients, 25%) cancers at the time of PDX collection. The PDXs were generated from either surgical resections or biopsies (Figure 8a) using tissue from the primary esophagogastric tumor or a metastatic site (Figure 8b). In addition, for some HER2-positive patients, we have derived two (9 patients) or three (1 patient) PDXs from the same patient at different timepoints within the treatment course. The large majority of PDXs from patients with metastatic HER2-positive cancers were generated from patients with treatment-refractory disease with progression on trastuzumab and chemotherapy containing regimens (Figure 8c). Other PDXs were derived from patients with newly diagnosed metastatic disease or with ongoing responses to trastuzumab-containing therapy. Moreover, we have generated several HER2-positive esophagogastric cancer PDXs from patients with localized disease, including PDXs from untreated tumors and tumors exposed to preoperative chemotherapy or chemoradiation (Figure 8d).

We have performed targeted sequencing of most of the HER2-positive PDXs using the MSK-IMPACT next-generation sequencing platform, with the latest version including 468 genes. The majority of these PDXs have corresponding clinical sequencing from patient tumors, allowing for analysis of genomic fidelity between patient and PDX samples. Frequently co-occurring alterations with HER2 amplifications include *TP53* mutations, cell-cycle gene alterations (i.e. *CDK12, CCDN3, CDKN2B, CCNE1*) and receptor tyrosine kinase alterations (such as *EGFR*), consistent with patient sequencing data.



b

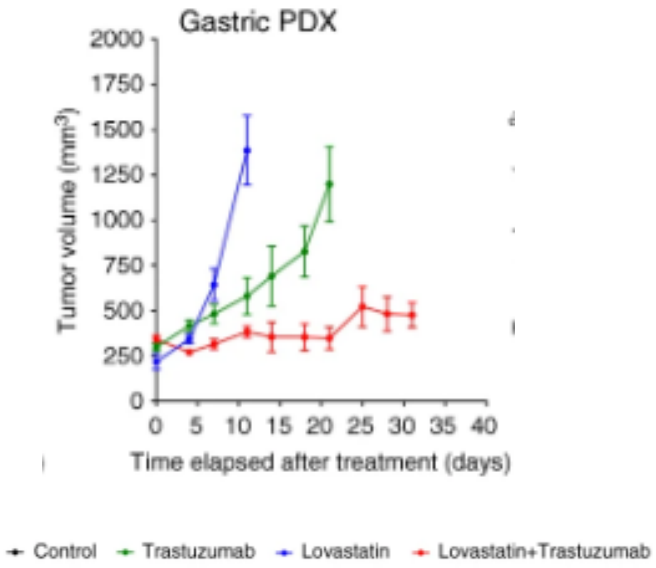


Figure 9: (a) Use of PDXs to image response to treatment. (b) Superior in vivo therapeutic efficacy of trastuzumab combined with lovastatin when compared with trastuzumab in nu/nu NSG mice bearing gastric PDXs (n≥8 mice per group).

As shown in figure 9, statin treatment increases tumor uptake and efficacy of trastuzumab. The use of gastric PDXs to image response to treatment and the therapeutic efficacy of trastuzumab combined with lovastatin increases our understanding of mechanisms of resistance and will assist in designing future studies.

Specific Aim 4

Generate highly liver metastatic PDX with in-vivo selection and therapy

Progression and passages of eight PDX models of HER2 gastric cancer for in vivo selection of metastasis.

Table 2:PDXs generated for *in vivo* liver selection

PDX ID	Clinical Key	Derivative
GAS CX	T3N1 GEJ adenocarcinoma	LVM1a
GAS DF1	T1N1M1 Gastric adenocarcinoma	LVM1a, b, and LVM2

Where, LVM1 stands for liver metastatic 1st passage line and LVM2 stands for liver metastatic 2nd passage line.

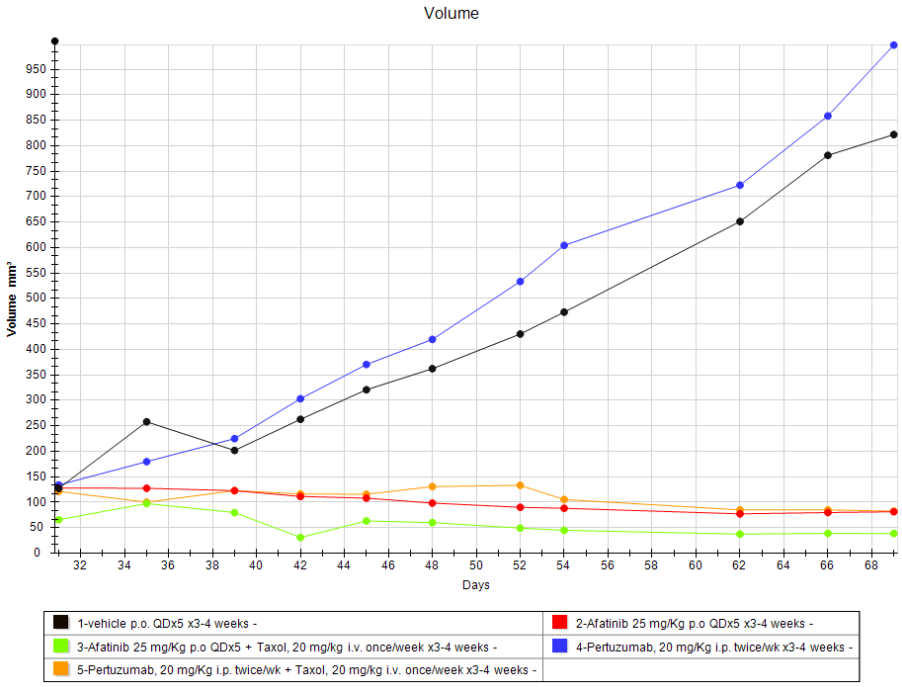


Figure 10: **GD PDX**: Determined the sensitivity of tumor GD to afatinib or pertuzumab + Taxol combination.

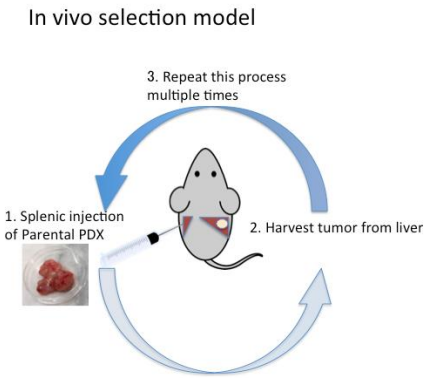


Figure 11: Schema of in-vivo selection model

Figure 11 shows single cell solution from parental PDXs are injected to spleen. Injected PDXs will colonize in liver through portal circulation. Harvest the colonized metastatic tumor and repeat the same process.



Figure 12:Ex-vivo image of highly liver metastatic derivative (LVM=upper and Parental=lower).

Table 3. List of highly liver metastatic PDX derivative

PDX ID	Clinical Key	Derivative
GAS DK	T3N0 Gastric Tubular adenocarcinoma	LVM1b
GAS DK	T3N0 Gastric Tubular adenocarcinoma	LVM1a
GAS CX	T3N1M1 GEJ cancer	LVM1a
GAS DQ	T1N0 Signet Ring cell Gastric cancer	LVM1a
GAS DC	Stage IV T3N1 GEJ Adenocarcinoma	LVM1a
GAS EK	Stage IV TXN0M1 GEJ adenocarcinoma	LVM1a
GAS DO	Stage IV T3N3M0 Gastric Tubular Adenocarcinoma	LVM2a
GAS DS	Stage IV T1N0M1 Gastric Signet Ring Cell Adenocarcinoma	LVM1a

micro RNA profiling of isogenic highly- or lowly- metastatic HER2 amplified gastric PDX

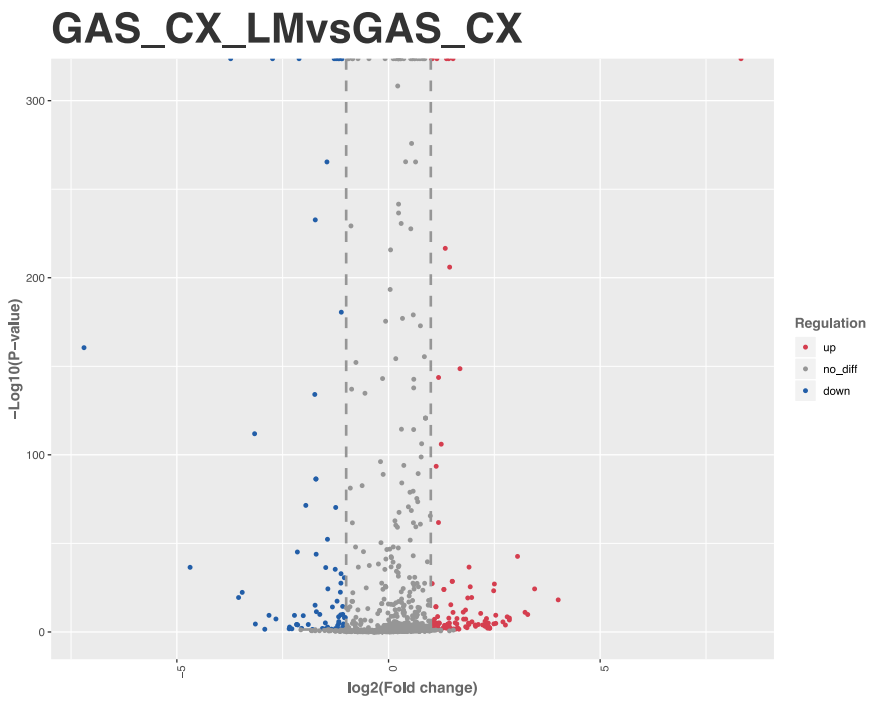


Figure 13: Volcano plot of up- or down- regulated micro RNAs

Sample: Gastric CX PDX, T3N1M0, tissue was taken from the stomach, HER2 amplified

Results: Most highly down regulated miRs with log2FC > 3 are annotated.

Table 2. List of top 20 differentially expressed miRs

Index	miR_name	miR_seq	up/down	fold_char	log2(fold	pvalue(ch	pvalue(fi
1	hsa-miR-1-3p	TGGAATGTAAAGAAGTATGTAT	down	0.01	-7.19	0.00E+00	########
2	hsa-miR-155-5p_R-1	TTAATGCTAATCGTGATAGGGGT	down	0.04	-4.69	5.06E-29	3.24E-37
3	hsa-miR-363-3p	AATTGCACGGTATCCATCTGTA	down	0.08	-3.73	0.00E+00	0.00E+00
4	hsa-miR-1911-5p	TGAGTACCGCCATGTCTGTTGGG	down	0.09	-3.54	3.48E-17	3.70E-20
5	hsa-miR-218-5p_R+2	TTGTGCTTGATCTAACCATGTGA	down	0.09	-3.46	7.96E-20	4.46E-23
6	hsa-miR-20b-5p	CAAAGTGCTCATAGTGCAGGTAG	down	0.11	-3.16	0.00E+00	########
7	bta-miR-1911_R+1	TGAGTACCGCCATGTCTGTTGGGA	down	0.11	-3.14	5.74E-05	3.37E-05
8	hsa-miR-548i	AAAAGTAATTGCGGATTTTGCC	down	0.13	-2.92	3.38E-02	2.90E-02
9	hsa-miR-1269b	CTGGACTGAGCCATGCTACTGG	down	0.14	-2.82	3.81E-09	4.21E-10
10	hsa-miR-486-5p	TCCTGTACTGAGCTGCCCCGAG	down	0.15	-2.74	0.00E+00	0.00E+00
11	hsa-miR-584-5p_R-1	TTATGGTTTGCCTGGGACTGA	down	0.16	-2.66	2.03E-07	4.72E-08
12	hsa-miR-6511b-3p_R-1	CCTCACCACCCCTTCTGCCTGC	down	0.20	-2.35	1.02E-02	1.72E-02
13	mmu-miR-3968_L-2_1ss14AT	AATCCCACTCCTGACACCA	down	0.20	-2.34	2.50E-03	1.72E-03
14	hsa-miR-4517_R+1	AAATATGATGAAACTCACAGCTGAGG	down	0.21	-2.28	1.37E-02	1.72E-02
15	mdo-miR-215_R+1_1ss20AC	ATGACCTATGAATTGACAGCCAT	down	0.21	-2.22	2.08E-09	4.49E-10
16	mmu-mir-3535-p3	AGATAGTCAAGTTCTGATC	down	0.22	-2.17	7.60E-05	6.56E-05
17	mmu-mir-3535-p5	AGATAGTCAAGTTCTGATC	down	0.22	-2.17	7.60E-05	6.56E-05
18	hsa-miR-181a-2-3p	ACCACTGACCGTTGACTGTACC	down	0.22	-2.15	7.18E-42	7.02E-46
19	PC-3p-43750_38	TATATATAGTATATGTGCATGT	down	0.23	-2.14	2.91E-04	1.10E-04
20	hsa-miR-10b-5p_R-1	TACCCTGTAGAACCGAATTTGT	down	0.23	-2.11	0.00E+00	0.00E+00

Known functions of top 5 down-regulated miRs in cancers

- miR-1-3p is known to regulate bladder cancer proliferation by up-regulating SFRP1 expression and is also known for inhibiting c-Met in NSCLC.
- miR-155 is known to be down regulated in FAP patients and modulate WNT signaling by targeting AXIN1 and TCF4.
- miR-363-3p is known to inhibit EMT and metastasis in CRC by targeting Sox4.
- miR-1911-5p is associated with metastasis phenotype in CRC.
- miR-218-5p_R+2 is known to inhibit cancer cell proliferation and migration via EGFR in NSCLC.

To identify a key gene in promoting gastric cancer liver metastasis, we generated an isogenic highly liver metastatic derivative from patient derived xenografts of gastric cancers (Gas PDXs) by *in vivo* selection. (Fidler, 1973) Iterative repeats of parental Gas PDXs injection to the portal circulation enriched highly liver metastatic Gas PDX sub-populations (Gas LVM PDXs). Over a decade, many groups including us (Loo et al., 2015; Ma et al., 2007; Pencheva et al., 2012; Tavazoie et al., 2008) have shown that differentially expressed micro RNAs regulate cancer metastasis. However, the role of differentially expressed micro RNAs in gastric cancer metastasis is little known, which motivated us to conduct micro RNA profiling of Gas LVM PDX and isogenic parental Gas PDX. We conducted micro RNA profiling of HER2 amplified Gas PDX, Gas CX and its LVM derivative, Gas CX LVM revealing 24 significantly differentially expressed micro RNAs with the cut off of log2FC=2 and p-value<0.05. Among the 24 highly significant micro RNAs, miR-1-3p is known to regulate bladder cancer proliferation by up-regulating sFRP1 expression(Shang et al., 2017). sFRP1 is known to promote gastric cancer proliferation by inhibiting TGF beta/Smad3 signaling(Peng et al., 2019). Taken together, miR-1-3p down-regulation we saw in our analysis might have an important regulatory role in gastric cancer metastasis although we must experimentally validate the hypothesis. In summary, micro RNA profiling of LVM and parental Gas PDX revealed novel differentially expressed micro RNAs and the experimental validation of those findings and further mechanistic investigation is highly warranted.

IMPACT

What opportunities for training and professional development has the project provided?

Reflecting her academic and research achievements, in 2018, Dr. Janjigian was appointed Chief of MSK's Gastrointestinal Oncology Service. This service is one of the largest at MSKCC and Dr. Janjigian's selection as its leader after an international search is a testament to her remarkable accomplishments.

How were the results disseminated to communities of interest?

National meetings and manuscripts published.

Cancer Discov. 2018 Jan;8(1):49-58. doi: 10.1158/2159-8290.CD-17-0787. Epub 2017 Nov 9. PMID: 29122777

Cancer Discov. 2019 Feb;9(2):199-209. doi: 10.1158/2159-8290.CD-18-0598. Epub 2018 Nov 21.PMID:30463996.

Janjigian et al ESMO 2019 conference Annals of Oncology (2019) 30 (5): 313. doi.org/10.1093/annonc/mdz247.143

Janjigian YY, Chou JF, Simmons M, et al: First-line pembrolizumab, trastuzumab, capecitabine and oxaliplatin in HER2-positive metastatic esophagogastric adenocarcinoma. 2019 Gastrointestinal Cancers Symposium. Abstract 62. Presented January 17, 2019.

Janjigian et al ASCO 2016 Journal of Clinical Oncology (2019) 37 (4): 62. 10.1200/JCO.2019.37.4_suppl.62

Janjigian et al ESMO 2016 conference Annals of Oncology (2016) 27 (6): 207-242. 10.1093/annonc/mdw371

Janjigian et al. First-line pembrolizumab and trastuzumab in HER2-positive esophagogastric cancer. Lancet Oncology- Submitted, under review.

What do you plan to do during the next reporting period to accomplish the goals?
N/A

What was the impact on technology transfer?
Nothing to report

What was the impact on society beyond science and technology?
Nothing to report

CHANGES/PROBLEMS

Changes in approach and reasons for change
N/A

Actual or anticipated problems or delays and actions or plans to resolve them
Nothing to report

Changes that had a significant impact on expenditures
Nothing to report

Significant changes in use or care of human subjects, vertebrate animals, biohazards, and/or select agents
Nothing to report

PRODUCTS

- **Publications, conference papers, and presentations**

Janjigian et al. First-line pembrolizumab and trastuzumab in HER2-positive esophagogastric cancer. Lancet Oncology- Submitted, under review.

Janjigian et al ESMO 2019 conference Annals of Oncology (2019) 30 (5): 313. doi.org/10.1093/annonc/mdz247.143

Janjigian YY, Chou JF, Simmons M, et al: First-line pembrolizumab, trastuzumab, capecitabine and oxaliplatin in HER2-positive metastatic esophagogastric adenocarcinoma. 2019 Gastrointestinal Cancers Symposium. Abstract 62. Presented January 17, 2019.

Janjigian et al ASCO 2019 Journal of Clinical Oncology (2019) 37 (4): 62. 10.1200/JCO.2019.37.4_suppl.62

Janjigian et al ESMO 2016 conference Annals of Oncology (2016) 27 (6): 207-242. 10.1093/annonc/mdw371

Janjigian Y, et al. Genetic predictors of response to systemic therapy in esophagogastric cancer. *Cancer Discov.* 2018 Jan;8(1):49-58.

Sanchez-Vega F, et al.EGFR and MET Amplifications Determine Response to HER2 Inhibition in ERBB2-Amplified Esophagogastric Cancer. *Cancer Discov.* 2019 February.

Pereira PMR, Sharma SK, Carter LM, Edwards KJ, Pourat J, Ragupathi A, **Janjigian YY**, Durack JC, Lewis JS. Caveolin-1 mediates cellular distribution of HER2 and affects trastuzumab binding and therapeutic efficacy. *Nat Commun*. 2018 December 3. PMID:30510281.

O'Donoghue JA, Lewis JS, Pandit-Taskar N, Fleming SE, Schoder H, Larson SM, Beylergil V1, Ruan S, Lyashchenko S, Zanzonico PB, Weber WA, Carrasquillo JA, **Janjigian YY**. Pharmacokinetics, biodistribution, and radiation dosimetry for 89Zr-trastuzumab in patients with esophagogastric cancer. *J Nucl Med*. 2017 Jun 21 PMID: 28637800.

Peng, J.X., Liang, S.Y., and Li, L. (2019). sFRP1 exerts effects on gastric cancer cells through GSK3beta/Rac1mediated restraint of TGFbeta/Smad3 signaling. Oncol Rep *41*, 224-234.

Shang, A., Yang, M., Shen, F., Wang, J., Wei, J., Wang, W., Lu, W., Wang, C., and Wang, C. (2017). MiR-1-3p Suppresses the Proliferation, Invasion and Migration of Bladder Cancer Cells by Up-Regulating SFRP1 Expression. Cell Physiol Biochem *41*, 1179-1188.

- **Books or other non-periodical, one-time publications.**

Nothing to report

- **Other publications, conference papers, and presentations**

Nothing to report

- **Website(s) or other Internet site(s)**

Nothing to report

- **Technologies or techniques**

Improved efficacy of tumor implantation to immune deficient mice

1. Dissect human tumor to 100mm3 pieces
2. With blunt edge of scissors, scrape off soft/whitish necrotic tissue
3. Cut the fragment to 20-30mm3 pieces by removing non-viable tissue

4. Implant these 20-30mm3 pieces in bilateral flank of immune deficient mice as described anywhere.

- **Inventions, patent applications, and/or licenses**

Nothing to report

- **Other Products**

Nothing to report

PARTICIPANTS & OTHER COLLABORATING ORGANIZATIONS

What individuals have worked on the project?

Personnel	Role	Percent effort
Yelena Janjigian	PD/PI	0.6
Christine Iacobuzio-Donahue	Co-PI	0.36
Francisco Sanchez-Vega	Post-Doctoral Associate	2.4
Hui-Yong Zhao	Laboratory Assistant	1.44
Brittanie Millang	Research Assistant	0.9

Has there been a change in the active other support of the PD/PI(s) or senior/key personnel since the last reporting period?
Nothing to report.

What other organizations were involved as partners?
Nothing to report.

SPECIAL REPORTING REQUIREMENTS

COLLABORATIVE AWARDS: ANNUAL REPORT SUBMITTED ON BEHALF OF DRS. LEWIS AND TAVAZOIE BY THE LEAD PI—DR. JANJIGIAN

REFERENCES:

Janjigian et al. First-line pembrolizumab and trastuzumab in HER2-positive esophagogastric cancer. Lancet Oncology- Submitted, under review.

Janjigian et al ESMO 2019 conference Annals of Oncology (2019) 30 (5): 313. doi.org/10.1093/annonc/mdz247.143

Janjigian YY, Chou JF, Simmons M, et al: First-line pembrolizumab, trastuzumab, capecitabine and oxaliplatin in HER2-positive metastatic esophagogastric adenocarcinoma. 2019 Gastrointestinal Cancers Symposium. Abstract 62. Presented January 17, 2019.

Janjigian et al ASCO 2019 Journal of Clinical Oncology (2019) 37 (4): 62. 10.1200/JCO.2019.37.4_suppl.62

Janjigian et al ESMO 2016 conference Annals of Oncology (2016) 27 (6): 207-242.

10.1093/annonc/mdw371

Janjigian Y, et al. Genetic predictors of response to systemic therapy in esophagogastric cancer. *Cancer Discov.* 2018 Jan;8(1):49-58.

Sanchez-Vega F, et al.EGFR and MET Amplifications Determine Response to HER2 Inhibition in ERBB2-Amplified Esophagogastric Cancer. *Cancer Discov.* 2019 February.

Pereira PMR, Sharma SK, Carter LM, Edwards KJ, Pourat J, Ragupathi A, **Janjigian YY**, Durack JC, Lewis JS. Caveolin-1 mediates cellular distribution of HER2 and affects trastuzumab binding and therapeutic efficacy. *Nat Commun*. 2018 December 3. PMID:30510281.

O'Donoghue JA, Lewis JS, Pandit-Taskar N, Fleming SE, Schoder H, Larson SM, Beylergil V1, Ruan S, Lyashchenko S, Zanzonico PB, Weber WA, Carrasquillo JA, **Janjigian YY**. Pharmacokinetics, biodistribution, and radiation dosimetry for 89Zr-trastuzumab in patients with esophagogastric cancer. *J Nucl Med*. 2017 Jun 21 PMID: 28637800.

Fidler, I.J. (1973). Selection of successive tumour lines for metastasis. Nat New Biol *242*, 148-149.
Loo, J.M., Scherl, A., Nguyen, A., Man, F.Y., Weinberg, E., Zeng, Z., Saltz, L., Paty, P.B., and Tavazoie, S.F. (2015). Extracellular metabolic energetics can promote cancer progression. Cell *160*, 393-406

Ma, L., Teruya-Feldstein, J., and Weinberg, R.A. (2007). Tumour invasion and metastasis initiated by microRNA-10b in breast cancer. Nature *449*, 682-688.

Pencheva, N., Tran, H., Buss, C., Huh, D., Drobnjak, M., Busam, K., and Tavazoie, S.F. (2012). Convergent multi-miRNA targeting of ApoE drives LRP1/LRP8-dependent melanoma metastasis and angiogenesis. Cell *151*, 1068-1082.

Tavazoie, S.F., Alarcon, C., Oskarsson, T., Padua, D., Wang, Q., Bos, P.D., Gerald, W.L., and Massague, J. (2008). Endogenous human microRNAs that suppress breast cancer metastasis. Nature *451*, 147-152.

Peng, J.X., Liang, S.Y., and Li, L. (2019). sFRP1 exerts effects on gastric cancer cells through GSK3beta/Rac1mediated restraint of TGFbeta/Smad3 signaling. Oncol Rep *41*, 224-234.

Shang, A., Yang, M., Shen, F., Wang, J., Wei, J., Wang, W., Lu, W., Wang, C., and Wang, C. (2017). MiR-1-3p Suppresses the Proliferation, Invasion and Migration of Bladder Cancer Cells by Up-Regulating SFRP1 Expression. Cell Physiol Biochem *41*, 1179-1188.

APPENDICES

Appendix A- Janjigian Y, et al. Genetic predictors of response to systemic therapy in esophagogastric cancer. *Cancer Discov.* 2018 Jan;8(1):49-58.

Appendix B- Sanchez-Vega F, et al.EGFR and MET Amplifications Determine Response to HER2 Inhibition in ERBB2-Amplified Esophagogastric Cancer. *Cancer Discov.* 2019 February.

Appendix C- Pereira PMR, Sharma SK, Carter LM, Edwards KJ, Pourat J, Ragupathi A, **Janjigian YY**,Durack JC, Lewis JS. Caveolin-1 mediates cellular distribution of HER2 and affects trastuzumab binding and therapeutic efficacy. *Nat Commun*. 2018 December 3. PMID:30510281.

Appendix D- O'Donoghue JA, Lewis JS, Pandit-Taskar N, Fleming SE, Schoder H, Larson SM, Beylergil V1, Ruan S, Lyashchenko S, Zanzonico PB, Weber WA, Carrasquillo JA, **Janjigian YY**. Pharmacokinetics, biodistribution, and radiation dosimetry for 89Zr-trastuzumab in patients with esophagogastric cancer. *J Nucl Med*. 2017 Jun 21 PMID: 28637800.

Appendix E- Janjigian et al ESMO 2016 conference Annals of Oncology (2016) 27 (6): 207-242.

Published OnlineFirst November 9, 2017; DOI: 10.1158/2159-8290.CD-17-0787

RESEARCH BRIEF

Genetic Predictors of Response to Systemic Therapy in Esophagogastric Cancer

Yelena Y. Janjigian[1], Francisco Sanchez-Vega[2,3], Philip Jonsson[3,4], Walid K. Chatila[2], Jaclyn F. Hechtman[5], Geoffrey Y. Ku[1], Jamie C. Riches[1], Yaelle Tuvy[1], Ritika Kundra[2], Nancy Bouvier[2], Efsevia Vakiani[5], Jianjiong Gao[2], Zachary J. Heins[2], Benjamin E. Gross[2], David P. Kelsen[1], Liying Zhang[5], Vivian E. Strong[6], Mark Schattner[1], Hans Gerdes[1], Daniel G. Coit[6], Manjit Bains[6], Zsofia K. Stadler[1], Valerie W. Rusch[6], David R. Jones[6], Daniela Molena[6], Jinru Shia[5], Mark E. Robson[1], Marinela Capanu[4], Sumit Middha[5], Ahmet Zehir[5], David M. Hyman[1], Maurizio Scaltriti[3,5], Marc Ladanyi[3,5], Neal Rosen[1], David H. Ilson[1], Michael F. Berger[2,3,5], Laura Tang[5], Barry S. Taylor[2,3,4], David B. Solit[1,2,3], and Nikolaus Schultz[2,3,4]

ABSTRACT

The incidence of esophagogastric cancer is rapidly rising, but only a minority of patients derive durable benefit from current therapies. Chemotherapy as well as anti-HER2 and PD-1 antibodies are standard treatments. To identify predictive biomarkers of drug sensitivity and mechanisms of resistance, we implemented prospective tumor sequencing of patients with metastatic esophagogastric cancer. There was no association between homologous recombination deficiency defects and response to platinum-based chemotherapy. Patients with microsatellite instability–high tumors were intrinsically resistant to chemotherapy but more likely to achieve durable responses to immunotherapy. The single Epstein–Barr virus–positive patient achieved a durable, complete response to immunotherapy. The level of *ERBB2* amplification as determined by sequencing was predictive of trastuzumab benefit. Selection for a tumor subclone lacking *ERBB2* amplification, deletion of *ERBB2* exon 16, and comutations in the receptor tyrosine kinase, RAS, and PI3K pathways were associated with intrinsic and/or acquired trastuzumab resistance. Prospective genomic profiling can identify patients most likely to derive durable benefit to immunotherapy and trastuzumab and guide strategies to overcome drug resistance.

SIGNIFICANCE: Clinical application of multiplex sequencing can identify biomarkers of treatment response to contemporary systemic therapies in metastatic esophagogastric cancer. This large prospective analysis sheds light on the biological complexity and the dynamic nature of therapeutic resistance in metastatic esophagogastric cancers. *Cancer Discov; 8(1); 49–58. ©2017 AACR.*

See related commentary by Sundar and Tan, p. 14.
See related article by Pectasides et al., p. 37.

INTRODUCTION

Esophagogastric cancer is the tumor type with the most rapidly increasing incidence in the United States, particularly in young patients (1). These tumors have a high metastatic potential and frequently recur. Recent large-scale sequencing initiatives, including the retrospective studies performed by The Cancer Genome Atlas (TCGA), have

[1]Department of Medicine, Memorial Sloan Kettering Cancer Center and Weill Cornell Medical College, New York, New York. [2]Marie-Josée & Henry R. Kravis Center for Molecular Oncology, Memorial Sloan Kettering Cancer Center, New York, New York. [3]Human Oncology and Pathogenesis Program, Memorial Sloan Kettering Cancer Center, New York, New York. [4]Department of Epidemiology-Biostatistics, Memorial Sloan Kettering Cancer Center, New York, New York. [5]Department of Pathology, Memorial Sloan Kettering Cancer Center, New York, New York. [6]Department of Surgery, Memorial Sloan Kettering Cancer Center, New York, New York.

Note: Supplementary data for this article are available at Cancer Discovery Online (http://cancerdiscovery.aacrjournals.org/).

Corresponding Author: Yelena Y. Janjigian, Memorial Sloan Kettering Cancer Center, 300 East 66th Street, Room 1033, New York, NY 10065. Phone: 646-888-4186; Fax: 646-888-4256; E-mail: janjigiy@mskcc.org

doi: 10.1158/2159-8290.CD-17-0787

©2017 American Association for Cancer Research.

Downloaded from cancerdiscovery.aacrjournals.org on January 22, 2020. © 2018 American Association for Cancer Research.

Published OnlineFirst November 9, 2017; DOI: 10.1158/2159-8290.CD-17-0787

revealed that most esophagogastric cancers are characterized by chromosomal instability with frequent amplifications of receptor tyrosine kinases (RTK; refs. 2–5). Additional molecularly defined esophagogastric cancer subsets that may be therapeutically relevant include those characterized by homologous recombination deficiency (HRD), Epstein–Barr virus (EBV)–related tumors, and tumors with hypermutation, in particular those with microsatellite instability (MSI; refs. 2–5).

The combination of a fluoropyrimidine and a platinum is the standard first-line systemic therapy for patients with esophagogastric cancer (6). For patients with human epidermal growth factor receptor 2 (HER2/*ERBB2*)–positive tumors, trastuzumab (a HER2-directed antibody) in combination with chemotherapy is standard of care (7). Pembrolizumab and nivolumab (anti–PD-1 antibodies) are approved for use in patients with chemotherapy-refractory esophagogastric cancer. Pembrolizumab was recently approved in the United States for programmed death-ligand 1 (PD-L1)–positive or MSI-high (MSI-H) esophagogastric cancer (8–10). However, PD-L1 status was not predictive of survival with nivolumab therapy in the ATTRACTION 2 study (11), and nivolumab is approved in Asia for treatment irrespective of PD-L1 status.

Despite the recent increase in therapeutic options, responses to systemic therapy in patients with esophagogastric cancer are most often short-lived, and less than 5% of patients with metastatic disease survive beyond 5 years (1). With the goal of identifying predictive biomarkers of response and molecular mechanisms of resistance to trastuzumab and immune checkpoint inhibitors, as a prelude to the development of rational combination strategies, we performed prospective targeted next-generation sequencing (NGS; ref. 12) and clinicopathologic analysis of patients with recurrent or metastatic esophagogastric cancer.

RESULTS

With the goal of identifying predictive biomarkers of drug response, we, in 2014, initiated an effort to perform prospective, targeted NGS analysis of paired tumor and normal samples from all patients with stage IV esophagogastric adenocarcinoma (Supplementary Tables S1 and S2) treated at our center. Tumors were analyzed using MSK-IMPACT, a capture-based, NGS platform that can detect mutations, copy-number alterations, and select rearrangements in 341 or more cancer genes (see Methods). Here, we report the results of the first 295 patients profiled along with accompanying prospectively captured detailed clinical annotation and treatment response data. The majority of samples were acquired from endoscopic biopsies of primary tumors. Unlike the TCGA dataset of early-stage tumors, this Memorial Sloan Kettering (MSK) cohort was comprised of specimens from predominantly younger patients with exclusively stage IV disease with detailed clinical annotation, including survival and therapeutic response data, available for all patients (Fig. 1A).

We achieved a mean sequencing coverage of 744× and identified an average of 5 nonsynonymous mutations per tumor sample (range, 1–63; Supplementary Table S3). MSI status was inferred from the sequencing data using a clinically validated algorithm (13), with MSI-H defined as an MSIsensor score ≥10 (Fig. 1B). MSI-H tumors possessed a high ratio of small insertions and deletions to substitutions, a mutational signature consistent with mismatch repair deficiency. Notably, only 9 samples in the MSK cohort were MSI-H (3%), which is significantly lower than the fraction in the TCGA cohort (16%, $P = 8e{-}10$, Fisher exact test, Fig. 1B). This difference is likely attributable to the higher prevalence of metastatic cancers in the MSK cohort, as MSI-H was a favorable prognostic marker in the TCGA cohort. EBV positivity could not be established from the targeted sequencing data and thus was not known for all patients. To assess for EBV in select patients receiving immunotherapy, Epstein–Barr encoding region *in situ* hybridization (EBER-ISH) was performed in 26 patients who received immunotherapy, with only a single patient testing positive.

The MSK cohort was comprised predominantly of tumors with a signature of chromosomal instability (CIN; 63%), characterized by a high degree of copy-number alterations and low mutational burden (Fig. 1C). *TP53* was the most frequently mutated gene (73%), followed by *ARID1A* (15%) and *CDKN2A* (12%). In total, 53% of patients had at least one potentially actionable alteration as defined by OncoKB (14), a precision oncology knowledge base that annotates the functional consequence and therapeutic implications of cancer mutations (Fig. 1D and E). Focal amplifications and mutations in receptor tyrosine kinases and members of the RAS and PI3K pathways were common in the CIN subset, with frequent oncogenic or likely oncogenic alterations in *ERBB2* (25%), *KRAS* (16%), *EGFR* (8%), *ERBB3* (7%), *PIK3CA* (7%), *FGFR2* (5%), and *MET* (5%). Genomically stable (GS) tumors (34%), conversely, were more frequently of diffuse histology (32% vs. 9%, $P = 3e{-}5$, Fisher test) and *CDH1*-mutant (20% vs. 7%, $P = 0.01$, Fisher test). A comparison of the non–MSI-H tumors to those in the TCGA cohort found few statistically significant differences (Fisher test, 15% FDR): *TP53* mutations were enriched in the MSK cohort (73% vs. 62%, q = 0.11), whereas *KMT2C* (2% vs. 9%, q = 0.06), *GRIN2A* (1% vs. 6%, q = 0.10), *PTPRD* (4% vs. 11%, q = 0.10), and *CTNNB1* (1% vs. 6%, q = 0.10) were less frequently mutated (Supplementary Fig. S1A). Notably, there were no significant differences in the alteration frequencies of any genes between primary and metastatic samples (Supplementary Fig. S1B).

To identify potential biomarkers of response to systemic chemotherapy in an unbiased manner, we correlated the genomic findings with treatment response and patient outcomes in the 187 patients with HER2$^-$ disease treated with first-line fluoropyrimidine/platinum. In this setting, the median progression-free survival (PFS) was similar to the published literature (6.9 vs. 5.3 months), with favorable overall survival (OS; 26.3 months vs. 10.2 months; ref. 15). In this analysis, no single mutant allele or gene, including those with a role in DNA repair pathways, such as *BRCA1/2*, was significantly associated with treatment response (Fig. 2A).

As an association between defects in homologous recombination and response to platinum-based chemotherapy has been identified in other cancer types, we inferred a surrogate marker for HRD from the copy-number data [large-scale

Downloaded from cancerdiscovery.aacrjournals.org on January 22, 2020. © 2018 American Association for Cancer Research.

Published OnlineFirst November 9, 2017; DOI: 10.1158/2159-8290.CD-17-0787

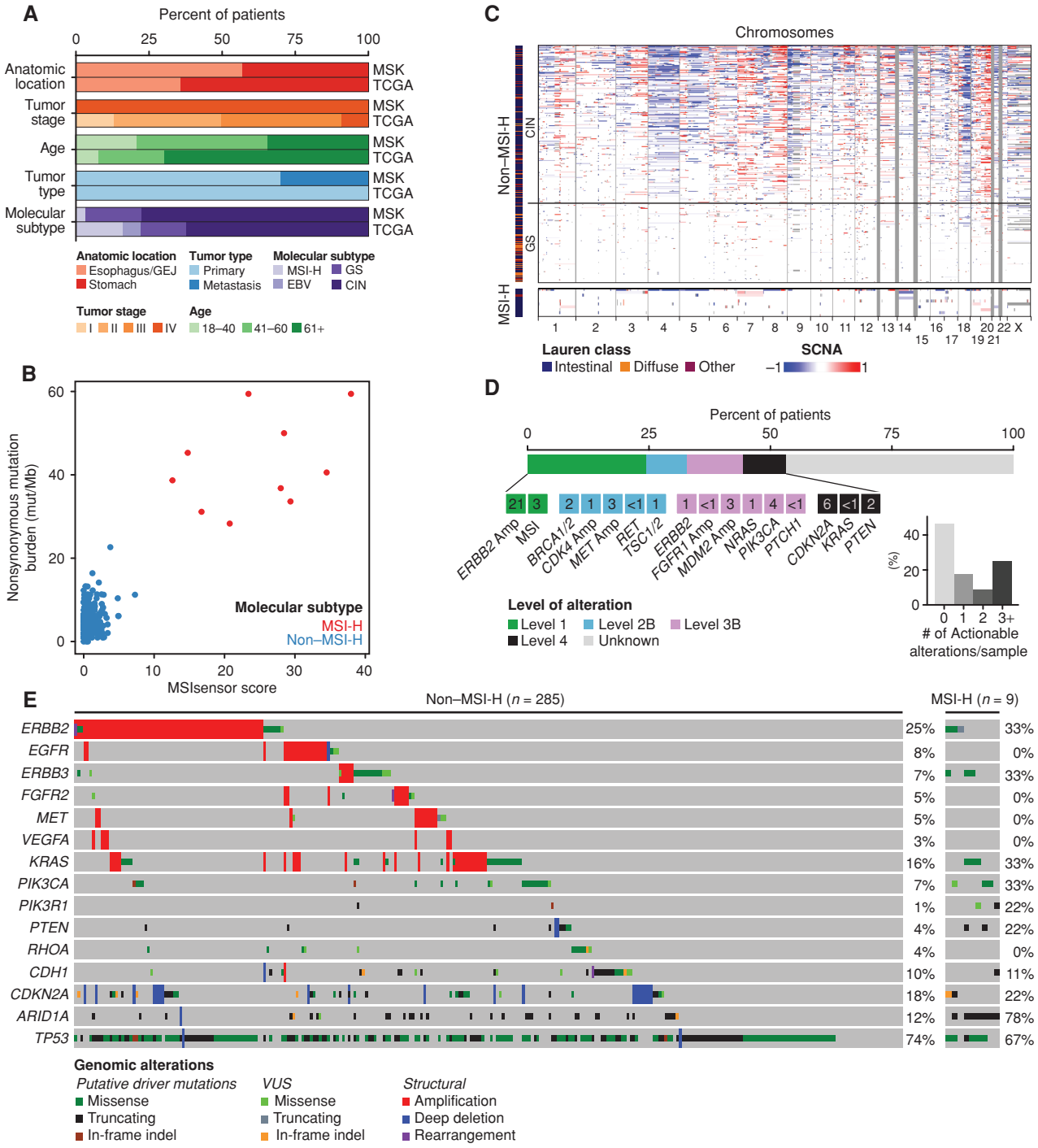


Figure 1. Molecular characterization of esophagogastric tumors. **A,** Comparison of clinical characteristics between the MSK and TCGA cohorts. **B,** Correlation between the MSIsensor score (x-axis) to nonsynonymous mutation burden (y-axis). Samples are colored according to the molecular subtype. **C,** DNA copy-number changes categorized by molecular subtype. Chromosomes are presented from left to right, samples from top to bottom. Regions of losses appear in shades of blue, whereas regions of gains are in shades of red. **D,** Highest level of clinical actionability across the cohort, as defined by OncoKB. Standard therapeutic implications include FDA-recognized or NCCN guideline–listed biomarkers that are predictive of response to an FDA-approved drug in a specific indication (level 1). Investigational therapeutic implications include FDA-approved biomarkers predictive of response to an FDA-approved drug detected in an off-label indication (level 2B), FDA- or non–FDA-recognized biomarkers that are predictive of response to novel targeted agents that have shown promising results in clinical trials (level 3B), and non–FDA-recognized biomarkers that are predictive of response to novel targeted agents on the basis of compelling preclinical data (level 4). **E,** Alterations of known drivers in esophagogastric cancer. Gene alteration types, patterns, and overall frequencies are shown for non–MSI-H and MSI-H tumors separately. Tumors are shown from left to right. Mutations are color-coded by type and by presumed oncogenicity, as defined by prior knowledge and recurrence (cancerhotspots.org). GEJ, gastroesophageal junction; NCCN, National Comprehensive Cancer Network; SCNA, somatic copy-number alterations; VUS, variant of unknown significance.

Downloaded from cancerdiscovery.aacrjournals.org on January 22, 2020. © 2018 American Association for Cancer Research.

Published OnlineFirst November 9, 2017; DOI: 10.1158/2159-8290.CD-17-0787

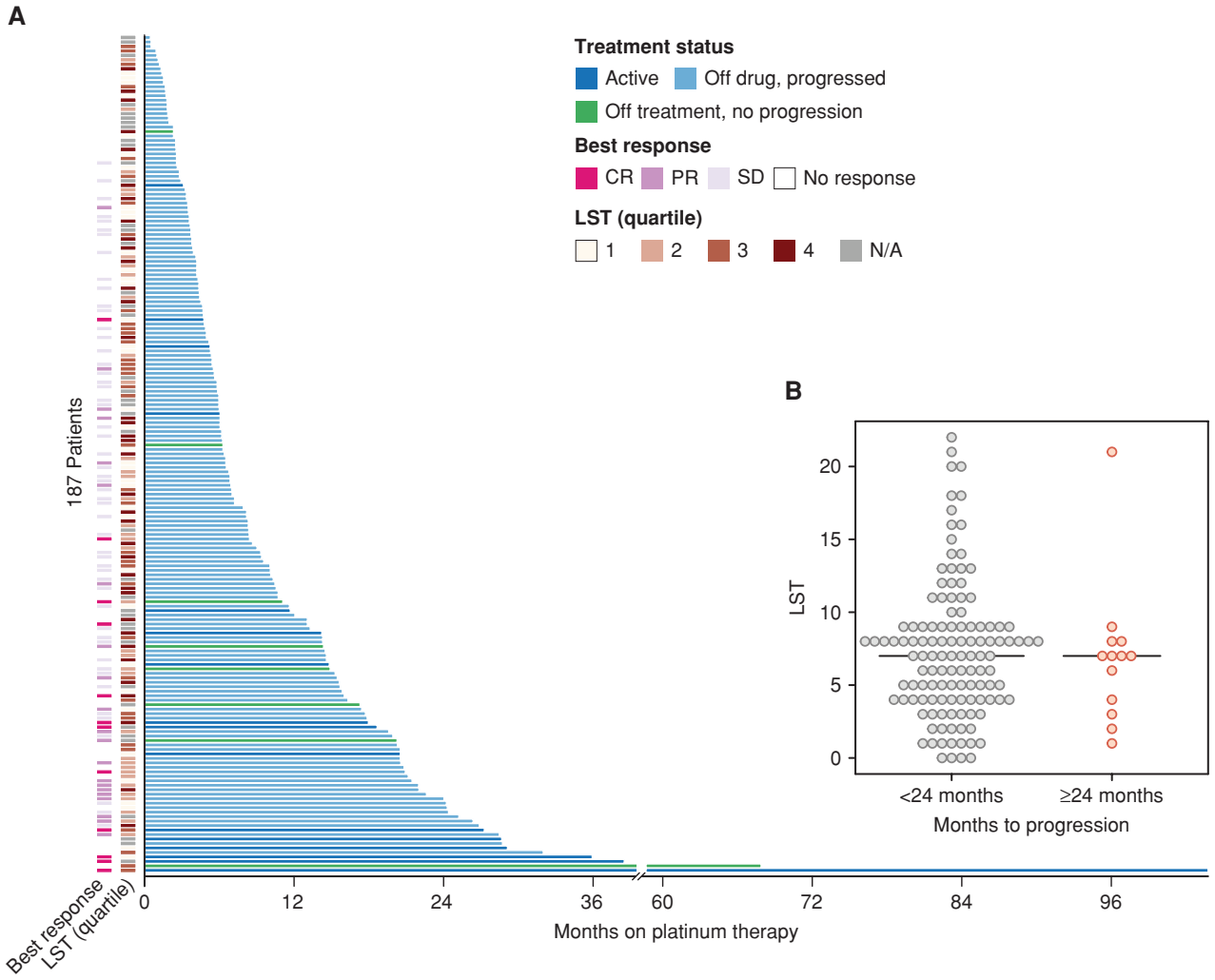


Figure 2. Genomic determinants of response to cytotoxic chemotherapy. **A,** Swimmer's plot showing months on first-line platinum-based therapy for 187 patients with metastatic, HER2⁻ esophageal cancer. The annotation tracks on the left of the y-axis indicate the patient's best response to platinum and the estimated LST score. The color of individual bars indicates the current status of the patient on this line of treatment. **B,** Distribution of LST scores in patients who progressed on platinum treatment before 24 months compared with patients with prolonged response (≥24 months). Horizontal bars represent the median by group. CR, complete response; PR, partial response; SD, stable disease.

state transitions (LST); refs. 16 and 17] and correlated the results with overall response and duration of treatment with chemotherapy. LST score was not predictive of PFS (HR = 0.99, $P = 0.947$, log-rank test) and was not higher in patients with responses to first-line therapy lasting over 24 months ($P = 0.6$, two-tailed t test; Fig. 2B). Notably, the majority of patients with prolonged response to platinum-based combination chemotherapy, including the 2 patients with the longest outlier responses (68 and 104 months, respectively), harbored no somatic alterations in known homologous recombination genes.

As outlined above, only 9 patients (3%) in the cohort had MSI-H tumors. Patients with MSI-H tumors suffered rapid disease progression on standard cytotoxic therapy, with a significantly shorter PFS on first-line chemotherapy when compared with non–MSI-H tumors (median PFS 4.8 vs. 6.9 months for non–MSI-H patients, HR = 0.4, $P = 0.027$, log-rank test; Fig. 3B), results consistent with those recently reported by the Adjuvant Gastric Chemotherapy MAGIC trial (18). On the basis of the sequencing results and prior data suggesting that MSI-H tumors arising in other disease sites may respond to immune checkpoint inhibitors, MSI-H patients who had progressed on standard cytotoxic chemotherapy were preferentially directed to immunotherapy. These patients received anti–PD-1 antibodies (durvalumab, pembrolizumab, and nivolumab), alone or in combination with anti-CTLA4 antibodies (ipilimumab, tremelimumab), on clinical trials or as part of compassionate-use programs. In total, 5 patients with MSI-H tumors and 35 patients with non–MSI-H tumors received immune checkpoint inhibitors, with time on therapy ranging from 0.3 to 44.7 months (Fig. 3A). Although 28% of patients had radiographic tumor regression with immunotherapy, responses were often transient, and the duration of response to immune checkpoint blockade was less than 6 months in all but 5 (12.5%)

Downloaded from cancerdiscovery.aacrjournals.org on January 22, 2020. © 2018 American Association for Cancer Research.

Published OnlineFirst November 9, 2017; DOI: 10.1158/2159-8290.CD-17-0787

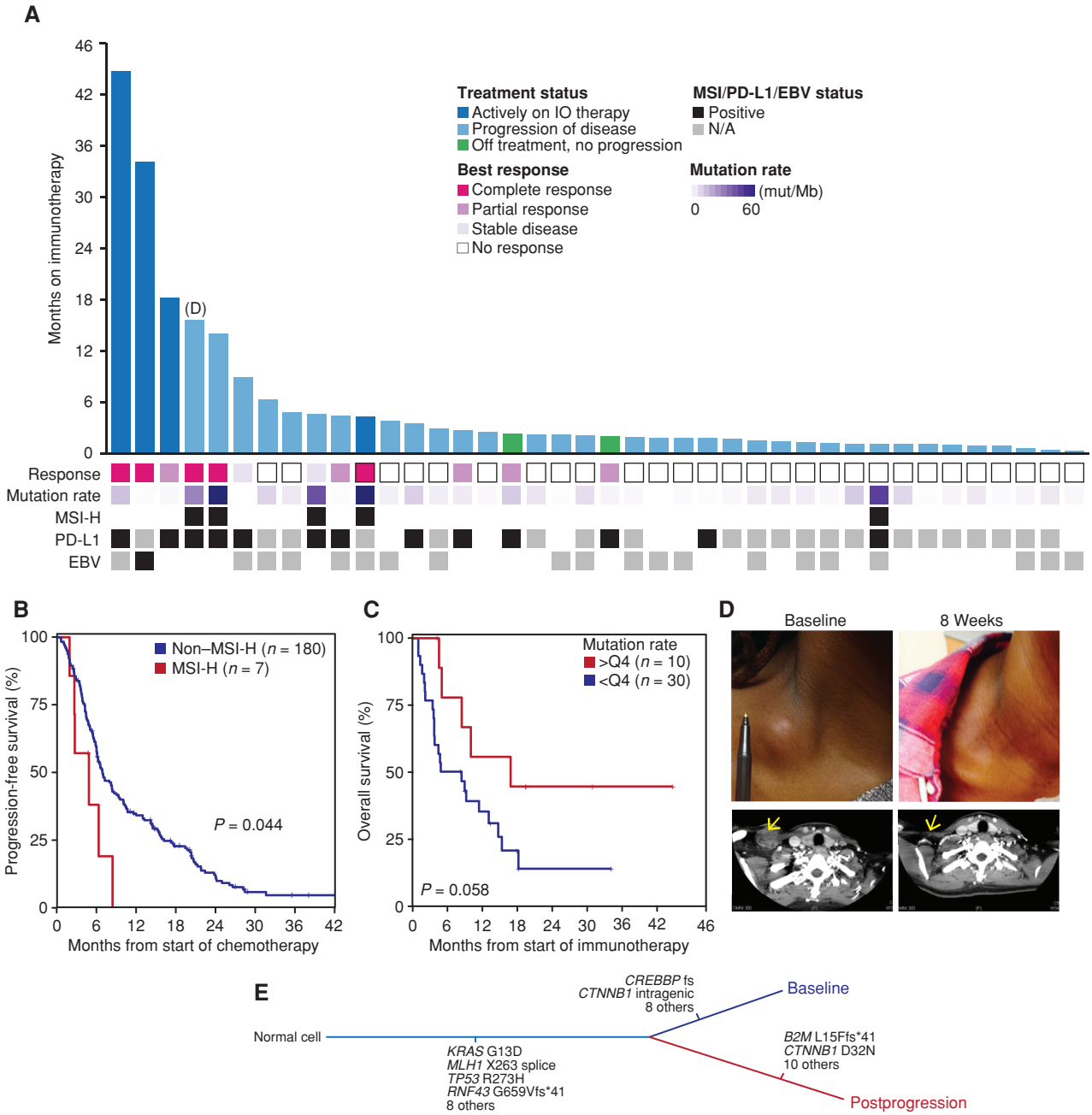


Figure 3. Genomic determinants of response to immune checkpoint inhibitors. **A,** Months on immune checkpoint inhibitors for 40 patients with metastatic, chemotherapy-refractory esophagogastric cancer. The annotation tracks below the x-axis indicate EBV and MSI status, mutational burden, and best response to immunotherapy (see legend). IO, immuno-oncology. **B,** Kaplan–Meier PFS on first-line platinum-based therapy for patients with MSI-H vs. non–MSI-H tumors, demonstrating shorter PFS and chemotherapy resistance in MSI-H esophagogastric cancers. **C,** Kaplan–Meier OS curve of patients receiving immunotherapy demonstrating favorable OS for those in the top quartile of tumor nonsynonymous mutational burden (those with >9.7 mut/Mb). **D,** Photograph and corresponding CT image showing complete response in biopsy-proven lymph-node metastases (yellow arrows) of a patient with stage IV MSI-H chemotherapy-refractory esophagogastric cancer treated with anti–PD-1 monotherapy in fourth-line setting. **E,** Genomic comparison of matched pre- and postprogression primary tumor samples from patient in **D**:12 mutations were private to the posttreatment sample, including a loss-of-function mutation in exon 1 of the *B2M* gene, which encodes β2-microglobulin.

patients. However, all 5 of these patients remain alive 19.5 to 44.7 months following initiation of immunotherapy despite prior rapid progression on standard fluoropyrimidine-, platinum-, taxane-, and irinotecan-based therapies. Of these 5 patients with durable responses to immunotherapy, 4 tumors tested positive for PD-L1, whereas 1 patient had insufficient tumor material for PD-L1 testing. Three of the 5 patients with durable immunotherapy responses had tumors with high mutational burden (59.4 mut/Mb, 28.3 mut/Mb, and 14.2 mut/Mb), and 2 of these 3 were MSI-H.

Downloaded from cancerdiscovery.aacrjournals.org on January 22, 2020. © 2018 American Association for Cancer Research.

Published OnlineFirst November 9, 2017; DOI: 10.1158/2159-8290.CD-17-0787

Overall, higher tumor mutational burden was associated with a better outcome on immunotherapy (Fig. 3C), with patients in the top quartile of tumor mutational burden (>9.7 mut/Mb) having the best outcomes (median OS 16.8 compared to 6.62 months for patients with lower mutational burdens; 2-year OS: 44% vs. 14%; HR = 0.40, log-rank test $P = 0.058$). As 2 of the 5 patients with durable outlier responses (>12 months) to immunotherapy had tumors with low mutational burden (1.9 and 3.3 mut/Mb), we explored these tumors in greater detail by performing EBV *in situ* hybridization. Notably, the outlier responder with the second longest duration on immunotherapy (>30 months and still on therapy) was EBV$^+$, the only EBV$^+$ tumor (of the 26 tested) in the cohort.

Of the 5 patients who achieved durable responses to immunotherapy lasting 12 months or longer, 2 have developed acquired resistance. One of these patients with acquired resistance to immune checkpoint blockade is highlighted in Fig. 3D. This patient had a PD-L1$^+$, MSI-H, chemotherapy-refractory tumor and achieved a complete response to anti–PD-1 monotherapy followed by disease progression in the distal esophageal tumor at 14 months. Genomic analysis of baseline and postprogression samples identified 33 somatic mutations, including 12 that were private to the posttreatment sample (Fig. 3E). Most notably, the posttreatment sample harbored a loss-of-function mutation in exon 1 of the *B2M* gene, which encodes for β2-microglobulin, loss of which was confirmed by immunohistochemistry. Mutations in *B2M* have been associated with acquired resistance to immune checkpoint blockade in melanoma (19). In the MSK cohort, 44% (4 of 9) of MSI-H tumors had likely deleterious alterations in *B2M*. Although the *B2M* mutation was acquired posttreatment in the patient highlighted in Fig. 3D, *B2M* mutations were present prior to therapy in other patients, and when present did not preclude response to checkpoint blockade.

The addition of trastuzumab to cytotoxic chemotherapy is standard of care in patients with esophagogastric cancer whose tumors overexpress HER2 protein. Of the 295 patients in the MSK cohort, 68 were HER2$^+$ based upon standard clinical criteria (IHC or FISH analysis; 44 had samples collected only pretreatment, 14 only posttreatment, 10 both pre- and posttreatment with trastuzumab). There was a strong correlation between *ERBB2* copy number as determined by sequencing and HER2 IHC/FISH (Supplementary Fig. S2). Overall, we observed a concordance rate of 93.7% between IHC/FISH and NGS, with a positive predictive value (PPV) of 90% and a negative predictive value (NPV) of 96.9%. A total of 50 patients with HER2$^+$ tumors collected before treatment received first-line trastuzumab. Of these, 92% (46/50) were *ERBB2*-amplified by NGS (ref. 20; Supplementary Table S4). Detailed analysis of the 4 discordant patients indicated that the discordance was attributed to either tumor heterogeneity for *ERBB2* amplification or equivocal IHC/FISH positivity. Additionally, the 4 patients with discordant cases exhibited significantly shorter PFS on first-line trastuzumab/chemotherapy compared with patients with *ERBB2*-amplified tumors by NGS (median PFS 5.8 vs. 14.0 months; $P = 1e{-}6$, log-rank test, Fig. 4A and B).

The level of *ERBB2* amplification by FISH has been shown to predict for sensitivity and prolonged survival with trastuzumab therapy in metastatic gastric cancer (21). Here, we also observed a strong correlation between the level of *ERBB2* amplification as quantitated by NGS and PFS on first-line trastuzumab, with patients in the top quartile of *ERBB2* amplification levels having a significantly longer PFS on trastuzumab (median PFS 24.3; Fig. 4B). Beyond *ERBB2* itself, we observed significant heterogeneity in the pattern of comutational events in the HER2$^+$ cohort. Patients with co-alterations in RTK–RAS–PI3K/AKT pathway genes had significantly shorter PFS (median PFS 8.4; Fig. 4A and B), suggesting that activation of this pathway may contribute to intrinsic trastuzumab resistance. In a multivariate analysis, *ERBB2* levels and co-alterations in the PI3K pathway independently contributed to the differences in PFS (Fig. 4C). Alterations in cell cycle–related genes, which were previously reported to be associated with less clinical benefit from trastuzumab-based therapy in an Asian population (22, 23), were not associated with response differences in the MSK cohort [median time on treatment for patients without a cell-cycle alteration was 12.2 months ($n = 23$), compared to 14.0 months for patients with a cell-cycle alteration ($n = 27$, $P = 0.11$, log-rank test)].

To identify mechanisms of acquired resistance, we analyzed matched tumors collected from individual patients both pre– and post–trastuzumab treatment. Given the small number of post–trastuzumab progression and paired samples in the prospective series, we augmented this cohort with a retrospective analysis of additional paired samples from 20 patients, assembling in total 23 matched pre- and post-trastuzumab tumor pairs. The site of clinical and radiographic disease progression determined the location of the second biopsy, with 11 biopsies obtained from the same anatomic site. Overall, the concordance between genomic alterations found in pre- and posttreatment samples was high, and most discordances were attributable to mutations found only in the posttreatment samples (Supplementary Fig. S3). In this paired sample analysis, we identified 2 patients with loss of *ERBB2* amplification and 1 patient with a focal *ERBB2* exon 16 deletion exclusively in the sample collected following disease progression on trastuzumab (Fig. 4C). In sum, in the 44 post-trastuzumab samples from patients who were HER2$^+$ by clinical IHC/FISH testing prior to treatment with trastuzumab, 7 (16%) were *ERBB2*$^-$ by targeted sequencing. HER2 IHC analysis of the postprogression samples used for NGS further confirmed that HER2 expression was either lost or significantly lower at the time of disease progression in all 7 of these patients as compared with their corresponding pretreatment samples. In 1 representative patient shown in Fig. 4D, the pre-trastuzumab tumor was IHC 3+/FISH>20 and *ERBB2* amplified by NGS, whereas the sample collected following disease progression on trastuzumab did not express HER2 protein (IHC 0) and had no evidence of *ERBB2* amplification by either FISH (FISH 1.1) or sequencing analysis (Fig. 4D); additionally, the sample had a newly acquired *PIK3CA* E545K mutation. Together, these results suggest that selection for an *ERBB2* nonamplified clone is a recurrent mechanism of trastuzumab resistance in esophagogastric cancer.

Downloaded from cancerdiscovery.aacrjournals.org on January 22, 2020. © 2018 American Association for Cancer Research.

Published OnlineFirst November 9, 2017; DOI: 10.1158/2159-8290.CD-17-0787

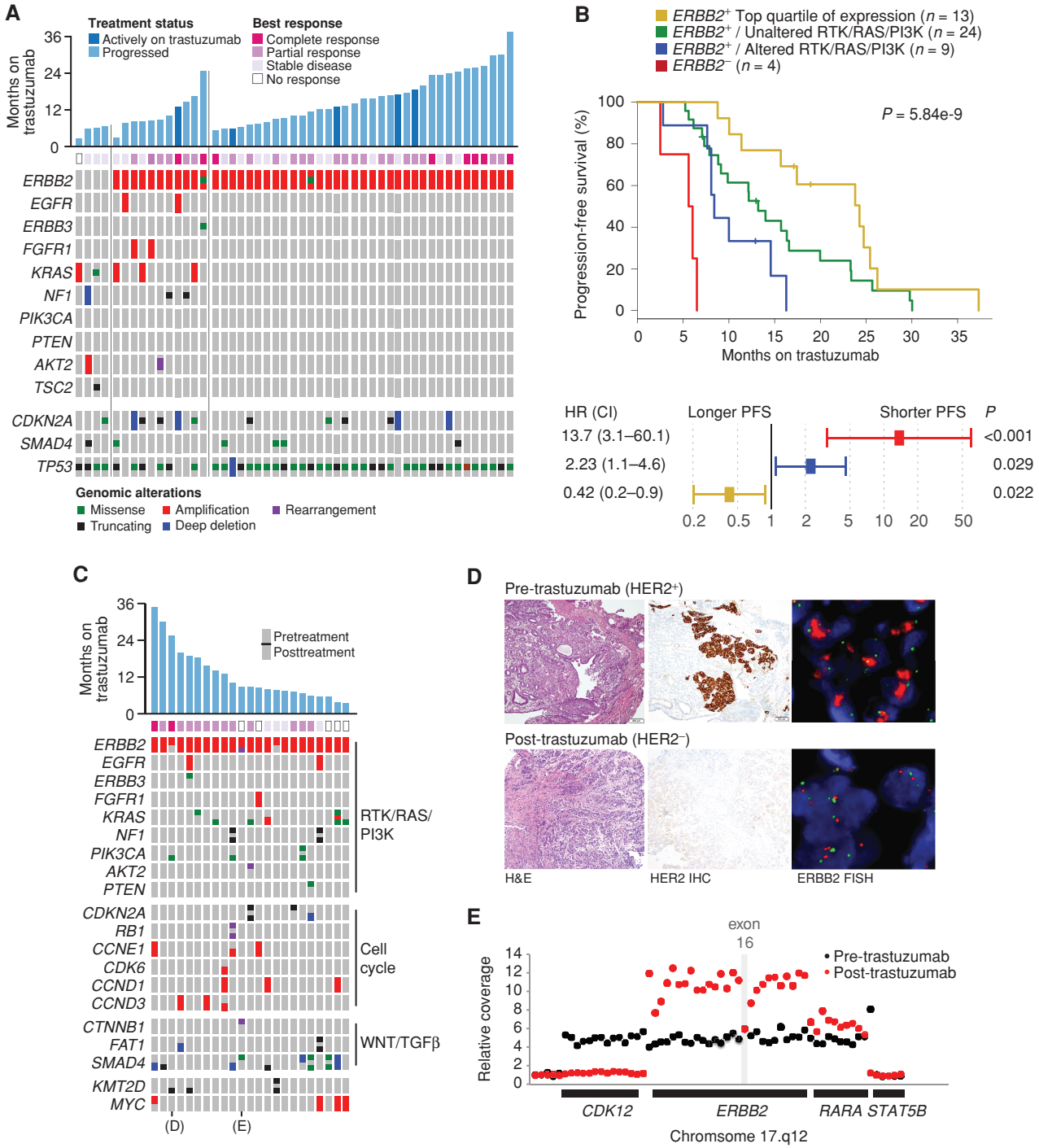


Figure 4. Intrinsic and acquired trastuzumab resistance. **A,** Duration, best response, and pretreatment genomic alterations for 50 patients with HER2+ metastatic esophagogastric cancer treated with first-line trastuzumab/chemotherapy. The first 4 tumors had no *ERBB2* amplification detected by sequencing, the next set of samples had co-alterations in the RTK/RAS/PI3K pathways, and the third set had no co-occurring alterations in these pathways. **B,** Kaplan–Meier PFS curves (top) and multivariate analysis (bottom) showing favorable outcome in patients with *ERBB2*-amplified and RTK/RAS/PI3K–wild-type tumors. Patients with tumors that were *ERBB2*− or *ERBB2* amplified and RTK/RAS/PI3K pathway–activated had significantly shorter time to progression on first-line trastuzumab therapy, and patients in the highest quartile of *ERBB2* levels as determined by sequencing had the best outcome. **C,** Analysis of somatic alterations in 23 pairs of matched pre- and post-trastuzumab samples. The oncoprint illustrates several oncogenic alterations, grouped by pathway, that are shared between or private to the paired pre- or posttreatment samples. The cells of the oncoprint are split, with the alteration status in the pre- and posttreatment samples shown in the top and bottom, respectively. **D,** A representative case illustrating loss of *ERBB2* amplification and HER2 protein expression in the posttreatment sample, confirmed by FISH and IHC, respectively. **E,** The structure of the acquired *ERBB2* exon 16 deletion in a post-trastuzumab specimen. The relative DNA-sequencing coverage is shown for each exon of *ERBB2* and the adjoining genes on chromosome 17, as well as select intragenic regions. The post-trastuzumab sample had a distinct, more focal, amplification that did not include exon 16 of *ERBB2*.

Downloaded from cancerdiscovery.aacrjournals.org on January 22, 2020. © 2018 American Association for Cancer Research.

Published OnlineFirst November 9, 2017; DOI: 10.1158/2159-8290.CD-17-0787

Among the notable somatic alterations in post-trastuzumab tumors not present in pretreatment tumors was a genomic rearrangement resulting in deletion of *ERBB2* exon 16 (Fig. 4E). This somatic alteration results in expression of the delta-16 HER2 variant, which is constitutively hyperphosphorylated compared with the wild-type isoform, and which has been shown to be resistant to anti-HER2 therapies in preclinical breast cancer models (24–26). Oncogenic comutations in *KRAS* were also identified in 1 tumor (1/50, 2%) collected prior to trastuzumab treatment and in 3 tumor samples (3/23, 13%) collected following disease progression. Similarly, known activating *PIK3CA* mutations were present in 1 (1/50, 2%) tumor collected prior to trastuzumab therapy and in 2 (2/23, 8.6%) tumors collected following disease progression. As the presence of a co-occurring alteration in the RTK/RAS/PI3K pathway in pretreatment tumors was associated with shorter time to progression on trastuzumab therapy, these results suggest that, along with secondary alterations to *ERBB2* and selection for a clone lacking *ERBB2* amplification, comutations that induce RAS or PI3K pathway activation may be mechanisms of both intrinsic and acquired resistance to trastuzumab in patients with esophagogastric cancer.

DISCUSSION

We report the largest experience with prospective NGS using a comprehensive cancer gene panel to guide therapy and identify predictive biomarkers of drug response in patients with esophagogastric cancer. We demonstrated that multiplex sequencing of tumor and matched blood samples from patients with esophagogastric cancer is efficient and permits interpretation and utilization of results in clinical practice. We generated an extensive dataset of manually reviewed mutations, copy-number alterations, and genomic rearrangements from 318 tumors from 295 patients with mature clinical annotation of treatment response and survival analyses on first-line platinum chemotherapy, trastuzumab, and immune checkpoint inhibitor therapy. All genomic and clinical data are publicly available through the cBioPortal for Cancer Genomics (refs. 27, 28; http://www.cbioportal.org/study?id=egc_msk_2017) to facilitate integration of this dataset with those generated by other institutions. Within the context of the AACR Project GENIE consortium (29), we have also committed to making all future data as part of our clinical sequencing of patients with esophagogastric cancer publicly available promptly upon data generation.

Based on FDA approval of trastuzumab and pembrolizumab, reflex *ERBB2* and MSI testing with the goal of guiding treatment selection in patients with esophagogastric cancer should now be standard practice. Among level 2 alterations identified in the MSK cohort, *BRCA1/2* alterations may have a role in identifying patients likely to respond to PARP inhibitors or platinum chemotherapies. Notably, among the potentially targetable kinase targets identified (*ERBB2, EGFR, MET, CDK4, FGFR1*), many were found to be concurrent in individual patients, suggesting that the clinical actionability of these mutations will likely depend on developing effective combination strategies.

NGS analysis identified patients with *ERBB2*-amplified or MSI-H tumors with high concordance with standard assays. Within the clinical HER2$^+$ cohort (as defined by IHC/FISH), patients with *ERBB2*-amplified, RAS/PI3K wild-type tumors derived the greatest benefit from trastuzumab-based therapy, with clinical benefit greatest in those patients with the highest levels of *ERBB2* amplification. Notably, 30% of clinical HER2$^+$ patients lacked *ERBB2* amplification by sequencing or had comutations in the RTK–RAS–PI3K pathway, and such patients had rapid disease progression and minimal benefit from trastuzumab-based therapy. *ERBB2* amplification as defined by NGS may thus be a more robust biomarker of clinically meaningful response to trastuzumab than current IHC/FISH testing. In several of the patients with HER2 discordance between FISH/IHC and NGS, discordance could be attributed to tumor heterogeneity in regard to *ERBB2* amplification. These results and the loss of *ERBB2* amplification in tumors collected postprogression on trastuzumab suggest that selection for a non–*ERBB2*-amplified clone is a common mechanism of acquired resistance to trastuzumab-based therapy in patients with esophagogastric cancer.

Patients with MSI-H tumors could be robustly identified by NGS. Our data indicate that in the metastatic setting MSI-H esophagogastric tumors are rare, but that such patients may represent a chemotherapy-refractory subset. Pembrolizumab was recently FDA approved for MSI-H tumors, irrespective of site of origin, and the data presented here suggest that immunotherapy should be considered in patients with MSI-H esophagogastric cancer early in their disease course, as such patients are unlikely to respond to cytotoxic chemotherapy. We also observed a complete and durable response (32 months and ongoing) to immune checkpoint blockade in the only patient with an EBV$^+$ tumor. This dramatic outlier response is consistent with the activity of immunotherapy in other virus-associated tumors, such as Merkel cell carcinoma (30), and suggests that routine EBV testing may aid in the prospective identification of patients with esophagogastric cancer most likely to benefit from immunotherapy.

A limitation of the current study was that the targeted capture approach used could not by definition detect alterations in genes not included in the assay design, epigenetic mechanisms of gene suppression such as promoter methylation of the *BRCA1/2* genes, or viral EBV DNA sequences. To address the latter, probes designed to capture viral DNA sequences will be included in future iterations of our clinical NGS platform. This study also highlights that tumor heterogeneity and acquisition of additional mutational events under the selective pressure of therapy is common in esophagogastric cancer. Sampling a single site of disease can never fully assess clonal complexity and tumor heterogeneity in patients with multisite metastatic disease. Therefore, circulating cell-free DNA methods capable of detecting genomic alterations present in genomically heterogeneous metastatic sites should be pursued in future studies of this disease.

Although the favorable OS we observed in the MSK cohort compared with the published literature may have been due in part to access to novel therapies such as immune checkpoint inhibitors, it also likely reflects the high proportion of patients with ECOG 0–1 functional status (90% of patients) who were thus sufficiently fit to receive second- and third-line therapies. Additional clinical factors such as a multidisciplinary approach, specialized nursing care, frequent symptom reporting, and

Downloaded from cancerdiscovery.aacrjournals.org on January 22, 2020. © 2018 American Association for Cancer Research.

Published OnlineFirst November 9, 2017; DOI: 10.1158/2159-8290.CD-17-0787

aggressive early intervention in a highly specialized practice likely further contributed to the favorable outcomes of patients with esophagogastric cancer in the MSK cohort compared with published data, and warrant future study.

In sum, the results reported here indicate that targeted sequencing methods can robustly identify established and investigational biomarkers of treatment response and drug resistance, including MSI status, *ERBB2* amplification, and others, and can potentially guide choice of therapy. Given the limited material available for genomic profiling and the high degree of genomic heterogeneity present in esophagogastric tumors, a multiplexed approach to the detection of multiple known biomarkers of response, possibly using tumor-derived cell-free DNA as input, will be needed to realize the promise of precision medicine in patients with this aggressive and often fatal disease.

METHODS

Patients with metastatic esophageal, gastric, and gastroesophageal junction adenocarcinoma receiving therapy at Memorial Sloan Kettering Cancer Center gave consent to an institutional review board–approved protocol for prospective tumor genomic profiling between February 2014 and February 2017. The studies were conducted in accordance with the Declaration of Helsinki, International Ethical Guidelines for Biomedical Research Involving Human Subjects (CIOMS), Belmont Report, or U.S. Common Rule.

All tumors were prospectively reviewed to confirm histologic subtype and Lauren classification, and to estimate tumor content. Of 376 tumors submitted for sequencing, 318 samples were included in the final analysis (see CONSORT diagram in Supplementary Fig. S4). We integrated genomic data with clinical characteristics, treatment history, response, and survival data (as of September 2017). OS time was measured from the date of diagnosis of stage IV disease until the date of death or last follow-up. PFS and OS on first-line platinum therapy and first-line chemotherapy with trastuzumab and immune checkpoint inhibitors in chemotherapy-refractory patients was calculated from the date of start of treatment to the date of radiographic disease progression, death, or last evaluation. Clinical HER2 status was based on HER2 protein expression by IHC (positive defined as 3+) or *ERBB2* gene amplification by FISH using College of American Pathologists (CAP)/American Society of Clinical Oncology (ASCO) criteria. IHC analysis of mismatch repair proteins, and beta 2 microglobulin (B2M), and Epstein–Barr encoding region *in situ* hybridization analysis was performed on a subset of tumors from patients treated with checkpoint inhibitors.

The MSK-IMPACT assay was performed in a Clinical Laboratory Improvement Amendments (CLIA)–certified laboratory, initially using a 341-gene panel and more recently 410- and 468-gene panels (Supplementary Table S5), as previously described, with results reported in the electronic medical record (12, 31). The assay is capable of detecting mutations, small insertions and deletions, copy-number alterations, and select structural rearrangements. In a previously published validation set, *ERBB2* amplification calls on this NGS assay had an overall concordance of 98.4% with the combined IHC/FISH results (20). The PPV and NPV of our NGS assay with respect to HER2 IHC/FISH were calculated in this cohort.

Tumors were assigned to consensus TCGA molecular subtypes: CIN, GS, EBV, and MSI-H (3). We assessed tumors for MSI using the MSIsensor method, and samples with a score ≥10 were classified as MSI-H. Tumors were characterized as GS if the fraction of the autosomal genome affected by DNA copy-number alterations of any kind (FGA) was less than 5%. We classified tumors that were neither EBV^+, MSI, or GS as CIN (chromosomal instability). The OncoKB Precision Oncology Knowledge Base was used (data from May 2017; ref. 14) to infer the oncogenic effect and clinical actionability of individual somatic mutations. Recurrent mutational hotspots were annotated using cancerhotspots.org (32). We inferred allele-specific DNA copy number using FACETS (33) to determine the zygosity of key mutant tumor suppressors as well as to generate estimates of tumor purity. We also inferred LST scores (34), based on the copy-number data, from tumors with an analytically estimated tumor purity greater than 20%. Samples with <20% tumor content were excluded from the analysis.

Disclosure of Potential Conflicts of Interest

Y.Y. Janjigian reports receiving commercial research grants from Boehringer Ingelheim, Bayer, Genentech/Roche, Bristol-Myers Squibb, Eli Lilly, and Merck, and is a consultant/advisory board member for Merck Serono, Bristol-Myers Squibb, Eli Lilly, Pfizer, and Merck. V.W. Rusch reports receiving commercial research support from Genelux, Inc. and is a consultant/advisory board member for Bristol-Myers Squibb. D. Molena has received honoraria from the speakers bureau of Novadaq. R.D.M. Hyman reports receiving commercial research grants from Puma Biotechnology, AstraZeneca, and Loxo Oncology, and is a consultant/advisory board member for Atara Biotherapeutics, AstraZeneca, Boehringer Ingelheim, CytomX, and Chugai. D.B. Solit has received honoraria from the speakers bureaus of Pfizer and Loxo Oncology. No potential conflicts of interest were disclosed by the other authors.

Authors' Contributions

Conception and design: Y.Y. Janjigian, V.E. Strong, M.E. Robson, N. Rosen, L. Tang, B.S. Taylor, D.B. Solit, N. Schultz

Development of methodology: Y.Y. Janjigian, J.F. Hechtman, J. Gao, L. Zhang, J. Shia, A. Zehir, M. Ladanyi, N. Rosen, L. Tang, B.S. Taylor, D.B. Solit, N. Schultz

Acquisition of data (provided animals, acquired and managed patients, provided facilities, etc.): Y.Y. Janjigian, G.Y. Ku, E. Vakiani, D.P. Kelsen, L. Zhang, M. Schattner, D.G. Coit, V.W. Rusch, D.R. Jones, D. Molena, J. Shia, M.E. Robson, A. Zehir, M. Ladanyi, L. Tang, D.B. Solit

Analysis and interpretation of data (e.g., statistical analysis, biostatistics, computational analysis): Y.Y. Janjigian, F. Sanchez-Vega, P. Jonsson, W.K. Chatila, J.F. Hechtman, J.C. Riches, E. Vakiani, L. Zhang, D.G. Coit, M. Bains, Z.K. Stadler, M. Capanu, S. Middha, A. Zehir, D.M. Hyman, M. Scaltriti, N. Rosen, D.H. Ilson, M.F. Berger, B.S. Taylor, D.B. Solit, N. Schultz

Writing, review, and/or revision of the manuscript: Y.Y. Janjigian, F. Sanchez-Vega, P. Jonsson, W.K. Chatila, G.Y. Ku, J.C. Riches, J. Gao, D.P. Kelsen, L. Zhang, V.E. Strong, D.G. Coit, Z.K. Stadler, V.W. Rusch, D.R. Jones, J. Shia, M.E. Robson, S. Middha, A. Zehir, D.M. Hyman, M. Scaltriti, M. Ladanyi, N. Rosen, M.F. Berger, L. Tang, B.S. Taylor, D.B. Solit, N. Schultz

Administrative, technical, or material support (i.e., reporting or organizing data, constructing databases): Y.Y. Janjigian, F. Sanchez-Vega, W.K. Chatila, Y. Tuvy, R. Kundra, N. Bouvier, Z.J. Heins, B.E. Gross, D.G. Coit, D.M. Hyman, D.B. Solit

Study supervision: Y.Y. Janjigian, F. Sanchez-Vega, V.E. Strong, D.B. Solit, N. Schultz

Other (obtained study biopsies and specimen): H. Gerdes

Acknowledgments

This study was supported by 2013 Conquer Cancer Foundation ASCO Career Development Award (Y.Y. Janjigian), Cycle for Survival Award (Y.Y. Janjigian and N. Schultz), the Department of Defense Congressionally Directed Medical Research Program CA 150646 (Y.Y. Janjigian), the Marie-Josée and Henry R. Kravis Center for Molecular Oncology, a National Cancer Institute Cancer Center Core Grant (P30-CA008748), the Robertson Foundation (B.S. Taylor and

Downloaded from cancerdiscovery.aacrjournals.org on January 22, 2020. © 2018 American Association for Cancer Research.

Published OnlineFirst November 9, 2017; DOI: 10.1158/2159-8290.CD-17-0787

N. Schultz), and the Center for Metastasis Research of the Sloan Kettering Institute (F. Sanchez-Vega).

Received July 24, 2017; revised October 20, 2017; accepted November 6, 2017; published OnlineFirst November 9, 2017.

REFERENCES

1. Siegel RL, Miller KD, Jemal A. Cancer Statistics, 2017. CA Cancer J Clin 2017;67:7–30.
2. Cancer Genome Atlas Research Network, Analysis Working Group: Asan University, BC Cancer Agency, Brigham and Women's Hospital, Broad Institute, Brown University, et al. Integrated genomic characterization of oesophageal carcinoma. Nature 2017;541:169–75.
3. Cancer Genome Atlas Research Network. Comprehensive molecular characterization of gastric adenocarcinoma. Nature 2014;513:202–9.
4. Cristescu R, Lee J, Nebozhyn M, Kim K-M, Ting JC, Wong SS, et al. Molecular analysis of gastric cancer identifies subtypes associated with distinct clinical outcomes. Nat Med 2015;21:449–56.
5. Secrier M, Li X, de Silva N, Eldridge MD, Contino G, Bornschein J, et al. Mutational signatures in esophageal adenocarcinoma define etiologically distinct subgroups with therapeutic relevance. Nat Genet 2016;48:1131–41.
6. Elimova E, Janjigian YY, Mulcahy M, Catenacci DV, Blum MA, Almhanna K, et al. It is time to stop using epirubicin to treat any patient with gastroesophageal adenocarcinoma. J Clin Oncol 2017;35:475–7.
7. Bang Y-J, Van Cutsem E, Feyereislova A, Chung HC, Shen L, Sawaki A, et al. Trastuzumab in combination with chemotherapy versus chemotherapy alone for treatment of HER2-positive advanced gastric or gastro-oesophageal junction cancer (ToGA): a phase 3, open-label, randomised controlled trial. Lancet 2010;376:687–97.
8. Muro K, Chung HC, Shankaran V, Geva R, Catenacci D, Gupta S, et al. Pembrolizumab for patients with PD-L1-positive advanced gastric cancer (KEYNOTE-012): a multicentre, open-label, phase 1b trial. Lancet Oncol 2016;17:717–26.
9. Le DT, Uram JN, Wang H, Bartlett BR, Kemberling H, Eyring AD, et al. PD-1 blockade in tumors with mismatch-repair deficiency. New Engl J Med 2015;372:2509–20.
10. Fuchs CS, Doi T, Jang RW-J, Muro K, Satoh T, Machado M, et al. KEYNOTE-059 cohort 1: efficacy and safety of pembrolizumab (pembro) monotherapy in patients with previously treated advanced gastric cancer. J Clin Oncol 2017;35:4003.
11. Kang Y-K, Boku N, Satoh T, Ryu M-H, Chao Y, Kato K, et al. Nivolumab in patients with advanced gastric or gastro-oesophageal junction cancer refractory to, or intolerant of, at least two previous chemotherapy regimens (ONO-4538-12, ATTRACTION-2): a randomised, double-blind, placebo-controlled, phase 3 trial. Lancet 2017; DOI: http://dx.doi.org/10.1016/S0140-6736(17)31827–5.
12. Zehir A, Benayed R, Shah RH, Syed A, Middha S, Kim HR, et al. Mutational landscape of metastatic cancer revealed from prospective clinical sequencing of 10,000 patients. Nat Med 2017;23:703–13.
13. Niu B, Ye K, Zhang Q, Lu C, Xie M, McLellan MD, et al. MSIsensor: microsatellite instability detection using paired tumor-normal sequence data. Bioinforma 2014;30:1015–6.
14. Chakravarty D, Gao J, Phillips SM, Kundra R, Zhang H, Wang J, et al. OncoKB: a precision oncology knowledge base. JCO Precis Oncol 2017. doi: 10.1200/PO.17.00011.
15. Ohtsu A, Shah MA, Van Cutsem E, Rha SY, Sawaki A, Park SR, et al. Bevacizumab in combination with chemotherapy as first-line therapy in advanced gastric cancer: a randomized, double-blind, placebo-controlled phase III study. J Clin Oncol 2011;29:3968–76.
16. Mirza MR, Monk BJ, Herrstedt J, Oza AM, Mahner S, Redondo A, et al. Niraparib maintenance therapy in platinum-sensitive, recurrent ovarian cancer. N Engl J Med 2016;375:2154–64.
17. Telli ML, Timms KM, Reid J, Hennessy B, Mills GB, Jensen KC, et al. Homologous recombination deficiency (HRD) score predicts response to platinum-containing neoadjuvant chemotherapy in patients with triple-negative breast cancer. Clin Cancer Res 2016;22:3764–73.
18. Smyth EC, Wotherspoon A, Peckitt C, Gonzalez D, Hulkki-Wilson S, Eltahir Z, et al. Mismatch repair deficiency, microsatellite instability, and survival: an exploratory analysis of the medical research council adjuvant gastric infusional chemotherapy (MAGIC) trial. JAMA Oncol 2017;3:1197–203.
19. Zaretsky JM, Garcia-Diaz A, Shin DS, Escuin-Ordinas H, Hugo W, Hu-Lieskovan S, et al. Mutations associated with acquired resistance to PD-1 blockade in melanoma. N Engl J Med 2016;375:819–29.
20. Ross DS, Zehir A, Cheng DT, Benayed R, Nafa K, Hechtman JF, et al. Next-generation assessment of human epidermal growth factor receptor 2 (ERBB2) amplification status: clinical validation in the context of a hybrid capture-based, comprehensive solid tumor genomic profiling assay. J Mol Diagn 2017;19:244–54.
21. Gomez-Martin C, Plaza JC, Pazo-Cid R, Salud A, Pons F, Fonseca P, et al. Level of HER2 gene amplification predicts response and overall survival in HER2-positive advanced gastric cancer treated with trastuzumab. J Clin Oncol 2013;31:4445–52.
22. Lee JY, Hong M, Kim ST, Park SH, Kang WK, Kim K-M, et al. The impact of concomitant genomic alterations on treatment outcome for trastuzumab therapy in HER2-positive gastric cancer. Sci Rep 2015;5:9289.
23. Kim J, Fox C, Peng S, Pusung M, Pectasides E, Matthee E, et al. Preexisting oncogenic events impact trastuzumab sensitivity in ERBB2-amplified gastroesophageal adenocarcinoma. J Clin Invest 2014;124:5145–58.
24. Castiglioni F, Tagliabue E, Campiglio M, Pupa SM, Balsari A, Ménard S. Role of exon-16-deleted HER2 in breast carcinomas. Endocr Relat Cancer 2006;13:221–32.
25. Turpin J, Ling C, Crosby EJ, Hartman ZC, Simond AM, Chodosh LA, et al. The ErbB2ΔEx16 splice variant is a major oncogenic driver in breast cancer that promotes a pro-metastatic tumor microenvironment. Oncogene 2016;35:6053–64.
26. Tagliabue E, Campiglio M, Pupa SM, Balsari A, Ménard S. The HER2 World: better treatment selection for better outcome. J Natl Cancer Inst Monogr 2009;2011:82–5.
27. Cerami E, Gao J, Dogrusoz U, Gross BE, Sumer SO, Aksoy BA, et al. The cBio cancer genomics portal: an open platform for exploring multidimensional cancer genomics data. Cancer Discov 2012;2:401–4.
28. Gao J, Aksoy BA, Dogrusoz U, Dresdner G, Gross B, Sumer SO, et al. Integrative analysis of complex cancer genomics and clinical profiles using the cBioPortal. Sci Signal 2013;6:pl1.
29. AACR Project GENIE Consortium. AACR project GENIE: powering precision medicine through an international consortium. Cancer Discov 2017;7:818–31.
30. Gulley JL, Rajan A, Spigel DR, Iannotti N, Chandler J, Wong DJL, et al. Avelumab for patients with previously treated metastatic or recurrent non-small-cell lung cancer (JAVELIN Solid Tumor): dose-expansion cohort of a multicentre, open-label, phase 1b trial. Lancet Oncol 2017;18:599–610.
31. Cheng DT, Mitchell TN, Zehir A, Shah RH, Benayed R, Syed A, et al. Memorial sloan kettering-integrated mutation profiling of actionable cancer targets (MSK-IMPACT): a hybridization capture-based next-generation sequencing clinical assay for solid tumor molecular oncology. J Mol Diagn 2015;17:251–64.
32. Chang MT, Asthana S, Gao SP, Lee BH, Chapman JS, Kandoth C, et al. Identifying recurrent mutations in cancer reveals widespread lineage diversity and mutational specificity. Nat Biotechnol 2016;34:155–63.
33. Shen R, Seshan VE. FACETS: allele-specific copy number and clonal heterogeneity analysis tool for high-throughput DNA sequencing. Nucleic Acids Res 2016;44:e131.
34. Marquard AM, Eklund AC, Joshi T, Krzystanek M, Favero F, Wang ZC, et al. Pan-cancer analysis of genomic scar signatures associated with homologous recombination deficiency suggests novel indications for existing cancer drugs. Biomark Res 2015;3:9.

Downloaded from cancerdiscovery.aacrjournals.org on January 22, 2020. © 2018 American Association for Cancer Research.

Published OnlineFirst November 9, 2017; DOI: 10.1158/2159-8290.CD-17-0787

AACR American Association for Cancer Research

CANCER DISCOVERY

Genetic Predictors of Response to Systemic Therapy in Esophagogastric Cancer

Yelena Y. Janjigian, Francisco Sanchez-Vega, Philip Jonsson, et al.

Cancer Discov 2018;8:49-58. Published OnlineFirst November 9, 2017.

Updated version	Access the most recent version of this article at: doi:10.1158/2159-8290.CD-17-0787
Supplementary Material	Access the most recent supplemental material at: http://cancerdiscovery.aacrjournals.org/content/suppl/2017/11/09/2159-8290.CD-17-0787.DC1

Cited articles	This article cites 32 articles, 7 of which you can access for free at: http://cancerdiscovery.aacrjournals.org/content/8/1/49.full#ref-list-1
Citing articles	This article has been cited by 16 HighWire-hosted articles. Access the articles at: http://cancerdiscovery.aacrjournals.org/content/8/1/49.full#related-urls

E-mail alerts	Sign up to receive free email-alerts related to this article or journal.
Reprints and Subscriptions	To order reprints of this article or to subscribe to the journal, contact the AACR Publications Department at pubs@aacr.org.
Permissions	To request permission to re-use all or part of this article, use this link http://cancerdiscovery.aacrjournals.org/content/8/1/49. Click on "Request Permissions" which will take you to the Copyright Clearance Center's (CCC) Rightslink site.

Downloaded from cancerdiscovery.aacrjournals.org on January 22, 2020. © 2018 American Association for Cancer Research.

Published OnlineFirst November 21, 2018; DOI: 10.1158/2159-8290.CD-18-0598

RESEARCH BRIEF

EGFR and *MET* Amplifications Determine Response to HER2 Inhibition in *ERBB2*-Amplified Esophagogastric Cancer

Francisco Sanchez-Vega[1,2], Jaclyn F. Hechtman[3], Pau Castel[2], Geoffrey Y. Ku[4], Yaelle Tuvy[4], Helen Won[1], Christopher J. Fong[1,2], Nancy Bouvier[1], Gouri J. Nanjangud[5], Joanne Soong[3], Efsevia Vakiani[3], Mark Schattner[4], David P. Kelsen[4], Robert A. Lefkowitz[6], Karen Brown[6], Mario E. Lacouture[4], Marinela Capanu[7], Marissa Mattar[8], Besnik Qeriqi[8], Fabiola Cecchi[9], Yuan Tian[9], Todd Hembrough[9], Rebecca J. Nagy[10], Richard B. Lanman[10], Steven M. Larson[6], Neeta Pandit-Taskar[6], Heiko Schöder[6], Christine A. Iacobuzio-Donahue[3], David H. Ilson[4], Wolfgang A. Weber[6], Michael F. Berger[1,2,3], Elisa de Stanchina[8], Barry S. Taylor[1,2,7], Jason S. Lewis[6], David B. Solit[1,2,4], Jorge A. Carrasquillo[6], Maurizio Scaltriti[2,3], Nikolaus Schultz[1,2,7], and Yelena Y. Janjigian[4]

ABSTRACT

The anti-HER2 antibody trastuzumab is standard care for advanced esophagogastric (EG) cancer with *ERBB2* (HER2) amplification or overexpression, but intrinsic and acquired resistance are common. We conducted a phase II study of afatinib, an irreversible pan-HER kinase inhibitor, in trastuzumab-resistant EG cancer. We analyzed pretreatment tumor biopsies and, in select cases, performed comprehensive characterization of postmortem metastatic specimens following acquisition of drug resistance. Afatinib response was associated with coamplification of *EGFR* and *ERBB2*. Heterogeneous ^{89}Zr-trastuzumab PET uptake was associated with genomic heterogeneity and mixed clinical response to afatinib. Resistance to afatinib was associated with selection for tumor cells lacking *EGFR* amplification or with acquisition of *MET* amplification, which could be detected in plasma cell-free DNA. The combination of afatinib and a MET inhibitor induced complete tumor regression in *ERBB2* and *MET* coamplified patient-derived xenograft models established from a metastatic lesion progressing on afatinib. Collectively, differential intrapatient and interpatient expression of HER2, EGFR, and MET may determine clinical response to HER kinase inhibitors in *ERBB2*-amplified EG cancer.

SIGNIFICANCE: Analysis of patients with *ERBB2*-amplified, trastuzumab-resistant EG cancer who were treated with the HER kinase inhibitor afatinib revealed that sensitivity and resistance to therapy were associated with *EGFR*/*ERBB2* coamplification and *MET* amplification, respectively. HER2-directed PET imaging and cell-free DNA sequencing could help guide strategies to overcome the emergence of resistant clones.

See related commentary by Klempner and Catenacci, p. 166.

[1]Marie-Josée and Henry R. Kravis Center for Molecular Oncology, Memorial Sloan Kettering Cancer Center, New York, New York. [2]Human Oncology and Pathogenesis Program, Memorial Sloan Kettering Cancer Center, New York, New York. [3]Department of Pathology, Memorial Sloan Kettering Cancer Center, New York, New York. [4]Department of Medicine, Memorial Sloan Kettering Cancer Center and Weill Cornell Medical College, New York, New York. [5]Molecular Cytogenetics Core Facility, Memorial Sloan Kettering Cancer Center, New York, New York. [6]Department of Radiology, Memorial Sloan Kettering Cancer Center, New York, New York. [7]Department of Epidemiology and Biostatistics, Memorial Sloan Kettering Cancer Center, New York, New York. [8]Antitumor Assessment Core Facility, Molecular Pharmacology Program, Memorial Sloan Kettering Cancer Center, New York, New York. [9]NantOmics, Rockville, Maryland. [10]Guardant Health, Inc., Redwood City, California.

Note: Supplementary data for this article are available at Cancer Discovery Online (http://cancerdiscovery.aacrjournals.org/).

Current address for P. Castel: Helen Diller Family Comprehensive Cancer Center, University of California, San Francisco, California; and current address for W.A. Weber: Department of Nuclear Medicine, Technical University Munich, Germany.

J.A. Carrasquillo, M. Scaltriti, N. Schultz, and Y.Y. Janjigian contributed equally to this article.

Corresponding Author: Yelena Y. Janjigian, Memorial Sloan Kettering Cancer Center and Weill Cornell Medical College, Division of Solid Tumor Oncology, 300 E 66th Street, Room 1033, New York, NY 10065. Phone: 646-888-4186; Fax: 646-888-4256; E-mail: janjigiy@mskcc.org

doi: 10.1158/2159-8290.CD-18-0598

©2018 American Association for Cancer Research.

Downloaded from cancerdiscovery.aacrjournals.org on January 22, 2020. © 2019 American Association for Cancer Research.

Published OnlineFirst November 21, 2018; DOI: 10.1158/2159-8290.CD-18-0598

INTRODUCTION

Esophagogastric (EG) cancer represents a substantial global health burden, with over a million patients diagnosed worldwide each year (1). The incidence of EG cancer is rising in developing countries, particularly in younger people (2). Up to 30% of EG tumors harbor *ERBB2*/HER2 amplification or overexpression (3–7). For these patients, trastuzumab (a HER2-directed antibody) improves survival when combined with first-line chemotherapy (3).

Although trastuzumab improves survival in patients with *ERBB2*-amplified EG cancer, disease progression typically still occurs within a year (3, 8). Therefore, novel treatment approaches are urgently needed for trastuzumab-resistant EG cancer. Unfortunately, the combination of trastuzumab and pertuzumab, an antibody that inhibits HER2 dimer formation, failed to improve survival in this population (9). Furthermore, neither lapatinib (a reversible EGFR/HER2 kinase inhibitor) nor trastuzumab emtansine (T-DM1, an antibody–drug conjugate consisting of trastuzumab linked to the cytotoxic agent DM1) were effective in patients with trastuzumab-refractory EG cancer (10, 11). However, improved outcomes were observed in subsets of patients with high tumor HER2 expression or *ERBB2* amplification detectable in plasma cell-free DNA (cfDNA) treated with lapatinib plus chemotherapy (11, 12). Resistance to lapatinib therapy has been associated with reactivation of EGFR and HER3 kinases (13, 14), and the irreversible pan-HER kinase inhibitor afatinib blocks HER2 (14 nmol/L), EGFR (0.5 nmol/L), as well as HER4 (1 nmol/L) kinase reactivation and can induce durable tumor regression in preclinical models of *ERBB2*-amplified EG cancer (14–17). Dual blockade with trastuzumab and lapatinib has also been shown to induce prolonged inhibition of HER3 and EGFR (14), mirroring the effect of single-agent afatinib, providing a rationale for combining HER2-directed therapies, an approach that is effective in patients with *ERBB2*-amplified breast cancer (18).

Building on these prior clinical and laboratory observations, we conducted a phase II study to determine the efficacy and safety of afatinib and afatinib/trastuzumab in patients with trastuzumab-refractory *ERBB2*-amplified EG cancer. Genomic analysis of tumor samples collected before treatment and at disease progression as well as functional imaging with ^{89}Zr-trastuzumab PET uncovered potential determinants of sensitivity and resistance to therapy. Moreover, in select patients who initially responded to afatinib but later progressed on therapy, we performed research autopsies to allow for analysis of multiple metastatic disease sites in order to explore the molecular basis for heterogeneous responses to afatinib.

RESULTS

Study Design and Summary of Clinical Outcomes

Patients were enrolled between March 2012 and April 2016. Eligible patients had a diagnosis of HER2-positive (IHC 3+, HER2:CEP17 FISH ratio ≥ 2.0) metastatic esophageal, gastroesophageal (GE) junction, or gastric adenocarcinoma with disease progression on at least one trastuzumab-containing regimen. Other inclusion criteria included RECIST 1.1 measurable disease, adequate performance status, and organ function. After the first 10 patients were enrolled, we noted that loss of HER2 was a potential mechanism of trastuzumab resistance (8), and thus the protocol eligibility was amended to mandate confirmation of HER2-positive status by IHC 3+, HER2:CEP17 FISH ratio ≥ 2.0, or next-generation sequencing (NGS) through analysis of a tumor sample collected following progression on trastuzumab and prior to afatinib therapy. In 3 patients treated with afatinib monotherapy (patients 4, 13, and 17), HER2 status following trastuzumab resistance could not be established because the repeat biopsy yielded inadequate tumor content (HER2 assessment details for each patient are provided in Supplementary Table S1). Dose reductions, management of toxicity, and criteria for treatment discontinuation are summarized in Supplementary Methods. Afatinib monotherapy was well tolerated, with diarrhea and skin rash the most common treatment-related adverse events. Grade 2 diarrhea requiring dose reductions was observed in 42% of patients treated with afatinib/trastuzumab despite the prophylactic use of loperamide. A more detailed summary of the adverse effects of afatinib and afatinib/trastuzumab is available in Supplementary Table S2. Detailed clinical information for all patients and tumor samples is given in Supplementary Table S3.

Twenty patients were treated with afatinib monotherapy administered orally at a dose of 40 mg daily. Five of these patients (25%) had tumor reduction according to RECIST 1.1 criteria (Fig. 1A). However, because of the short duration of response in some patients, the RECIST 1.1 objective partial response rate was only 10% (2 of 20 patients). The median progression-free survival was 2 months (95% CI, 1.8–3.51 months), with 3 patients (15%) progression-free at 4 months (95% CI, 3%–33%). Median overall survival for patients treated with afatinib was 7 months (95% CI, 3–11 months).

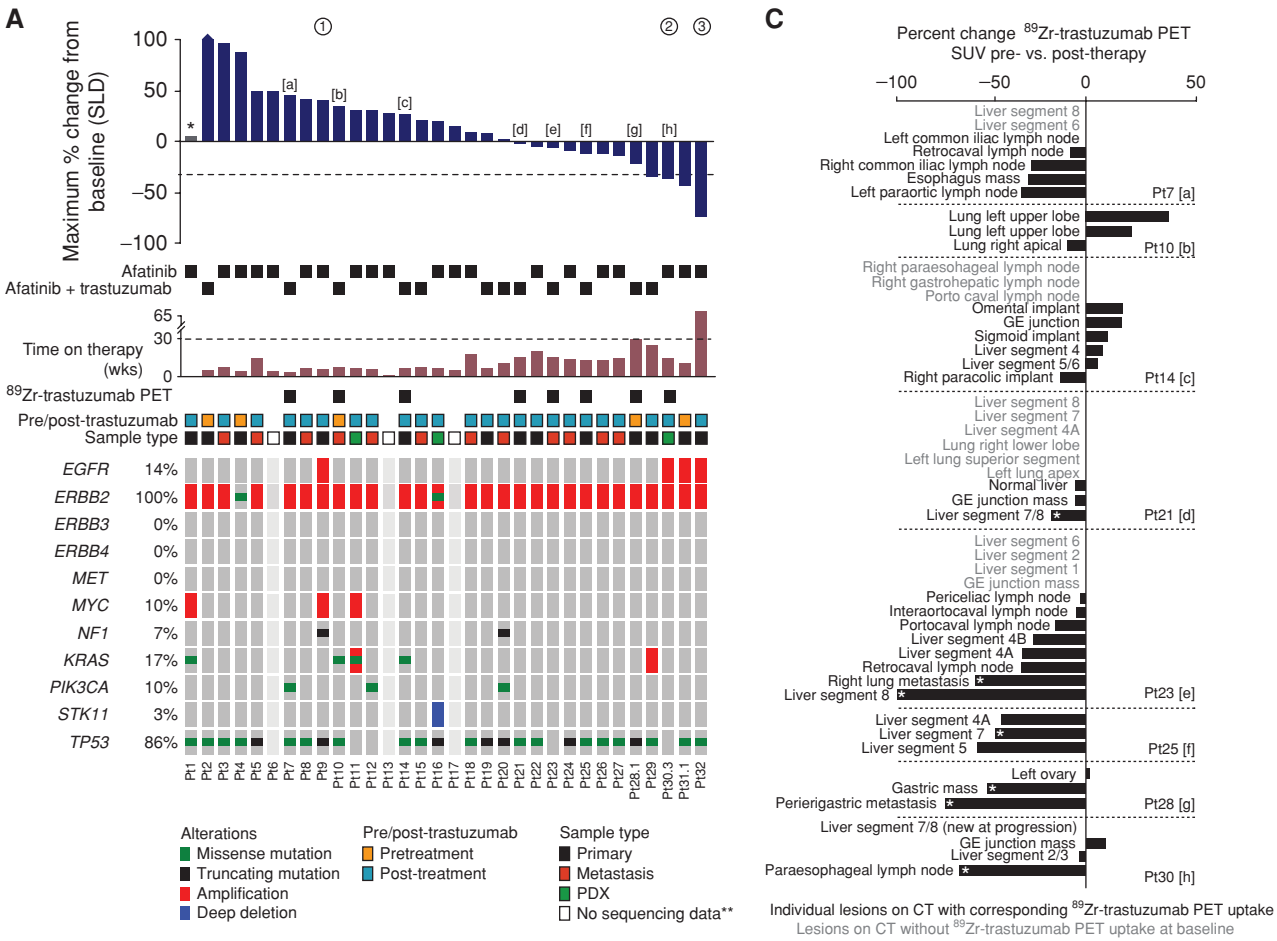
Given the modest clinical benefit of afatinib monotherapy and preclinical data in patient-derived xenograft (PDX) models suggesting greater efficacy with a HER kinase inhibitor/trastuzumab combination (13–15), a second cohort of 12 patients was treated with afatinib 30 mg daily in combination with trastuzumab 4 mg/kg every 2 weeks. One patient (8%) treated with the afatinib/trastuzumab combination achieved a RECIST 1.1 partial response, and 2 (17%) had disease control for ≥ 4 months (95% CI, 2.6%–41.3%). This was a heavily pretreated population. Across the afatinib and afatinib/trastuzumab cohorts, 75% and 33% of patients, respectively, had progressed on 2 or more trastuzumab-based combination therapies prior to study enrollment (see baseline patient characteristics in Supplementary Table S4 and prior treatment details in Supplementary Table S5).

Tumor Regression on Afatinib Is Associated with Coamplification of *ERBB2* and *EGFR*

To identify molecular determinants of afatinib response, we performed biopsies after trastuzumab therapy but prior to initiation of afatinib or afatinib/trastuzumab in all patients. Only 24 of 32 post-trastuzumab progression biopsies (75%) yielded sufficient tumor material for genomic analysis (Fig. 1A), highlighting the logistic challenges associated with tumor genomic characterization in patients with advanced EG cancer.

Downloaded from cancerdiscovery.aacrjournals.org on January 22, 2020. © 2019 American Association for Cancer Research.

Published OnlineFirst November 21, 2018; DOI: 10.1158/2159-8290.CD-18-0598



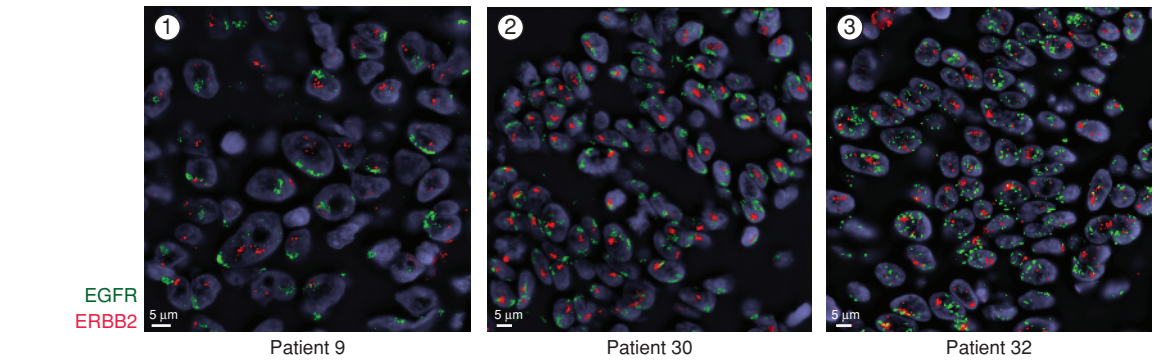


Figure 1. Individual treatment outcomes of 20 patients treated with afatinib and 12 patients treated with afatinib and trastuzumab. **A,** Percentage best change from baseline in the target lesion assessed by RECIST 1.1. Relevant clinical features (time on therapy, type of sequenced sample, and collection time point of the sequenced sample) plus key genomic alterations in sequenced samples are shown for each patient. SLD, sum of longest diameter on CT scan. Pt1 to Pt32 are IDs for all the patients in the study. For patients with multiple sequenced samples, the sample included in the oncoprint is designed after a decimal. *, Nonevaluable. **, Sample uninformative due to low tumor content. **B,** Dual probe *EGFR* and *ERBB2* FISH from patients 9, 30, and 32, all of which were collected prior to protocol treatment, demonstrated diffuse and uniform *ERBB2* and *EGFR* coamplification in virtually all tumor cells. There was no additional tissue for dual probe FISH for patient 31. **C,** Percent change in ^{89}Zr-trastuzumab PET SUV pre- versus post-therapy for each individual lesion on CT in 1 patient treated with afatinib monotherapy and 7 patients treated with afatinib/trastuzumab. White stars inside the bar plots denote lesions with resolution of uptake to baseline SUV.

Downloaded from cancerdiscovery.aacrjournals.org on January 22, 2020. © 2019 American Association for Cancer Research.

Published OnlineFirst November 21, 2018; DOI: 10.1158/2159-8290.CD-18-0598

For 5 of the remaining 8 patients (63%), pre-trastuzumab tumor biopsies yielded sufficient tumor material for genomic analysis (Fig. 1A). Tumors were analyzed using the MSK-IMPACT assay, a capture-based NGS platform that detects mutations, copy-number alterations, and select rearrangements in up to 468 cancer-associated genes (see Methods; refs. 19, 20). The OncoKB knowledge base was used to distinguish alterations with known functional relevance from variants of unknown significance (21). Notably, the 3 patients with the highest percentage tumor regression on afatinib (patients 30, 31, and 32) had coamplification of *ERBB2* and *EGFR* (mean RECIST 1.1 percent change from baseline of −29% vs. +24%; $P = 0.025$, one-sided Wilcoxon rank-sum test; Fig. 1A; Supplementary Table S6). Using dual probe FISH, we confirmed that the *EGFR* and *ERBB2* coamplifications detected by NGS of bulk tumor were the result of concurrent amplification of both genes in the same tumor cells (Fig. 1B; Supplementary Fig. S1). Patients whose tumors harbored *KRAS* (14%), *PIK3CA* (10%), or *NF1* (7%) mutations had rapid disease progression on afatinib monotherapy (Fig. 1A). These data are consistent with prior results demonstrating that mutations in the RAS and PI3K pathways are associated with trastuzumab resistance in *ERBB2*-amplified EG cancer (8, 12, 22–25). *MYC* amplification, although identified in only 3 patients, was associated with a lower likelihood of RECIST response ($P = 0.04$, one-sided Wilcoxon rank-sum test; Fig. 1A).

Patient 9 was the only nonresponder with *EGFR/ERBB2* coamplification. However, afatinib resistance in this case may be explained by co-occurrence of *MYC* amplification and a truncating mutation in *NF1* (Fig. 1A). Furthermore, we noticed that EGFR amplification and expression, by dual probe FISH and selected reaction monitoring–mass spectrometry (SRM-MS), respectively, was lower in that patient compared with the responders. The combination of afatinib and trastuzumab did not show greater clinical activity. As was observed in the afatinib monotherapy cohort, patients with comutations in the RAS or PI3 kinase pathways experienced rapid disease progression on afatinib/trastuzumab therapy (Fig. 1A).

Homogenous ^{89}Zr-Trastuzumab Uptake on Pretreatment PET May Predict for Therapeutic Sensitivity

We previously reported that ^{89}Zr-trastuzumab localizes to HER2-positive EG tumors as measured by PET imaging (26). Furthermore, in contrast to ^{18}F-FDG and ^{18}F-FLT PET, ^{89}Zr-trastuzumab PET could noninvasively differentiate HER2-positive from HER2-negative EG cancers preclinically (15). As downregulation of HER2 expression by afatinib is associated with afatinib sensitivity in preclinical models (15), we hypothesized that functional imaging with ^{89}Zr-trastuzumab PET could identify afatinib-sensitive and afatinib-resistant tumor sites prior to evidence of clinical progression. To test this hypothesis, we performed ^{89}Zr-trastuzumab PET imaging before treatment and before the first CT assessment (after 3–5 weeks on therapy) in 8 patients, one treated with afatinib monotherapy and seven with afatinib/trastuzumab.

All patients demonstrated ^{89}Zr-trastuzumab tumor uptake in at least one disease site prior to therapy initiation. In the pretreatment scans, we observed a wide range in median standardized uptake values (SUV) among patients and among lesions in individual patients (median SUVmax 15.6; range, 6.4–23.8; Fig. 1C; Supplementary Table S7). Four patients (50%) had visible metastases on CT that did not exhibit ^{89}Zr-trastuzumab uptake on PET, indicating pretreatment intrapatient HER2 expression heterogeneity among disease sites. All 4 of these patients demonstrated disease progression within 6 weeks. Even when mean ^{89}Zr-trastuzumab uptake declined 3 to 5 weeks after therapy, we observed intrapatient lesion-to-lesion variability in this change (Fig. 1C). Notably, the 3 patients with the strongest tumor regression on afatinib and afatinib/trastuzumab therapy had uniformly high ^{89}Zr-trastuzumab uptake (SUV >5) in all lesions visualized on CT (see Fig. 1C). These data suggest that homogenous pretreatment ^{89}Zr-trastuzumab uptake may be a marker of afatinib sensitivity and that heterogeneous uptake at baseline or variable ^{89}Zr-trastuzumab PET response may be indicators of poor response to afatinib in *ERBB2*-amplified EG cancer.

Differential Intrapatient and Interpatient Expression of the HER2, EGFR, and MET Kinases May Determine Clinical Response to HER Kinase Inhibitors in *ERBB2*-Amplified EG Cancer

To further explore the molecular basis of the variable lesion-to-lesion ^{89}Zr-trastuzumab uptake observed in individual patients and to identify potential mechanisms of afatinib resistance, we obtained consent to perform warm autopsies on 3 patients (patients 28, 30, and 31) who initially responded to afatinib but later developed disease progression. Patients 28 and 30 had undergone pre- and post-treatment ^{89}Zr-trastuzumab PET imaging. Patient 30 had presented with metastatic HER2-positive EG cancer initially treated with preoperative carboplatin, paclitaxel, and radiotherapy, followed by 5-fluorouracil, oxaliplatin, and trastuzumab, with transient tumor response and disease progression after 7 months. Liver biopsies performed pretreatment and following progression on trastuzumab revealed uniform, diffuse *ERBB2* and *EGFR* coamplification (within the same tumor cells; Fig. 1B; Supplementary Fig. S1). The patient achieved maximal tumor regression of 37% by RECIST 1.1 on afatinib monotherapy, followed by disease progression at week 16. ^{89}Zr-trastuzumab PET imaging pre-afatinib demonstrated tracer uptake in a GE junction tumor (the primary disease site), in a retroesophageal lymph node, and in a metastasis in liver segment 2/3 (Fig. 2A). After 3 weeks of afatinib therapy, repeat PET demonstrated variable change in ^{89}Zr-trastuzumab uptake in these lesions (see Fig. 2A). Specifically, there was a decline in ^{89}Zr-trastuzumab uptake at the retroesophageal lymph node site (−67% change in SUV and resolution to background activity) but persistently high ^{89}Zr-trastuzumab uptake (−4% change in SUV) at the site of the segment 2/3 liver metastasis. Tracer uptake at the site of the GE junction tumor also remained high on afatinib therapy (+10% change in SUV), and a new segment 7/8 liver lesion not observed on pretreatment CT and PET scans was now visualized by ^{89}Zr-trastuzumab PET at week 3 (Fig. 2A). This segment 7/8 liver lesion first visualized at 3 weeks by ^{89}Zr-trastuzumab PET increased progressively in size from treatment initiation to disease progression (Fig. 2A). Notably, clear radiographic progression at this disease site occurred despite ongoing response/stability in the retroesophageal lymph nodes and

Downloaded from cancerdiscovery.aacrjournals.org on January 22, 2020. © 2019 American Association for Cancer Research.

Published OnlineFirst November 21, 2018; DOI: 10.1158/2159-8290.CD-18-0598

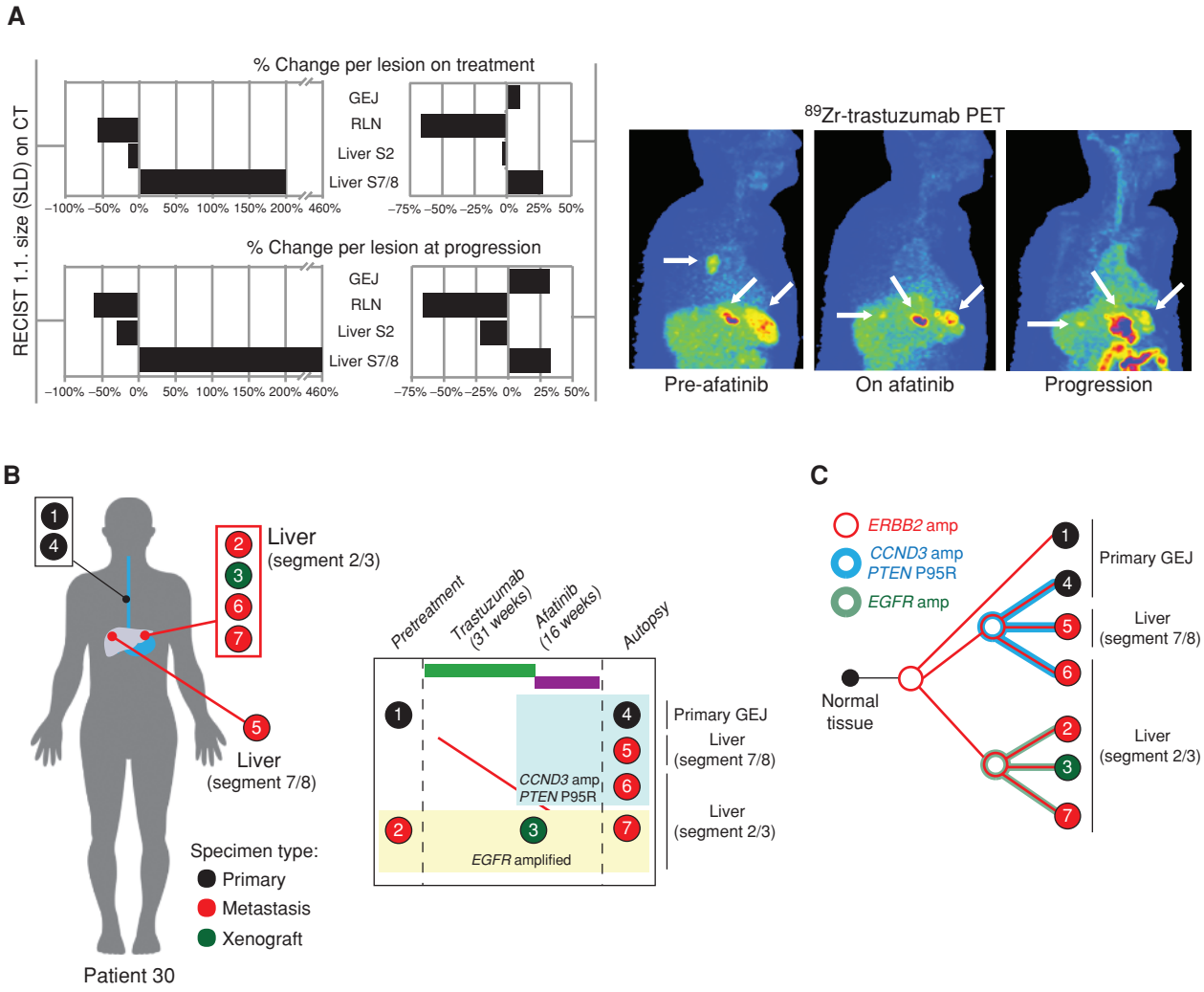


Figure 2. Intrapatient disease heterogeneity and selection for a non–*EGFR*-amplified tumor clone as mechanisms of afatinib resistance in patient 30. **A,** Radiographic tumor assessment using ^{89}Zr-trastuzumab PET and conventional CT scan, with corresponding bar graphs. ^{89}Zr-trastuzumab PET values in SUV and CT measurements in mm. ^{89}Zr-trastuzumab PET images include 3 panels: left (pre-afatinib) is a baseline pretreatment image showing uptake in segment 2/3 liver metastasis (SUV 16.4), GE junction (GEJ; SUV 21.5), and retroesophageal lymph node (RLN; SUV 9.1); middle (on afatinib) corresponds to 3 weeks post-treatment initiation, showing resolution of retroesophageal lymph node (SUV 3.0) with decrease in size but persistent high uptake in segment 2/3 liver lesion (SUV 15.8), similar uptake in GE junction (SUV 23.7), and a new lesion in liver segment 7/8 which appeared on ^{89}Zr-trastuzumab PET (SUV 8.6); right (progression) shows postprogression ^{89}Zr-trastuzumab PET uptake in GE junction (SUV 28.5) and segment 7/8 liver lesion (SUV 9.0), decreased uptake in liver segment 2/3 (SUV 12.3), and ongoing resolution of retroesophageal lymph node. **B,** Genomic comparison of matched pre- and post-treatment primary and liver segment 2/3 and post-treatment progression liver segment 7/8 obtained at warm autopsy. *EGFR* amplification was unique to the segment 2/3 liver lesion with ongoing response. The enlarging GE junction tumor and segment 7/8 liver metastasis were not *EGFR* amplified. In addition to a likely pathogenic mutation in *PTEN* (P95R, also present in a segment 2/3 liver lesion), the nonresponding metastases acquired an amplification of *CCND3*. SUV, standardized uptake value on ^{89}Zr-trastuzumab PET; SLD, sum of longest diameter on CT scan. **C,** Phylogenetic tree showing the inferred patterns of clonal evolution for the samples described in **B**.

other liver lesions on both CT and ^{89}Zr-trastuzumab PET imaging.

Following discontinuation of afatinib treatment, the patient clinically deteriorated and died, after which we performed an autopsy to collect tumor tissue from the primary tumor site and all visible metastatic sites (Fig. 2B). MSK-IMPACT sequencing was then performed on all tumor tissues and a matched normal blood specimen to explore the clonal and evolutionary relationships among disease sites. Whereas *ERBB2* amplification was clonal and shared among all the sampled disease sites, *EGFR* amplification was identified in only the pre-afatinib liver biopsy and in only 1 of the 3 tumor sites collected postmortem (liver segment 3).

These results indicate that *EGFR* amplification defined a distinct subclone that colonized liver segment 2/3 but branched off from other clones before trastuzumab and afatinib therapy (Fig. 2C). Notably, we observed heterogeneity of *EGFR* copy-number status in two geographically separate regions of the large segment 2/3 liver lesion: one area positive and the other area negative for *EGFR* amplification. The progressing disease sites at autopsy, although all lacking *EGFR* amplification and possessing additional private

Downloaded from cancerdiscovery.aacrjournals.org on January 22, 2020. © 2019 American Association for Cancer Research.

Published OnlineFirst November 21, 2018; DOI: 10.1158/2159-8290.CD-18-0598

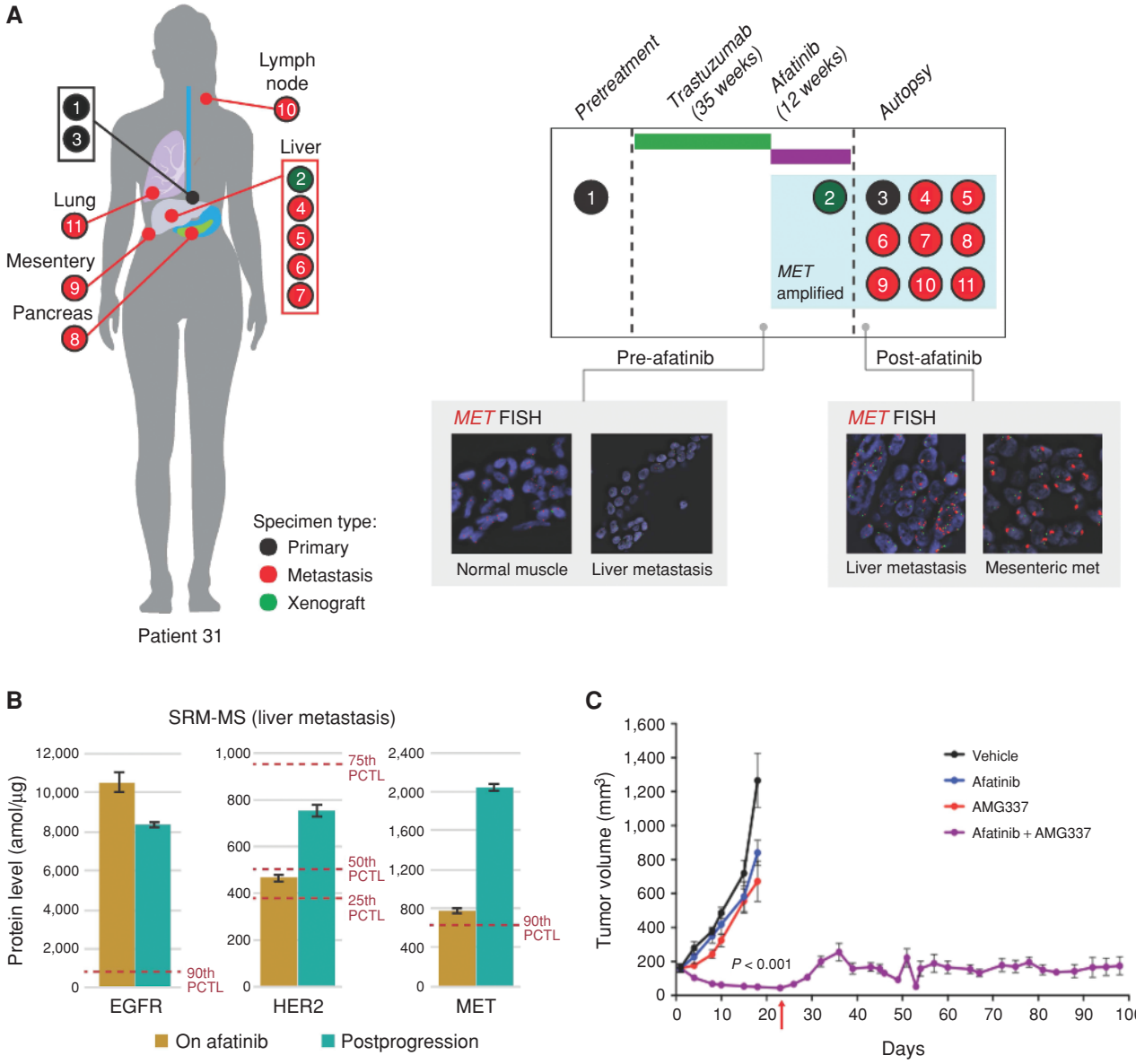


Figure 3. Acquired *MET* amplification as a mechanism of afatinib resistance in patient 31 with *EGFR*- and *ERBB2*-amplified EG cancer. **A,** Genomic comparison of matched pretreatment biopsy with post-treatment metastases obtained at warm autopsy demonstrating acquired *MET* amplification. **B**, SRM-MS analysis of liver metastasis sample obtained on afatinib with postprogression autopsy sample revealing increased MET and HER2 as well as decreased EGFR expression. PCTL, percentile. **C,** Efficacy of afatinib and afatinib/AMG 337 in a *MET/EGFR/ERBB2*-amplified PDX model established from patient 31. The combination of afatinib/AMG 337 resulted in complete tumor response at 21 days in *MET/EGFR/ERBB2*-amplified PDX. Red arrow indicates when the mice were rechallenged with the afatinib/AMG 337 combination following discontinuation of drug treatment, with durable tumor control again achieved.

mutations, were clonally related and defined by a likely functional shared mutation in *PTEN* (P95R), and a focal amplification of *CCND3*. In sum, these data suggest that preexistent heterogeneity of *EGFR* amplification may account for the patient's mixed response to afatinib therapy, with drug resistance arising through selection for a preexistent *EGFR* wild-type, *ERBB2*-amplified clone with additional coalterations of *PTEN* and *CCND3*.

A second patient (patient 31), a 61-year-old with stage IV gastric adenocarcinoma that was metastatic at diagnosis, had a 6-month transient response to first-line fluorouracil/oxaliplatin in combination with trastuzumab. Tumor genomic profiling of a liver metastasis collected post-trastuzumab identified *ERBB2* and *EGFR* coamplification, and the patient subsequently received afatinib monotherapy, achieving a confirmed partial response (best response 43% tumor regression by RECIST 1.1), followed by clinical progression at 12 weeks (Fig. 3). The patient succumbed to the disease within 6 weeks of afatinib discontinuation. Lesions in the primary tumor as well as the liver, pancreas, mesentery, lung, and lymph

Downloaded from cancerdiscovery.aacrjournals.org on January 22, 2020. © 2019 American Association for Cancer Research.

Published OnlineFirst November 21, 2018; DOI: 10.1158/2159-8290.CD-18-0598

nodes were collected at autopsy and subjected to tumor molecular profiling. A comparison of the sequencing results from postmortem tumor specimens and the primary tumor biopsy specimens collected prior to afatinib/trastuzumab treatment demonstrated a *TP53* R248W mutation in all disease sites. *MET* amplification was, however, detected only in the post-afatinib progression sites. This *MET* amplification was further confirmed using FISH (MET/Cen 7 >10; Fig. 3A). SRM-MS analysis of tumor samples collected at autopsy also confirmed uniformly high MET protein expression in all progressing lesions (Supplementary Table S8). Notably, a liver metastasis sampled both during afatinib therapy and at autopsy showed increased MET and HER2 as well as decreased EGFR protein expression in the postprogression versus on-treatment samples (Fig. 3B).

Amplification of *MET* has been previously proposed as a resistance mechanism to HER2 blockade in HER2-positive gastric cancer (23, 27–29). To determine whether *MET* amplification was sufficient to confer afatinib resistance in this patient, we studied a PDX model generated from a postprogression sample collected following progression on afatinib. We treated mice bearing this PDX with either afatinib, the MET kinase inhibitor AMG 337, a combination of both agents, or the vehicles only as control. Neither afatinib nor AMG 337 alone had an effect on PDX growth (Fig. 3C). However, the afatinib/AMG 337 combination induced durable tumor regression. By day 21, tumors were no longer palpable and treatment was halted, which resulted in subsequent tumor progression that by day 35 had reached a mean volume of ~300 mm^3. The mice were then rechallenged with the afatinib/AMG 337 combination, with durable tumor control again achieved.

A third patient (patient 28) had stage IV *ERBB2*-amplified gastric cancer metastatic to the peritoneal cavity. This patient had a prolonged 24-month response to first-line trastuzumab, fluorouracil, and oxaliplatin. The tumor collected post-trastuzumab progression had *ERBB2* amplification, but in contrast to the afatinib-sensitive patients described above, we did not observe *EGFR* coamplification in tumor or plasma cfDNA analysis (Supplementary Table S9). Pretreatment imaging showed ^{89}Zr-trastuzumab PET tracer uptake in the primary gastric mass, a peritoneal perigastric metastasis, and a left ovarian metastasis (Fig. 4A). A repeat scan following 5 weeks of afatinib/trastuzumab showed resolution of tracer uptake in the perigastric metastasis and the primary gastric mass but persistently elevated uptake in the ovarian metastasis, the site of eventual disease progression. A subsequent CT demonstrated regression of the perigastric peritoneal metastasis on afatinib/trastuzumab combination therapy, with an overall reduction of 22% in measurable disease by RECIST 1.1 criteria. The patient remained on afatinib/trastuzumab for 31 weeks, with subsequent disease progression manifested as an enlargement of the ovarian metastasis. cfDNA analysis at the time of disease progression on combined afatinib/trastuzumab revealed persistent *ERBB2* amplification, in addition to *MET* amplification that was not present in the pretreatment tumor biopsy (Fig. 4B and C; Supplementary Table S9). The progressing ovarian metastasis was subsequently resected, and tumor genomic profiling of this treatment-resistant disease site confirmed *ERBB2* and *MET* coamplification. Given the acquired *MET* amplification on afatinib/trastuzumab therapy, the patient was treated with afatinib in combination with cabozantinib, a multitargeted kinase inhibitor that inhibits MET among other kinase targets. Despite an initial decline in tumor markers, the patient clinically deteriorated and died. Analysis of multiple disease sites collected at autopsy revealed *MET* amplification only in the progressing ovarian metastasis and in a new perirectal metastasis not detected by pretreatment imaging. By contrast, the perigastric metastasis and the primary tumor site did not harbor a *MET* amplification, and both demonstrated ongoing response to afatinib/trastuzumab combination therapy (Fig. 4C). On dual *EGFR/ERBB2* FISH, there was heterogeneity within the perirectal metastasis, with all cells demonstrating *ERBB2* amplification but a mixture of non-*EGFR*–amplified and low-level *EGFR*-amplified cells (Fig. 4D). This heterogeneity was reflected in the observed *EGFR* amplification as detected by cfDNA (Fig. 4B).

DISCUSSION

We report the results of a phase II study of afatinib monotherapy and combined afatinib and trastuzumab combination therapy in patients with trastuzumab-resistant EG cancer. Integral to this study were analyses of pretreatment tumor biopsies with the goal of identifying determinants of afatinib sensitivity and, in responding patients, evolutionary analyses of samples collected following disease progression at the time of warm autopsy, to explore the effect of tumor heterogeneity on drug response. We observed that coamplification of *EGFR* was associated with clinical benefit with afatinib in *ERBB2*-amplified EG cancer and believe that this hypothesis should be further investigated in a larger cohort of EG patients. Because prior phase II results showed no meaningful response to afatinib in patients with *EGFR*-amplified EG tumors lacking *ERBB2* amplification, our data suggest that patients with coamplification of both *ERBB2* and *EGFR* may be most likely to respond to pan-HER kinase inhibitors such as afatinib (16). Coamplification of *ERBB2* and *EGFR* was not, however, required for afatinib response, as the combination of afatinib with trastuzumab showed modest clinical activity in *ERBB2*-amplified tumors lacking *EGFR* amplification. Furthermore, EGFR-selective inhibitors such as cetuximab and gefitinib have demonstrated activity in *EGFR*-amplified tumors lacking *ERBB2* amplification, suggesting that these agents may have a different efficacy profile than afatinib (30–33).

In this study, we performed warm autopsies with the goal of sampling multiple tumor sites to explore the relationship between intrapatient tumor heterogeneity and treatment response. In each case, the paired analysis of drug-sensitive and drug-resistant tumor sites identified a likely resistance mechanism. More specifically, we observed that afatinib resistance was associated with selection for a tumor clone that either lacked a sensitizing amplification (*EGFR* amplification) or had gained a resistance amplification (*MET* amplification). The results support the hypothesis that the limited efficacy of targeted kinase inhibitors in EG cancer is the result of rapid selection for or against driver amplifications that are heterogeneously present within an

Downloaded from cancerdiscovery.aacrjournals.org on January 22, 2020. © 2019 American Association for Cancer Research.

Published OnlineFirst November 21, 2018; DOI: 10.1158/2159-8290.CD-18-0598

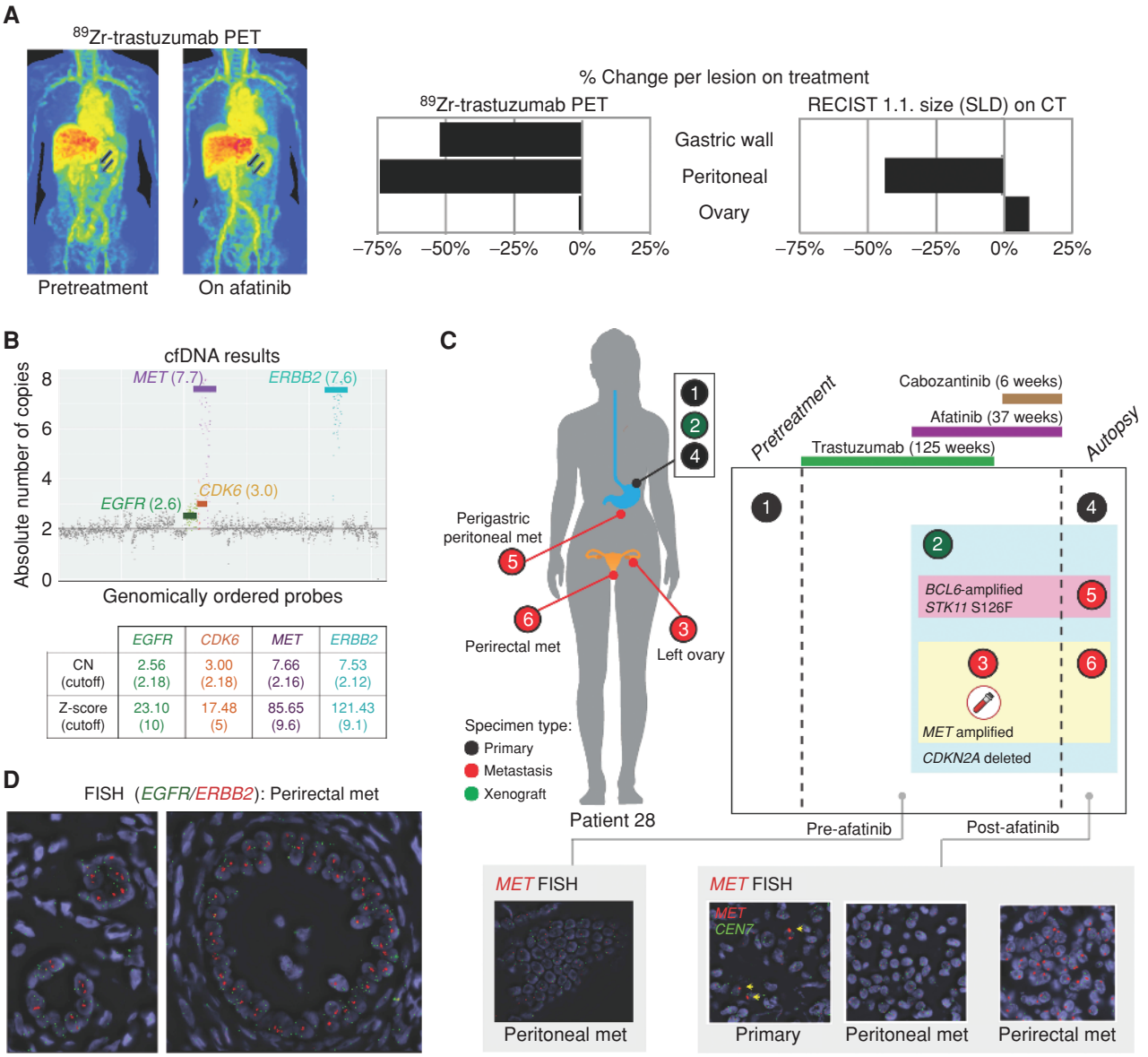


Figure 4. Noninvasive detection of acquired *MET* amplification as a mechanism of afatinib/trastuzumab resistance using cfDNA. **A,** Radiographic tumor assessment using ^{89}Zr-trastuzumab PET and conventional CT scan, with corresponding bar graphs in patient 28. ^{89}Zr-trastuzumab PET values in SUV and CT measurements in mm. Left, a baseline pretreatment ^{89}Zr-trastuzumab PET image showing uptake in a left ovary metastasis (SUV 5.1) not visible in this projection, perigastric peritoneal metastasis (SUV 7.2, lower arrow), and gastric mass (SUV 8.2, upper arrow). Right, ^{89}Zr-trastuzumab PET 5 weeks post-treatment initiation, showing resolution of uptake in the perigastric peritoneal metastasis (SUV 1.8) and gastric mass (SUV 3.9) and persistently high uptake in the left ovarian metastasis (SUV 5.2) not seen on maximum intensity projection (MIP) images. **B,** cfDNA analysis at the time of disease progression on afatinib/trastuzumab, demonstrating *ERBB2* and *MET* amplification (results for additional time points are provided in Supplementary Table S9). **C,** Genomic comparison of matched pretreatment biopsy with post-treatment tumor tissue collected from the left ovarian metastasis and subsequently at rapid autopsy, demonstrating acquired *MET* amplification unique to the progressing lesions. The perigastric metastasis (met) and the primary tumor, both of which demonstrated ongoing response to afatinib/trastuzumab, did not harbor *MET* amplification. **D,** Dual probe *EGFR* and *ERBB2* FISH from a perirectal tumor biopsy collected after treatment demonstrated *ERBB2* amplification and low-level gain of *EGFR* in a subset of tumor cells.

individual patient, a hypothesis consistent with a recently published study of matched primary and metastatic biopsies that noted that amplifications of *ERBB2, EGFR*, and *MET* were frequently discordant between primary and metastatic tumor sites (34).

Notably, we were able to generate a PDX model from a drug-resistant tumor site in one of the patients in whom treatment resistance was associated with selection for a *MET*-coamplified tumor. Analysis of this PDX model in the laboratory indicated that whereas afatinib and the MET inhibitor AMG 337 had no activity when used alone, cotreatment with both induced complete tumor regression, thus confirming that *MET* amplification was sufficient to induce afatinib resistance in this patient. Also notably, in one of the 2 patients, we were able to noninvasively detect the *MET* amplification by analyzing tumor-derived DNA in plasma (cfDNA),

Downloaded from cancerdiscovery.aacrjournals.org on January 22, 2020. © 2019 American Association for Cancer Research.

Published OnlineFirst November 21, 2018; DOI: 10.1158/2159-8290.CD-18-0598

suggesting that cfDNA analysis could noninvasively identify patients for whom EGFR and MET kinase inhibitor combinations would be most appropriate.

In the current study, we also show that HER2-directed functional PET imaging using ^{89}Zr-trastuzumab can noninvasively identify tumor heterogeneity, which may be predictive of subsequent drug response. Although the number of patients imaged was small, we did observe resolution of ^{89}Zr-trastuzumab uptake on PET imaging at some disease sites at early time points with tumor regression at these same sites on subsequent CT scans. These results suggest that HER2-directed PET imaging may represent a potential noninvasive tool to predict therapy response within weeks of therapy initiation. Early increases in ^{89}Zr-trastuzumab uptake may also be useful in identifying treatment-resistant disease sites prior to visible disease progression on traditional CT or MRI imaging. Hence, the potential uses of ^{89}Zr-trastuzumab PET could extend beyond detection of HER2-positive lesions to include facilitation of individualized patient care and management.

In summary, we find that concurrent amplification of *EGFR* and *ERBB2* is associated with response to the HER kinase inhibitor afatinib in patients with trastuzumab-refractory EG cancer. Heterogeneous uptake of ^{89}Zr-trastuzumab measured noninvasively by PET was associated with disease progression. Analyses of multiple disease sites sampled at the time of disease progression indicated several potential mediators of afatinib resistance, including loss of *EGFR* amplification and gain of *MET* amplification.

METHODS

Study Design and Treatment

This was a single-institution investigator-initiated phase II study of oral afatinib 40 mg daily (cohort 1) or afatinib 30 mg daily with intravenous trastuzumab 4 mg/kg every 2 weeks (cohort 2). The study protocol and all amendments were approved by the Memorial Sloan Kettering institutional review board, and the protocol was conducted in accordance with the Declaration of Helsinki, International Ethical Guidelines for Biomedical Research Involving Human Subjects (CIOMS), the Belmont Report, and the US Common Rule. All patients provided written informed consent. A CONSORT diagram is provided as Supplementary Fig. S2.

Study Assessments

The primary endpoint of the study was overall clinical benefit defined as best overall response rate (ORR; stable disease, complete or partial response) at 4 months. Adverse events were assessed according to National Cancer Institute Common Terminology Criteria for Adverse Events (CTCAE) version 4.0.

Biomarkers

To identify predictive biomarkers of response and molecular mechanisms of resistance, NGS, FISH, IHC, and PDX studies were prespecified in the initial version of the protocol, which was later amended to also include ^{89}Zr-trastuzumab PET imaging. Patients were also enrolled to a separate institutional review board–approved tissue procurement protocol, which provided consent for the mass spectrometry, plasma cfDNA, and autopsy studies. cfDNA collected during treatment of patient 28 was analyzed using the Guardant360 assay (35). The MSK-IMPACT assay was performed initially using a 341-gene and later 410-gene and 468-gene panels (Supplementary Table S10), as previously described (8). Multicolor FISH was performed using a probe mix containing equal parts of custom Kreatech *MET* (7q31) red, *EGFR* (7p11) green, and *ERBB2* (17q12) blue FISH probes (Leica Biosystems). HER2, EGFR, and MET protein levels were quantitated by targeted mass spectrometry (SRM-MS) using the NantOmics processing pipeline, as previously described (36–38). High protein expression was set by SRM level for MET ≥ 1,500 amol/μg, EGFR ≥ 1,200 amol/μg, and HER2 ≥ 750 amol/μg (36–38).

Statistical Analysis

Each treatment group was evaluated separately for the primary endpoint of ORR, cohort 1 using a Simon two-stage study design (39) with 80% power to reject the null hypothesis of ORR 5% (insufficient drug activity), assuming that the true ORR was 20%, with one-sided $\alpha = 0.05$. In the first stage, 13 patients were treated with afatinib, and based on 2 responses, accrual was expanded in stage 2 to 19 additional patients. After 20 patients were treated with afatinib, the trial was amended based on synergy observed in preclinical models to combined afatinib and trastuzumab (cohort 2). Cohort 2 was evaluated using the exact binomial single-stage design with unacceptable response rate of 7% against an acceptable response rate of 25% (at least 5 of 26 responding). Accrual was stopped after only 1 response was observed out of 12 patients treated in cohort 2, and because afatinib with trastuzumab was poorly tolerated.

CT and ^{89}Zr-Trastuzumab PET Assessments

CT or MRI scans were performed at baseline and every 8 weeks thereafter with response assessments quantified using RECIST 1.1 criteria. Best overall responses were derived from tumor measurements provided by the study-site radiologist. In patients who were willing to undergo additional imaging, ^{89}Zr-trastuzumab PET imaging was performed before treatment and before the first CT assessment (after 3–5 weeks on therapy) as an exploratory objective to assess early changes on protocol therapy. We have previously reported on the pharmacokinetics and serial biodistribution of ^{89}Zr-trastuzumab in patients with HER2-positive EG cancer (NCT02023996; ref. 26). Trastuzumab conjugated with desferrioxamine and radiolabeled with ^{89}Zr was administered intravenously as previously described (26). The ^{89}Zr-trastuzumab images were reviewed together with available conventional CT/MRI for concordance of tumor targeting. Heterogeneity of tumors was assessed on a per-lesion basis by aligning ^{89}Zr-trastuzumab PET and CT/MRI images on a Hermes Medical Imaging workstation. Intrapatient heterogeneity was defined as ^{89}Zr-trastuzumab PET-positive imaging in some but not all lesions identified on CT/MRI (see Supplementary Table S7).

Data Availability

All genomic and clinical data from this study are publicly available through the cBioPortal for Cancer Genomics (http://cbioportal.org/study?id=egc_msk_afatinib_2018; refs. 40, 41).

Disclosure of Potential Conflicts of Interest

P. Castel has ownership interest (including stock, patents, etc.) in Venthera and is a consultant/advisory board member for Venthera and Quartz Therapeutics. G.Y. Ku reports receiving commercial research support from Pieris and is a consultant/advisory board member for the same. M.E. Lacouture reports receiving a commercial research grant from RJR Fund, reports receiving other commercial research support from Veloce, Berg, US BIotest, and BMS, is a consultant/advisory board member for Boehringer Ingelheim, Roche/Genentech, BMS, AstraZeneca, Amgen, Symphogen, EMD Serono, Janssen, and Novartis, and has received other remuneration from Harborside Press and Wiley. T. Hembrough is President, Proteomics at NantOmics and has ownership interest (including stock, patents, etc.) in NantOmics and NantHealth. R.B. Lanman is Chief Medical

Downloaded from cancerdiscovery.aacrjournals.org on January 22, 2020. © 2019 American Association for Cancer Research.

Published OnlineFirst November 21, 2018; DOI: 10.1158/2159-8290.CD-18-0598

Officer at Guardant Health, Inc., is on the Board of Directors of Biolase, Inc., has ownership interest (including stock, patents, etc.) in Guardant Health, Inc., Biolase, Inc., and Forward Medical, Inc., and is a consultant/advisory board member for Forward Medical, Inc. S.M. Larson reports receiving commercial research grants from Genentech, Inc., Wilex AG, Telix Pharmaceuticals Ltd., and Regeneron Pharmaceuticals Inc., has ownership interest (including stock, patents, etc.) in Imaginab, Inc., Samus Therapeutics Inc., Elucida Oncology Inc., Voreyda Theranostics Inc., and YMABS Therapeutic Inc., is a consultant/advisory board member for Cynvec LLC, Eli Lilly, Prescient Therapeutics Limited, Advanced Therapeutic Partners, Gerson Lehman Group, Progenics, and Janssen Pharmaceuticals Inc., and has received other remuneration from Fonde de Research Sante, Quebec. M.F. Berger is a consultant/advisory board member for Roche. J.S. Lewis reports receiving a commercial research grant from Eli Lilly and other commercial research support from Genentech. D.B. Solit is a consultant/advisory board member for Pfizer, Loxo Oncology, Illumina, and Intezyne. J.A. Carrasquillo reports receiving commercial research grants from Genentech, Gilead, Regeneron, and y-mab. M. Scaltriti reports receiving commercial research grants from Puma Biotechnology, Menarini Ricerche, Immunomedics, and Daiichi Sankio, has ownership interest (including stock, patents, etc.) in Medendi Medical Travel, and is a consultant/advisory board member for Menarini Ricerche, ADC Pharma, and Biocience Institute. Y.Y. Janjigian reports receiving commercial research grants from Boehringer Ingelheim, Bayer, Genentech/Roche, Eli Lilly, and Merck and is a consultant/advisory board member for Merck Serono, Bristol-Myers Squibb, Eli Lilly, Pfizer, Bayer, Imugene, and Merck. No potential conflicts of interest were disclosed by the other authors.

Authors' Contributions

Conception and design: R.A. Lefkowitz, R.B. Lanman, D.B. Solit, J.A. Carrasquillo, M. Scaltriti, N. Schultz, Y.Y. Janjigian

Development of methodology: P. Castel, T. Hembrough, R.B. Lanman, S.M. Larson, W.A. Weber, E. de Stanchina, D.B. Solit, J.A. Carrasquillo, N. Schultz, Y.Y. Janjigian

Acquisition of data (provided animals, acquired and managed patients, provided facilities, etc.): J.F. Hechtman, P. Castel, G.Y. Ku, G.J. Nanjangud, J. Soong, E. Vakiani, M. Schattner, D.P. Kelsen, R.A. Lefkowitz, K. Brown, M.E. Lacouture, M. Mattar, B. Qeriqi, F. Cecchi, Y. Tian, T. Hembrough, R.B. Lanman, N. Pandit-Taskar, H. Schöder, C.A. Iacobuzio-Donahue, W.A. Weber, E. de Stanchina, J.S. Lewis, D.B. Solit, J.A. Carrasquillo, Y.Y. Janjigian

Analysis and interpretation of data (e.g., statistical analysis, biostatistics, computational analysis): F. Sanchez-Vega, J.F. Hechtman, H. Won, C.J. Fong, M.E. Lacouture, M. Capanu, T. Hembrough, R.B. Lanman, S.M. Larson, H. Schöder, D.H. Ilson, W.A. Weber, M.F. Berger, B.S. Taylor, D.B. Solit, J.A. Carrasquillo, M. Scaltriti, N. Schultz, Y.Y. Janjigian

Writing, review, and/or revision of the manuscript: F. Sanchez-Vega, J.F. Hechtman, P. Castel, C.J. Fong, G.J. Nanjangud, E. Vakiani, M. Schattner, D.P. Kelsen, R.A. Lefkowitz, M.E. Lacouture, M. Capanu, R.J. Nagy, R.B. Lanman, S.M. Larson, N. Pandit-Taskar, H. Schöder, D.H. Ilson, M.F. Berger, B.S. Taylor, J.S. Lewis, D.B. Solit, J.A. Carrasquillo, M. Scaltriti, N. Schultz, Y.Y. Janjigian

Administrative, technical, or material support (i.e., reporting or organizing data, constructing databases): F. Sanchez-Vega, J.F. Hechtman, Y. Tuvy, N. Bouvier, E. Vakiani, M.E. Lacouture, M. Mattar, R.J. Nagy, S.M. Larson, C.A. Iacobuzio-Donahue, J.S. Lewis, D.B. Solit, J.A. Carrasquillo

Study supervision: F. Sanchez-Vega, D.B. Solit, J.A. Carrasquillo, M. Scaltriti, N. Schultz, Y.Y. Janjigian

Other (administration of the imaging study drug, technical supervision of imaging, and interpretation of imaging data): N. Pandit-Taskar

Other (image acquisition and interpretation): H. Schöder

Other (contributed to these aspects in the FDG PET data): J.A. Carrasquillo

Acknowledgments

This clinical research was funded by Boehringer Ingelheim Pharmaceuticals Inc., Ingelheim. Boehringer Ingelheim Pharmaceuticals Inc. provided afatinib. ClinicalTrials.gov trial registration ID: NCT01522768. This study was supported by the 2013 Conquer Cancer Foundation ASCO Career Development Award (Y.Y. Janjigian), 2014 and 2016 Mr. William H. Goodwin and Mrs. Alice Goodwin and the Commonwealth Foundation for Cancer Research and The Center for Experimental Therapeutics at Memorial Sloan Kettering Cancer Center (Y.Y. Janjigian and J.S. Lewis), the Cancer Center Support Grant (P30 CA008748), U54 OD020355 01 (E. de Stanchina), Marie-Josée and Henry R. Kravis Center for Molecular Oncology, Robertson Foundation (B.S. Taylor and N. Schultz), Brown Performance Fund for Innovation in Cancer Informatics (F. Sanchez-Vega), 2015 Cycle for Survival Award (Y.Y. Janjigian and N. Schultz), and the Department of Defense Congressionally Directed Medical Research Program (CA 150646; Y.Y. Janjigian).

Received May 25, 2018; revised October 5, 2018; accepted November 15, 2018; published first November 21, 2018.

REFERENCES

1. Ferlay J, Soerjomataram I, Dikshit R, Eser S, Mathers C, Rebelo M, et al. Cancer incidence and mortality worldwide: sources, methods and major patterns in GLOBOCAN 2012. Int J Cancer 2015;136:E359–86.
2. Siegel RL, Miller KD, Jemal A. Cancer statistics, 2017. CA: Cancer J Clin 2017;67:7–30.
3. Bang Y-J, Van Cutsem E, Feyereislova A, Chung HC, Shen L, Sawaki A, et al. Trastuzumab in combination with chemotherapy versus chemotherapy alone for treatment of HER2-positive advanced gastric or gastro-oesophageal junction cancer (ToGA): a phase 3, open-label, randomised controlled trial. Lancet 2010;376:687–97.
4. Janjigian YY, Werner D, Pauligk C, Steinmetz K, Kelsen DP, Jäger E, et al. Prognosis of metastatic gastric and gastroesophageal junction cancer by HER2 status: a European and USA International collaborative analysis. Ann Oncol 2012;23:2656–62.
5. Cancer Genome Atlas Research Network. Comprehensive molecular characterization of gastric adenocarcinoma. Nature 2014;513:202–9.
6. Cancer Genome Atlas Research Network. Integrated genomic characterization of oesophageal carcinoma. Nature 2017;541:169–75.
7. Liu Y, Sethi NS, Hinoue T, Schneider BG, Cherniack AD, Sanchez-Vega F, et al. Comparative molecular analysis of gastrointestinal adenocarcinomas. Cancer Cell 2018;33:721–35.e8.
8. Janjigian YY, Sanchez-Vega F, Jonsson P, Chatila WK, Hechtman JF, Ku GY, et al. Genetic predictors of response to systemic therapy in esophagogastric cancer. Cancer Discov 2018;8:49–58.
9. Tabernero J, Hoff PM, Shen L, Ohtsu A, Shah MA, Cheng K, et al. Pertuzumab plus trastuzumab and chemotherapy for HER2-positive metastatic gastric or gastro-oesophageal junction cancer (JACOB): final analysis of a double-blind, randomised, placebo-controlled phase 3 study. Lancet Oncol 2018;19:1372–84.
10. Thuss-Patience PC, Shah MA, Ohtsu A, Van Cutsem E, Ajani JA, Castro H, et al. Trastuzumab emtansine versus taxane use for previously treated HER2-positive locally advanced or metastatic gastric or gastro-oesophageal junction adenocarcinoma (GATSBY): an international randomised, open-label, adaptive, phase 2/3 study. Lancet Oncol 2017;18:640–53.
11. Satoh T, Xu R-H, Chung HC, Sun G-P, Doi T, Xu J-M, et al. Lapatinib plus paclitaxel versus paclitaxel alone in the second-line treatment of HER2-amplified advanced gastric cancer in Asian populations: TyTAN—a randomized, phase III study. J Clin Oncol 2014;32:2039–49.
12. Kim ST, Banks KC, Pectasides E, Kim SY, Kim K, Lanman RB, et al. Impact of genomic alterations on lapatinib treatment outcome and

Downloaded from cancerdiscovery.aacrjournals.org on January 22, 2020. © 2019 American Association for Cancer Research.

Published OnlineFirst November 21, 2018; DOI: 10.1158/2159-8290.CD-18-0598

cell-free genomic landscape during HER2 therapy in HER2+ gastric cancer patients. Ann Oncol 2018;29:1037–48.
13. Wainberg ZA, Anghel A, Desai AJ, Ayala R, Luo T, Safran B, et al. Lapatinib, a dual EGFR and HER2 kinase inhibitor, selectively inhibits HER2-amplified human gastric cancer cells and is synergistic with trastuzumab in vitro and in vivo. Clin Cancer Res 2010;16:1509–19.
14. Leto SM, Sassi F, Catalano I, Torri V, Migliardi G, Zanella ER, et al. Sustained inhibition of HER3 and EGFR is necessary to induce regression of HER2-Amplified gastrointestinal carcinomas. Clin Cancer Res 2015;21:5519–31.
15. Janjigian YY, Viola-Villegas N, Holland JP, Divilov V, Carlin SD, Gomes-DaGama EM, et al. Monitoring afatinib treatment in HER2-positive gastric cancer with 18F-FDG and 89Zr-trastuzumab PET. J Nucl Med 2013;54:936–43.
16. Kwak EL, Shapiro GI, Cohen SM, Becerra CR, Lenz H-J, Cheng W-F, et al. Phase 2 trial of afatinib, an ErbB family blocker, in solid tumors genetically screened for target activation. Cancer 2013;119:3043–51.
17. Li D, Ambrogio L, Shimamura T, Kubo S, Takahashi M, Chirieac LR, et al. BIBW2992, an irreversible EGFR/HER2 inhibitor highly effective in preclinical lung cancer models. Oncogene 2008;27:4702–11.
18. Baselga J, Bradbury I, Eidtmann H, Di Cosimo S, de Azambuja E, Aura C, et al. Lapatinib with trastuzumab for HER2-positive early breast cancer (NeoALTTO): a randomised, open-label, multicentre, phase 3 trial. Lancet 2012;379:633–40.
19. Cheng DT, Mitchell TN, Zehir A, Shah RH, Benayed R, Syed A, et al. Memorial Sloan Kettering-Integrated Mutation Profiling of Actionable Cancer Targets (MSK-IMPACT): a hybridization capture-based next-generation sequencing clinical assay for solid tumor molecular oncology. J Mol Diagn 2015;17:251–64.
20. Zehir A, Benayed R, Shah RH, Syed A, Middha S, Kim HR, et al. Mutational landscape of metastatic cancer revealed from prospective clinical sequencing of 10,000 patients. Nat Med 2017;23:703–13.
21. Chakravarty D, Gao J, Phillips SM, Kundra R, Zhang H, Wang J, et al. OncoKB: a precision oncology knowledge base. JCO Precis Oncol 2017;2017.
22. Kim J, Fox C, Peng S, Pusung M, Pectasides E, Matthee E, et al. Preexisting oncogenic events impact trastuzumab sensitivity in ERBB2-amplified gastroesophageal adenocarcinoma. J Clin Investig 2014;124:5145–58.
23. Pietrantonio F, Fucà G, Morano F, Gloghini A, Corso S, Aprile G, et al. Biomarkers of primary resistance to trastuzumab in HER2-positive metastatic gastric cancer patients: the AMNESIA case–control study. Clin Cancer Res 2018;24:1082–9.
24. Díaz-Serrano A, Angulo B, Dominguez C, Pazo-Cid R, Salud A, Jiménez-Fonseca P, et al. Genomic profiling of HER2-positive gastric cancer: PI3K/Akt/mTOR pathway as predictor of outcomes in HER2-positive advanced gastric cancer treated with trastuzumab. Oncol 2018;23:1092–102.
25. Klempner SJ, Chao J. Toward optimizing outcomes in Her2-positive gastric cancer: timing and genomic context matter. Ann Oncol 2018;29:801–2.
26. O'Donoghue JA, Lewis JS, Pandit-Taskar N, Fleming SE, Schöder H, Larson SM, et al. Pharmacokinetics, biodistribution, and radiation dosimetry for Zr-trastuzumab in patients with esophagogastric cancer. J Nucl Med 2018;59:161–6.
27. Chen C-T, Kim H, Liska D, Gao S, Christensen JG, Weiser MR. MET activation mediates resistance to lapatinib inhibition of HER2-amplified gastric cancer cells. Mol Cancer Ther 2012;11:660–9.
28. Zhang Z, Wang J, Ji D, Wang C, Liu R, Wu Z, et al. Functional genetic approach identifies MET, HER3, IGF1R, INSR pathways as determinants of lapatinib unresponsiveness in HER2-positive gastric cancer. Clin Cancer Res 2014;20:4559–73.
29. Goltsov AA, Fang B, Pandita TK, Maru DM, Swisher SG, Hofstetter WL. HER2 confers resistance to foretinib inhibition of MET-amplified esophageal adenocarcinoma cells. Ann Thorac Surg 2018;105:363–70.
30. Zhang L, Yang J, Cai J, Song X, Deng J, Huang X, et al. A subset of gastric cancers with EGFR amplification and overexpression respond to cetuximab therapy. Sci reports 2013;3:2992.
31. Luber B, Deplazes J, Keller G, Walch A, Rauser S, Eichmann M, et al. Biomarker analysis of cetuximab plus oxaliplatin/leucovorin/5-fluorouracil in first-line metastatic gastric and oesophago-gastric junction cancer: results from a phase II trial of the Arbeitsgemeinschaft Internistische Onkologie (AIO). BMC Cancer 2011;11:509.
32. Petty RD, Dahle-Smith A, Stevenson DAJ, Osborne A, Massie D, Clark C, et al. Gefitinib and EGFR gene copy number aberrations in esophageal cancer. J Clin Oncol 2017;35:2279–87.
33. Maron SB, Alpert L, Kwak HA, Lomnicki S, Chase L, Xu D, et al. Targeted therapies for targeted populations: anti-EGFR treatment for -amplified gastroesophageal adenocarcinoma. Cancer Discov 2018;8:696–713.
34. Pectasides E, Stachler MD, Derks S, Liu Y, Maron S, Islam M, et al. Genomic heterogeneity as a barrier to precision medicine in gastroesophageal adenocarcinoma. Cancer Discov 2018;8:37–48.
35. Lanman RB, Mortimer SA, Zill OA, Sebisanovic D, Lopez R, Blau S, et al. Analytical and clinical validation of a digital sequencing panel for quantitative, highly accurate evaluation of cell-free circulating tumor DNA. PloS One 2015;10:e0140712.
36. Catenacci DVT, Liao W-L, Zhao L, Whitcomb E, Henderson L, O'Day E, et al. Mass-spectrometry-based quantitation of Her2 in gastroesophageal tumor tissue: comparison to IHC and FISH. Gastric Cancer 2016;19:1066–79.
37. Hembrough T, Thyparambil S, Liao W-L, Darfler MM, Abdo J, Bengali KM, et al. Selected reaction monitoring (SRM) analysis of epidermal growth factor receptor (EGFR) in formalin fixed tumor tissue. Clin proteomics 2012;9:5.
38. Catenacci DVT, Liao W-L, Thyparambil S, Henderson L, Xu P, Zhao L, et al. Absolute quantitation of Met using mass spectrometry for clinical application: assay precision, stability, and correlation with MET gene amplification in FFPE tumor tissue. PloS One 2014;9:e100586.
39. Simon R. Optimal two-stage designs for phase II clinical trials. Control Clin Trials 1989;10:1–10.
40. Gao J, Aksoy BA, Dogrusoz U, Dresdner G, Gross B, Sumer SO, et al. Integrative analysis of complex cancer genomics and clinical profiles using the cBioPortal. Sci Signal 2013;6:pl1.
41. Cerami E, Gao J, Dogrusoz U, Gross BE, Sumer SO, Aksoy BA, et al. The cBio cancer genomics portal: an open platform for exploring multidimensional cancer genomics data. Cancer Discov 2012;2:401–4.

Downloaded from cancerdiscovery.aacrjournals.org on January 22, 2020. © 2019 American Association for Cancer Research.

Published OnlineFirst November 21, 2018; DOI: 10.1158/2159-8290.CD-18-0598

AACR American Association for Cancer Research

CANCER DISCOVERY

EGFR and *MET* Amplifications Determine Response to HER2 Inhibition in *ERBB2*-Amplified Esophagogastric Cancer

Francisco Sanchez-Vega, Jaclyn F. Hechtman, Pau Castel, et al.

Cancer Discov 2019;9:199-209. Published OnlineFirst November 21, 2018.

Updated version	Access the most recent version of this article at: doi:10.1158/2159-8290.CD-18-0598
Supplementary Material	Access the most recent supplemental material at: http://cancerdiscovery.aacrjournals.org/content/suppl/2018/11/21/2159-8290.CD-18-0598.DC1

Cited articles	This article cites 40 articles, 13 of which you can access for free at: http://cancerdiscovery.aacrjournals.org/content/9/2/199.full#ref-list-1
Citing articles	This article has been cited by 4 HighWire-hosted articles. Access the articles at: http://cancerdiscovery.aacrjournals.org/content/9/2/199.full#related-urls

E-mail alerts	Sign up to receive free email-alerts related to this article or journal.
Reprints and Subscriptions	To order reprints of this article or to subscribe to the journal, contact the AACR Publications Department at pubs@aacr.org.
Permissions	To request permission to re-use all or part of this article, use this link http://cancerdiscovery.aacrjournals.org/content/9/2/199. Click on "Request Permissions" which will take you to the Copyright Clearance Center's (CCC) Rightslink site.

Downloaded from cancerdiscovery.aacrjournals.org on January 22, 2020. © 2019 American Association for Cancer Research.

nature COMMUNICATIONS

ARTICLE

DOI: 10.1038/s41467-018-07608-w OPEN

Caveolin-1 mediates cellular distribution of HER2 and affects trastuzumab binding and therapeutic efficacy

Patrícia M.R. Pereira[1], Sai Kiran Sharma[1], Lukas M. Carter[1], Kimberly J. Edwards[1], Jacob Pourat[1], Ashwin Ragupathi[1], Yelena Y. Janjigian[2], Jeremy C. Durack[1,3] & Jason S. Lewis[1,3,4,5,6]

Human epidermal growth factor receptor 2 (HER2) gene amplification and/or protein overexpression in tumors is a prerequisite for initiation of trastuzumab therapy. Although HER2 is a cell membrane receptor, differential rates of endocytosis and recycling engender a dynamic surface pool of HER2. Since trastuzumab must bind to the extracellular domain of HER2, a depressed HER2 surface pool hinders binding. Using in vivo biological models and cultures of fresh human tumors, we find that the caveolin-1 (CAV1) protein is involved in HER2 cell membrane dynamics within the context of receptor endocytosis. The translational significance of this finding is highlighted by our observation that temporal CAV1 depletion with lovastatin increases HER2 half-life and availability at the cell membrane resulting in improved trastuzumab binding and therapy against HER2-positive tumors. These data show the important role that CAV1 plays in the effectiveness of trastuzumab to target HER2-positive tumors.

[1] Department of Radiology, Memorial Sloan Kettering Cancer Center, New York, NY 10065, USA. [2] Department of Medicine, Memorial Sloan Kettering Cancer Center and Weill Cornell Medical College, New York, NY 10065, USA. [3] Department of Radiology, Weill Cornell Medical College, New York, NY 10065, USA. [4] Molecular Pharmacology Program, Memorial Sloan Kettering Cancer Center, New York, NY 10065, USA. [5] Department of Pharmacology, Weill Cornell Medical College, New York, NY 10065, USA. [6] Radiochemistry and Molecular Imaging Probes Core, Memorial Sloan Kettering Cancer Center, New York, NY 10065, USA. Correspondence and requests for materials should be addressed to J.S.L. (email: lewisj2@mskcc.org)

Unrestrained activation of human epidermal growth factor receptor 2 (HER2) contributes to aberrant tumor growth; and HER2 gene amplification, messenger RNA or protein overexpression, has been observed in patients with breast or ovarian cancer[1]. HER2 overexpression has also been reported in patients with gastric cancer, bladder carcinomas, gallbladder, and extrahepatic cholangiocarcinomas[2]. HER2 has no known ligand, but remains the most preferred dimerization partner to potentiate downstream oncogenic signaling by members of the HER family. Prior to the development of targeted anti-HER2 therapy, patients with HER2-positive tumors demonstrated reduced disease-free survival compared to patients whose tumors expressed low levels of HER2[3]. These findings established HER2 as a therapeutic target and a tumor biomarker. Over the past two decades, clinical evidence has unequivocally demonstrated that the inhibition of this oncogene improves treatment outcomes, and has led to the emergence of several effective anti-HER2 therapies[4].

Among these agents, anti-HER2 therapeutic antibodies (e.g., trastuzumab and pertuzumab), antibody-drug conjugates (ADCs, e.g., trastuzumab emtansine; TDM1), and trastuzumab imaging agents (when radio- or fluorescently-labeled[5–8]) have changed the prognosis of both breast and gastric cancer patients. However, heterogeneity in HER2 expression or equivocal HER2 status warrants attention in trastuzumab-based imaging and therapeutic strategies[9–13]. A lack of correlation between histologic HER2-positivity and tumor uptake of, e.g., zirconium-89 (^{89}Zr)-labeled trastuzumab has been observed in patients with breast cancer[7,14]. These results suggest that determination of overall amplification and/or overexpression of HER2 alone are insufficient to predict response to treatment with trastuzumab.

Clinically, the anti-tumor activity of trastuzumab is attributed to more than a single mechanism of action. Direct action of the antibody is premised on receptor downregulation and subsequent alterations to intracellular signaling including attenuation of downstream pro-tumorigenic cell signaling, inhibition of HER2 shedding, and inhibition of tumor angiogenesis. On the other hand, indirect action due to activation of an immune response via antibody dependent cell-mediated cytotoxicity (ADCC) has also been proposed as a mechanism of action for this drug[15–17]. Trastuzumab binding to cancer cells is highly dependent on the availability of HER2 at the cell membrane. The current status of patient selection for trastuzumab therapy is based on HER2-positivity using DNA- and protein-based assays[18]. However, these assays could overestimate HER2-positivity, as some of the stained antigen may be intracellular and, therefore, unavailable to engage trastuzumab at the tumor cell surface. This would translate as minimal benefit to such patients from trastuzumab-based therapy since the antibody can only target HER2 available at the cell membrane.

Notably, cell-surface receptors involved in tumor development are characterized by abnormal trafficking from the cell membrane to intracellular compartments[19,20]. Distinct from HER2, endocytosis of the other members of the HER family occurs after ligand binding[20]. Although HER2 has no known ligand, the open conformation of the extracellular domain contributes to the dynamics of the HER2 surface pool[21,22]. The localization of HER2 at the membrane is a heterogeneous and dynamic process[19,23,24] governed by differential rates of endocytosis and recycling[20,24,25]. In addition to cell membrane expression, HER2 localizes in the cytoplasm[26] and nucleus[27].

Several studies have demonstrated that at the cell membrane, HER2 is localized in caveolae domains[28]. Caveolae are caveolin-1 (CAV1) enriched subdomains of the plasma membrane, which are deregulated in cancer cells and contain a high content of cholesterol and sphingolipids[29,30]. Others have demonstrated that HER2 co-localizes with the lipid-raft marker GM1[31] and interacts with the lipid-raft associated oncoprotein mucin-1-c[32]. After binding to the extracellular domain of HER2, the tumor suppressor opioid binding protein/cell adhesion molecule like (OPCML) induces HER2 degradation through the caveolae-associated endosomal pathway[32]. Importantly, the depletion of membrane cholesterol results in HER2 confinement at the cell membrane[33].

Intrinsic defects in the endocytic machinery responsible for HER2 downregulation correlate with unresponsiveness to trastuzumab therapy[34]. It is suggested that caveolae-mediated endocytosis is involved in resistance to treatment with TDM1 and trastuzumab[35,36]. We hypothesize that modulation of the caveolae membrane domains could promote stability of HER2 at the cell membrane and improve binding of trastuzumab to target cells. In this study, we demonstrate how CAV1 can influence HER2 expression and stability at the cell membrane.

Results

HER2 interacts with CAV1. To address cell-surface HER2 stability in CAV1-positive vs. CAV1 negative cells, we first explored protein–protein associations between HER2 and CAV1 in a panel of cancer cell lines (Fig. 1a and Supplementary Fig. 1a, b). Mining the Cancer Cell Line Encyclopedia database[37] for breast, gastric and bladder cancer lines revealed that protein expression of HER2 is inversely correlated with that of CAV1, bearing a Spearman's rank correlation coefficient (r) of −0.54 ($P < 0.0001$, Spearman's correlation). Western blot analysis of a panel of 14 cell lines supported the inverse correlation between HER2 and CAV1 protein expression ($r = -0.58$, $P = 0.03$, Spearman's correlation). UMUC14 bladder, NCIN87 gastric, BT474 and SKBR3 breast cancer cell lines exhibited the highest ratio of HER2-to-CAV1 protein levels (Fig. 1a) and were chosen for use in subsequent in vitro and in vivo experiments. HER2–CAV1 protein associations were also correlated using the STRING database, which allows for the determination of protein–protein interactions based on experimental and computationally predicted associations. This analysis yielded a high-confidence association value (score ≥ 0.700, Supplementary Fig. 1c). The network generated for HER2 and CAV1 proteins using the STRING database revealed that CAV1 has a negative molecular action on HER2. Altogether, these findings support a seesaw effect between CAV1 and HER2 proteins.

CAV1 contributes to cell membrane HER2 density. Given that CAV1 associates with HER2 and that CAV1 expression in malignancies may be clinically significant for cancer diagnosis[29,30], we sought to determine if CAV1 expression is correlated with HER2 density at the cell membrane. We observed that HER2 does not exhibit predominant membrane localization in all cell clusters of NCIN87 (HER2-positive gastric cancer cell line[8]) tumor xenografts (Fig. 1b). These observations are consistent with recent reports of HER2-positive gastric tumors having different HER2 densities at the cell membrane[38]. In cancer cells where CAV1 is absent, HER2 is exclusively present at the cell membrane (Fig. 1c highlighted by the dashed white circles 1 and 3). On the other hand, cancer cells expressing CAV1 exhibit reduced HER2 staining at the cell membrane (Fig. 1c highlighted by the dashed white circles 2 and 4). Consistent with these findings, immunofluorescence staining of HER2-positive tumor samples obtained from gastric cancer patients revealed that cells with high expression of CAV1 have low membrane staining of HER2 (Fig. 1d). In HER2-positive tumor samples containing low expression levels of CAV1, HER2 exhibits predominant membrane staining. Altogether, the immunofluorescence analyses of

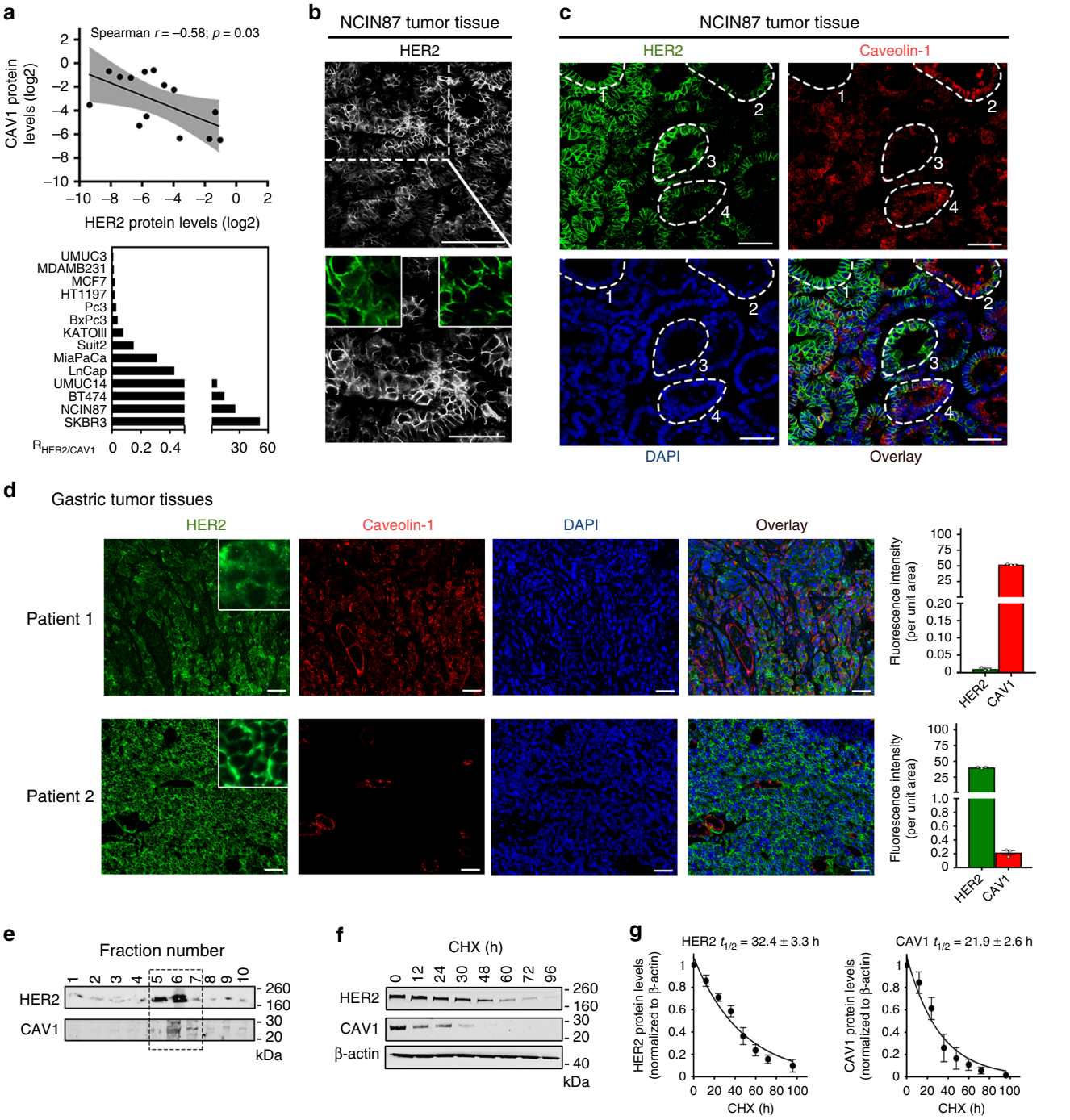
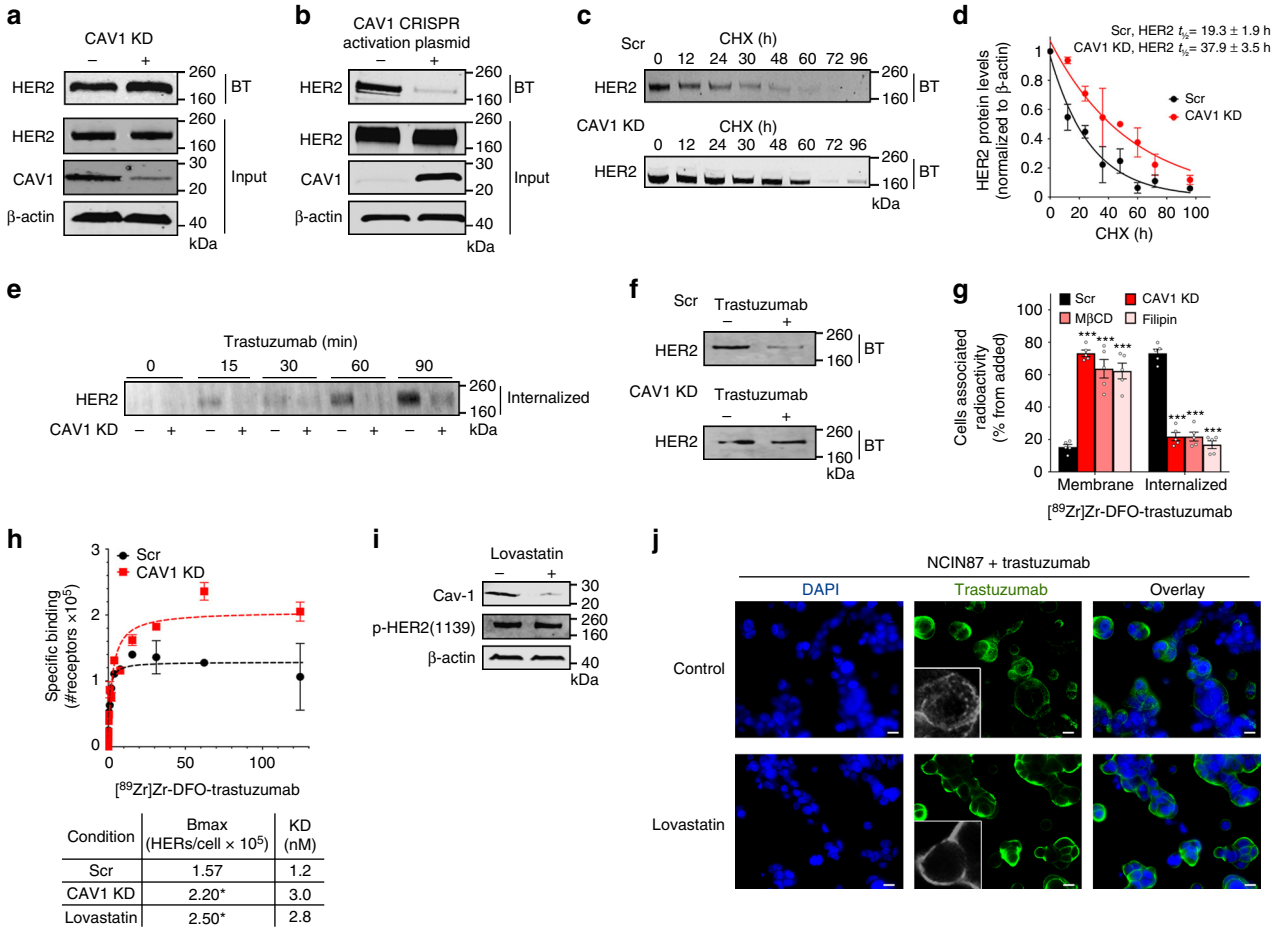


Fig. 1 Seesaw effect between CAV1 and HER2 proteins. **a** Association between CAV1 and HER2 in gastric (NCIN87, KATOIII), bladder (HT1197, UMUC14, UMUC3), breast (MDAMB231, MCF-7, BT474, SKBR3), pancreatic (BxPc3, MiaPaCa, Suit2) and prostate (LnCap, Pc3) cancer cells. The level of CAV1 (*y*-axis) and HER2 (*x*-axis) are expressed as the ratio of protein/β-actin control, as determined by western blot analysis (upper panel). The non-parametric one-tailed Spearman test was used to determine the correlation coefficients. $R_{HER2/CAV1}$, ratio of HER2-to-CAV1 protein levels as determined by western blot analysis from total extracts (lower panel). **b** Confocal images of immunofluorescence staining of HER2 in s.c. NCIN87 gastric tumors from athymic nude mice, showing that HER2 does not exhibit a predominant membrane staining. Scale bars: 100 μm and 50 μm (inset). **c** Confocal images of immunofluorescence staining of HER2 and CAV1 in s.c. NCIN87 gastric tumors from athymic nude mice. HER2 presence at the cell membrane in cells where CAV1 is absent (cell clusters 1 and 3) and HER2 almost absent at the cell membrane in cells where CAV1 is present (cell clusters 2 and 4). Scale bars: 50 μm. **d** Confocal images and quantification (mean ± S.E.M, $n = 3$) of immunofluorescence staining of HER2 and CAV1 in human HER2-positive gastric tumors containing high (Patient 1) and low (Patient 2) expression of CAV1. HER2 predominant presence at the cell membrane in CAV1-negative tumors (Patient 2). Scale bars: 50 μm. **e** Western blot analysis of the distribution of HER2 and CAV1 in caveolae fractions isolated from NCIN87 cells. **f** Western blot of HER2 and CAV1 in the total lysates of NCIN87 cells after blocking protein synthesis with 80 μg mL^{-1} CHX for 0, 12, 24, 30, 48, 60, 72, and 96 h. CHX cyclohexamide. **g** HER2 and CAV1 have similar half-lives. Half-lives calculated after western blot analysis of Fig. 1f. Density of western blot bands was quantified by scanning densitometry with ImageJ software. Half-lives were calculated as the time required for protein decrease to 50% of its initial level (mean ± S.E.M, $n = 4$)

preclinical and clinical samples indicate that CAV1 expression plays a role in HER2 antigen density at the cell membrane.

Additional subcellular fractionation experiments confirmed that HER2 is present, with CAV1, in the same lipid-rich fractions (Fig. 1e). HER2 and CAV1 half-lives were estimated in cells treated with an inhibitor of protein biosynthesis, cycloheximide, CHX (Fig. 1f, g and Supplementary Fig. 2). The actin-normalized HER2 or CAV1 protein expression levels (relative to t = 0) were plotted over time, and protein half-life was estimated from a monophasic exponential fit using GraphPad Prism (Fig. 1g). The estimated half-life of HER2 was similar to CAV1 in NCIN87 gastric, BT474 and SKBR3 breast cancer cell lines. Collectively, these results support the association between CAV1 and HER2.

Depletion of CAV1 improves trastuzumab binding. The inverse correlation between CAV1 and HER2 expression led us to investigate if depletion of CAV1 would result in improved HER2 stability at the cell membrane. To this end, we first used a pool of three target-specific 20–25 nucleotides (nt) small-interfering RNA (siRNA) to knockdown CAV1 protein (Supplementary Fig. 3a). Cell-surface biotinylation experiments were performed to analyze HER2 expression and localization in the plasma membrane. siRNA-mediated knockdown of CAV1 slightly increased (1.4 ± 0.2, mean ± S.E.M, $n = 3$) HER2 at the cell membrane for NCIN87 cells (Fig. 2a) and UMUC14 cells (Supplementary Fig. 3b), without alteration of total HER2 protein levels. In contrast, when we used clustered regularly interspaced short palindromic repeats (CRISPR) activation plasmid to increase CAV1, we found that forced CAV1 overexpression promotes loss of HER2 at the cell membrane (Fig. 2b and Supplementary Fig. 3c). While CAV1 depletion resulted in a slight increase in cell-surface HER2, a more pronounced effect of knocking down CAV1 was demonstrated by the extended half-life



Condition	Bmax (HERs/cell × 10^5)	KD (nM)
Scr	1.57	1.2
CAV1 KD	2.20*	3.0
Lovastatin	2.50*	2.8

Fig. 2 In vitro CAV1 depletion increases HER2 stability at the cell membrane. **a** Western blot of biotinylated cell surface-associated HER2 along with HER2 and CAV1 in total lysates of NCIN87 cells transfected with CAV1 siRNA or scrambled control siRNA constructs or **b** transfected with CAV1 CRISPR activation plasmid or control CRISPR activation plasmid. HER2 protein levels increase at the cell surface after CAV1 depletion (1.4 ± 0.2, mean ± S.E.M, $n = 3$). BT biotinylation. **c** Western blot of biotinylated cell surface-associated HER2 in NCIN87 cells transfected with CAV1 siRNA or scrambled control siRNA constructs and blocking protein synthesis with 80 μg mL^{-1} CHX. CHX cyclohexamide. **d** Half-lives of cell surface-associated HER2 (mean ± S.E.M, $^*P < 0.05$ based on a Student's *t*-test, $n = 5$). **e**, **f** Western blot analysis of internalized HER2 (**e**) or cell surface-associated HER2 (**f**) on NCIN87 cells transfected with either control or CAV1 siRNA and treated with 1 μM trastuzumab. **g** Membrane-bound and internalized [^{89}Zr]Zr-DFO-trastuzumab before and after CAV1 knockdown or CAV1 depletion with methyl-β-cyclodextrin (MβCD) or filipin in NCIN87 cancer cells (bars, $n = 5$, mean ± S.E.M, $^{***}P < 0.001$ based on a Student's *t*-test). **h** NCIN87 cells transfected with CAV1 siRNA or scrambled control siRNA constructs were incubated with [^{89}Zr]Zr-DFO-trastuzumab (0 to 125 μM) for 3 h at 4 °C (upper panel). Specific binding of [^{89}Zr]Zr-DFO-trastuzumab (black circles, red squares) and non-linear regression curve fit (dotted lines). Data are presented as mean ± S.E.M, $n = 3$. Binding parameters (lower panel) of [^{89}Zr]Zr-DFO-trastuzumab to NCIN87 cells scrambled control, treated with CAV1 siRNA or with lovastatin ($^*P < 0.05$ based on a Student's *t*-test, $n = 5$). **i** Western blot of CAV1 and phosphorylated HER2 proteins from total extracts of NCIN87 cells incubated with 25 μM of lovastatin for 4 h. β-actin was used as a loading control. **j** Confocal images of immunofluorescence of HER2 in NCIN87 cells incubated with 1 μM trastuzumab for 90 min in the presence and absence of lovastatin. Scale bars: 20 μm

($P < 0.05$, Student's *t*-test) of HER2 at the cell membrane (Fig. 2c, d and Supplementary Fig. 3d, e) in NCIN87, UMUC14, and BT474 cancer cells. Knockdown of CAV1 in HER2-positive SKBR3 breast cancer cell line, did not impact the HER2 cell-surface half-life (Supplementary Fig. 3f) plausibly due to the low levels of caveolae in this cell line[31] (Supplementary Fig. 1a). In direct comparison, the membrane-bound HER2 half-life was 2.2-, 1.5-, and 2.0-fold higher in CAV1-depleted NCIN87, UMUC14 and BT474 cells, respectively.

Following trastuzumab binding, HER2 is internalized from the plasma membrane and accumulates in sorting endosomes. Thereafter, it can either recycle back to the cell surface or be degraded in the lysosomes[39]. We sought to investigate if decreased trastuzumab-mediated HER2 internalization could be achieved by a temporal and acute depletion of CAV1. To this end, trastuzumab was allowed to bind HER2 on NCIN87 cells treated with a scrambled (Scr) siRNA (control) vs. cells treated with a CAV1-depleting siRNA. The cells were allowed to undergo trastuzumab-mediated endocytosis for at least 90 min after surface biotinylation, and the internalized fraction of HER2 was evaluated via immunoblotting (Fig. 2e and Supplementary Fig. 4a). Incubation with trastuzumab depresses the surface pool of HER2 (Fig. 2f) as the receptor is internalized in a time-dependent manner. Notably, compared to scr cells, a marked decrease in HER2 endocytosis was observed in CAV1-depleted NCIN87 cells. Cellular fractionation of CAV1-depleted cancer cells treated with ^{89}Zr-labeled trastuzumab revealed a significant increase ($P < 0.001$, Student's *t*-test) in membrane-associated radioactivity (Fig. 2g and Supplementary Fig. 4b). Increased membrane-associated ^{89}Zr-labeled trastuzumab was also observed upon depletion of cholesterol using methyl-β-cyclodextrin (MβCD) and filipin (Fig. 2g and Supplementary Fig. 4b). Next, the binding profile of ^{89}Zr-labeled trastuzumab in competitive radioligand saturation-binding assays confirmed that CAV1 knockdown increased HER2 density on the cell membrane (B_{max}) (Fig. 2h and Supplementary Fig. 4c). Altogether, these data indicate that CAV1 depletion stabilizes HER2 at the cell membrane and improves the tumor avidity for trastuzumab on HER2-positive cancer cells.

CAV1 can be downregulated in vivo by lovastatin. Premised on our in vitro findings, we expected that HER2-positive tumors containing high levels of CAV1 would have a low surface pool of HER2. This in turn would impact the ability of trastuzumab to target and treat HER2-positive cancer cells. Therefore, we sought to investigate whether CAV1 depletion might result in an increased uptake of trastuzumab in tumor xenografts and human tumor samples. However, to date, there are no commercially available CAV1-specific modulators. Nevertheless, protein levels of CAV1 can be reduced by disruption of cholesterol-rich membrane domains using cholesterol-lowering drugs[30,39].

Lovastatin is one such commercially available drug that is prescribed worldwide to normalize lipid content in individuals having high blood cholesterol levels. In our study, lovastatin was used as a pharmacological modulator of CAV1. Previous studies have reported that 25 μM of lovastatin reduces the protein expression of CAV1 in vitro[40]. In our studies, the active form of lovastatin effectively depleted CAV1 expression in NCIN87 cells without altering phosphorylated HER2 levels (Fig. 2i). Thus, we further explored the potential role of lovastatin as a CAV1 modulator in the context of trastuzumab binding to NCIN87 cells. A potent role for the active form of lovastatin in increasing trastuzumab binding to cancer cells was also demonstrated via competitive radioligand saturation-binding assays (Fig. 2h and Supplementary Fig. 4c). These results seem to indicate that the increased binding of trastuzumab to HER2-positive cancer cells after treatment with lovastatin is a result of an overall increase in the binding between trastuzumab and HER2. Using fluorescence microscopy, trastuzumab was found not only on the surface of cancer cells, but also in intracellular vesicles (Fig. 2j and Supplementary Movie 1). However, in the presence of lovastatin, trastuzumab exhibited predominant membrane staining (Fig. 2j and Supplementary Movie 2). Lovastatin's inhibition of the enzyme 3-hydroxyl-3-methylgutarylcoenzyme A (HMG-CoA) reductase (HMGCR) is known to result in the decrease of mevalonate and its downstream products (e.g., cholesterol). In the presence of lovastatin, cells exhibited an increase in membrane-associated ^{89}Zr-labeled trastuzumab, an effect that is rescued by the addition of mevalonate to the cell culture (Fig. 3a and Supplementary Fig. 4d). Additional studies demonstrated that an increment in membrane cholesterol content has the opposite effect (Fig. 3a and Supplementary Fig. 4d). In sum, our findings suggest that lovastatin may be able to pharmacologically modulate HER2 endocytosis through a CAV1-mediated mechanism.

Further to these findings, we explored the efficiency of lovastatin to deplete CAV1 in NCIN87 xenografts. Two doses of lovastatin (8.3 mg kg^{-1} of mice), administered within 12 h of each other, was established as the most efficient treatment regimen that yielded a significant reduction in the total levels of CAV1 protein (Fig. 3b). Since the extracellular domain of HER2 is known to shed in vivo, we evaluated the impact of lovastatin treatment on this phenomenon. Specifically, treatment with lovastatin reduced HER2 shedding by approximately 50% in vitro using NCIN87 cells vs. 70% in NCIN87 xenografts (Fig. 3c). HER2 localization at the plasma membrane was increased in NCIN87 xenografts treated with lovastatin vs. saline-treated control mice (Fig. 3d–f and Supplementary Fig. 5). No further reduction of CAV1 concomitant with an increase in cell surface HER2 in tumors could be observed when mice were treated with lovastatin for longer than 60 h. Collectively, these results demonstrate that CAV1 can be temporally modulated in vitro and in vivo via pharmacological treatment with a statin.

CAV1 depletion increases tumor avidity for trastuzumab. To determine the impact of lovastatin-mediated CAV1 depletion on trastuzumab's binding to HER2-positive tumors, a pilot study was performed using separate bilateral xenografts of UMUC14 bladder cancer and NCIN87 gastric cancer (Supplementary Fig. 6). The active form of lovastatin (0.44 mg kg^{-1}) was injected into the tumor on the left flank while the right-flank tumor was used as a control (CT). To noninvasively monitor the effect of this treatment, mice were injected intravenously (i.v.) with ^{89}Zr-labeled trastuzumab at 4 h post-administration of lovastatin. An additional intratumoral injection of lovastatin was performed simultaneously with the injection of ^{89}Zr-labeled trastuzumab. Notably, there was a significant difference in the uptake of ^{89}Zr-labeled trastuzumab between the lovastatin vs. CT tumors (Supplementary Fig. 6a, b). At 48 h post-injection of ^{89}Zr-labeled trastuzumab, NCIN87 CT tumors had an uptake of 19.7 ± 11.8% ID g^{-1}, while tumors treated with lovastatin yielded an uptake of 41.6 ± 10.7 % ID g^{-1}. Similarly, the uptake of the radiotracer in UMUC14 xenografts was 13.6 ± 3.6% ID g^{-1} in CT tumors vs. 19.9 ± 3.6% ID g^{-1} in lovastatin-treated tumors (Supplementary Fig. 6c, d). The higher accumulation of trastuzumab in NCIN87 tumors vs. UMUC14 is a result of higher HER2 expression in NCIN87 cells (Supplementary Fig. 1a).

Encouraged by the results of this pilot study, we performed in vivo studies in mice bearing unilateral NCIN87 tumors (Fig. 4a and Supplementary Fig. 7). Since lovastatin is clinically prescribed

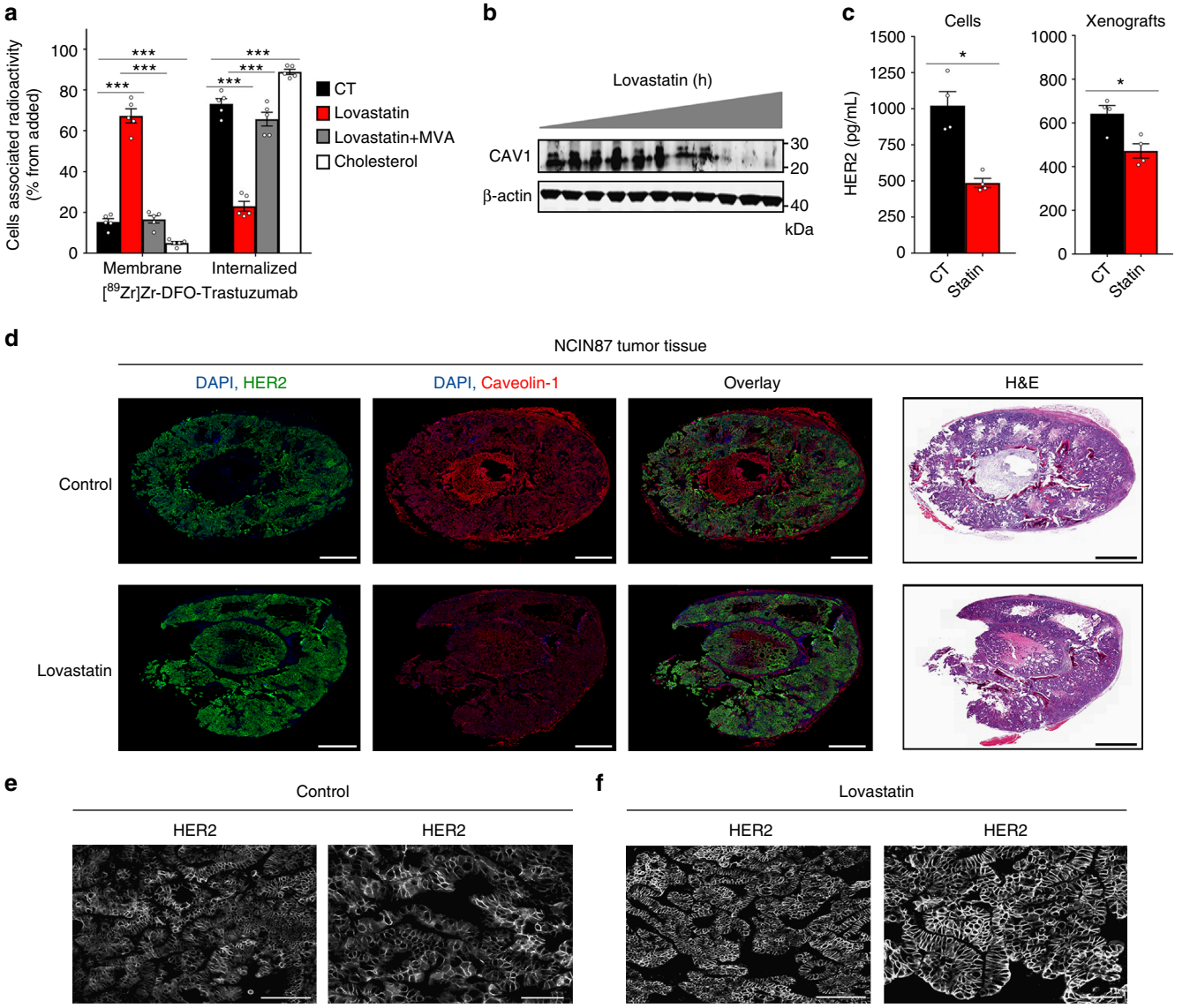
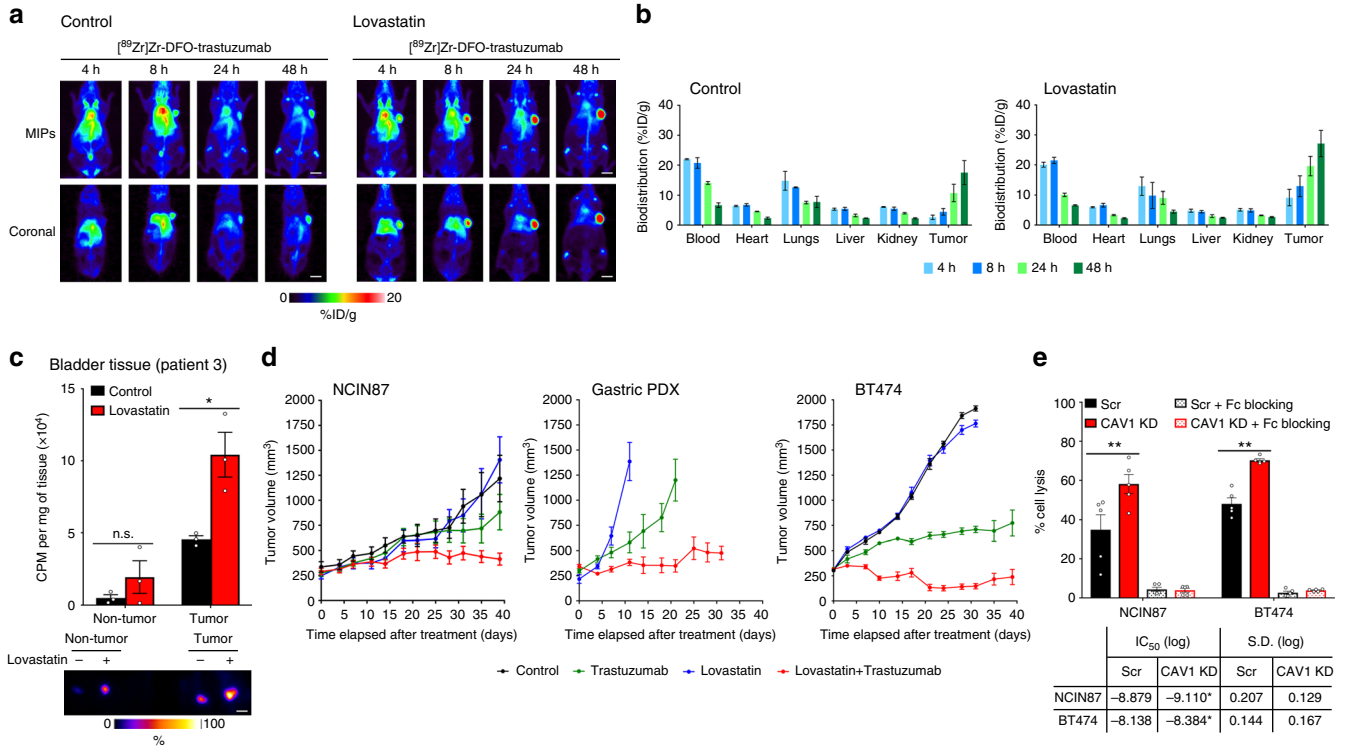


Fig. 3 In vivo CAV1 modulation with statin improves HER2 stability at the cell membrane. **a** Membrane-bound and internalized [^{89}Zr]Zr-DFO-trastuzumab before and after CAV1 depletion with 25 μM of lovastatin for 4 h in NCIN87 cancer cells. Increase in membrane-bound trastuzumab is rescued when cells are treated with lovastatin in the presence of 200 μM mevalonic acid (MVA). Treatment of NCIN87 cancer cells with a MβCD solution saturated with cholesterol increases [^{89}Zr]Zr-DFO-trastuzumab internalization (bars, $n = 5$, mean ± S.E.M, $^{**}P < 0.01$, $^{***}P < 0.001$ based on a Student's *t*-test, $n = 4$). **b** Western blot of CAV1 in the total lysates of NCIN87 s.c. tumors from athymic nude mice. Lovastatin (8.3 mg kg^{-1} of mice) was orally administrated twice with an interval of 12 h between each administration. Tumor lysates were prepared between 0 and 48 h after the second dose of lovastatin and analyzed by western blot. **c** Treatment with lovastatin decreases HER2 shedding as determined by ELISA experiments (bars, $n = 4$, mean ± S.E.M, $^{*}P < 0.05$ based on a Student's *t*-test). **d** Fluorescence staining (HER2 and CAV1) and H&E stain of tissue sections of s.c. NCIN87 gastric tumors from athymic nude mice. Lovastatin (8.3 mg kg^{-1} of mice) was orally administrated twice with an interval of 12 h between each administration. Tumor sections were prepared at 48 h after the first dose of lovastatin. Scale bars: 100 μm. **e**, **f** Lovastatin increases cell membrane HER2 in NCIN87 tumors. Confocal images of immunofluorescence staining of HER2 in s.c. NCIN87 gastric tumors from athymic nude mice, non-treated (**e**) or treated with lovastatin (**f**). Images are two representative sections of two different xenografts. Lovastatin (8.3 mg kg^{-1} of mice) was orally administrated twice with an interval of 12 h between each administration. Tumor sections were prepared at 48 h after the first dose of lovastatin. Scale bars: 100 μm (left) and 50 μm (right)

as an orally administered formulation, further studies were performed using oral administration of lovastatin 12 h prior and at the same time of trastuzumab injection. The 12 h window was chosen since immunoblotting and immunofluorescence data demonstrated that CAV1 was significantly reduced in the tumor with a concomitant increase in HER2 at the cell membrane at this time point (Fig. 3). Control mice were orally administered saline instead of lovastatin. Longitudinal PET imaging of these mice revealed tumors that were clearly delineated as early as 4 h post-injection of trastuzumab and yielded high contrast images at 48 h post-injection of the radiotracer (Fig. 4a). Ex vivo biodistribution studies further validated our findings from PET imaging (Fig. 4b). The saline-treated cohort yielded a radiopharmacologic profile typical of ^{89}Zr-labeled trastuzumab, which shows a gradual accretion into the HER2-positive tumors (2.6 ± 1.3% ID g^{-1} at 4 h to 17.5 ± 6.9% ID g^{-1} at 48 h). On the other hand, xenograft mice treated with lovastatin yielded a remarkably high tumor uptake of 9.1 ± 4.6% ID g^{-1} as early as 4 h post-injection of ^{89}Zr-labeled trastuzumab, which rose to 27.1 ± 7.6 at 48 h. High tumor-to-background ratios were achieved in mice pretreated



	IC_{50} (log)		S.D. (log)	
	Scr	CAV1 KD	Scr	CAV1 KD
NCIN87	–8.879	–9.110*	0.207	0.129
BT474	–8.138	–8.384*	0.144	0.167

Fig. 4 Statin treatment increases tumor uptake and efficacy of trastuzumab. **a** Representative coronal and MIPs PET images and **b** biodistribution data at 4, 8, 24, and 48 h p.i. of [^{89}Zr]Zr-DFO-trastuzumab in athymic nude mice bearing s.c. gastric tumors. Lovastatin (8.3 mg kg^{-1} of mice) was orally administrated 12 h prior and at the same time as the tail vein injection of [^{89}Zr]Zr-DFO-trastuzumab (8.14–10.18 Mbq, 80–100 µg protein). Bars, $n = 4$ mice per group, mean ± S.E.M. MIPs maximum intensity projection. %ID g^{-1}, percentage of injected dose per gram. Scale bars: 5 mm. **c** Uptake (upper panel) and autoradiography (lower panel) of [^{89}Zr]Zr-DFO-trastuzumab in organotypic cultures of non-tumor and tumor human bladder tissues. Organotypic cultures were incubated with 25 µM of lovastatin for 4 h prior and at the same time as the addition of [^{89}Zr]Zr-DFO-trastuzumab. Slices were harvested at 3 h after incubation with [^{89}Zr]Zr-DFO-trastuzumab. Bars, $n = 3$, mean ± S.E.M, *$P < 0.05$ based on a Student's *t*-test. CPM counts per minute. Scale bars: 500 µm. **d** Superior in vivo therapeutic efficacy of trastuzumab combined with lovastatin when compared with trastuzumab in *nu/nu* female mice bearing NCIN87 gastric and BT474 breast xenografts, and NSG mice bearing gastric PDXs ($n \geq 8$ mice per group). Intraperitoneal trastuzumab administration 5 mg kg^{-1} weekly (during 5 weeks) was started at day 0. Lovastatin (4.15 mg kg^{-1} of mice) was orally administrated 12 h prior and at the same time as the intraperitoneal injection of trastuzumab. **e** Ability of trastuzumab to mediate in vitro ADCC as determined with peripheral blood mononuclear cells (PBMCs) from healthy donors, in Scr and CAV1-depleted cancer cells (upper panel). Bars, $n = 5$, mean ± S.E.M, **$P < 0.01$ based on a Student's *t*-test. Trastuzumab IC_{50} response as determined with engineered Jurkat cells stably expressing the FcγRIIIa receptor, in Scr and CAV1-depleted cancer cells (lower panel)

with lovastatin (Supplementary Fig. 7a, b). The tumor uptake of a radiolabeled isotype control IgG was significantly low and comparable in both CT mice as well as those treated with lovastatin (Supplementary Fig. 7c). These results indicate that a temporal depletion of CAV1 by lovastatin increases cell surface HER2, which in turn enhances the avidity of HER2-positive tumors for trastuzumab and accelerates tumor uptake of ^{89}Zr-trastuzumab.

In addition to the conventional in vitro and in vivo studies, our findings were validated in organotypic cultures of fresh human bladder tumors. Tissues of HER2-positive bladder tumors were sliced immediately upon harvest during surgery, and grown in culture-plate inserts[41]. Viability assays of tumor slices revealed no significant loss of viable cells (Supplementary Fig. 8a, b) during 96 h of ex vivo culture ($P < 0.05$, Student's *t*-test). After ex vivo treatment with the active form of lovastatin, the tumor slices showed an increased uptake of ^{89}Zr-trastuzumab ($P < 0.05$, Student's *t*-test; Fig. 4c). In non-tumor bladder tissue, lovastatin treatment did not significantly increase tissue accumulation of ^{89}Zr-trastuzumab. Western blot analysis revealed a decrease in CAV1 protein expression after lovastatin treatment (Supplementary Fig. 8c), lending further support to our central hypothesis that temporal CAV1 depletion increases trastuzumab binding to HER2-positive tumors. Additionally, through this experiment, we were able to demonstrate the utility of organotypic cultures as a potential ex vivo biological model to study the accumulation of target-specific radiolabeled antibodies in clinically relevant tumor tissues.

CAV1 depletion enhances trastuzumab therapeutic efficacy. To assess the efficacy of trastuzumab treatment when combined with CAV1 depletion in vivo, we conducted therapy studies in mice bearing NCIN87 gastric and BT474 breast, and gastric cancer PDXs. The gastric PDX model was established by implantation of HER2-positive and CAV1-positive gastric tumor tissue from Patient 1 (Fig. 1d) in immunodeficient NOD-SCID gamma (NSG) mice. Mice were treated weekly with 5 mg kg^{-1} of trastuzumab for 5 weeks. Two doses of lovastatin (4.15 mg kg^{-1}) were orally administrated 12 h prior and at the same time as the intraperitoneal injection of trastuzumab. No difference was seen between the vehicle and lovastatin groups (Fig. 4d). Mice treated with either trastuzumab alone or trastuzumab combined with lovastatin showed tumor growth inhibition. However, the therapeutic efficacy of trastuzumab combined with lovastatin was significantly improved compared with trastuzumab alone. Taken

together, these results show that the in vivo therapeutic efficacy of trastuzumab is remarkably improved when the tumors are temporally depleted of CAV1—despite the latter being a transient effect.

One of the mechanisms of action of trastuzumab is by inducing tumor cell death via ADCC. A prerequisite to this phenomenon is the binding of trastuzumab to HER2 on tumor cells. Thus, trastuzumab-mediated ADCC is an effect that is closely related with HER2 density at cell membrane[42]. We attempted to study in vitro ADCC upon CAV1 depletion in NCIN87 gastric and BT474 breast cancer cells (T) using peripheral blood mononuclear cells (PBMCs) from healthy donors and engineered Jurkat cells as effector cells (E) that stably express the FcγRIIIa receptor. CAV1-depleted NCIN87 and BT474 cancer cells showed increased in vitro ADCC when PBMCs were used as effector cells (E:T ratio = 50:1, Fig. 4e). When engineered Jurkat cells were used as effector cells, CAV1 depletion in NCIN87 and BT474 cancer cells resulted in a decrease in IC_{50} values (E/T = 15:1, Fig. 4e and Supplementary Fig. 9).

Discussion

Endocytosis of receptors of the EGFR family is a complex biological process that remains to be completely understood. Nevertheless, intrinsic defects in this process have been demonstrated to influence therapeutic outcomes in EGFR-directed therapies[25,34,43]. Treatment of HER2-positive tumors with trastuzumab is premised on the presence of HER2 on the membrane of tumor cells. Therefore, the stability and availability of cell surface HER2 is an important predictor of trastuzumab efficacy. In the work at hand, we show that CAV1 knockdown reduces HER2 internalization and extends the half-life of HER2 at the cell membrane while concomitantly decreasing HER2 shedding without altering HER2 activity. Furthermore, accumulation of cell surface HER2 in response to pharmacological depletion of CAV1 was observed using preclinical xenograft models and organotypic cultures derived from freshly harvested human tumors. The discovery that CAV1 modulates cellular distribution of HER2 may have direct therapeutic implications for antibody-mediated targeting of HER2 and the use of such antibodies for molecular imaging and therapy of HER2-positive tumors.

CAV1 has been shown to regulate downstream signaling by members of the HER family[19,20,23,44] and interferes with the uptake/activity of a wide variety of antibodies or ADCs targeting the HER family[29,36,44–46]. Here, we show that the inverse correlation between cellular expression of CAV1 and HER2 directly affects the stability and localization of HER2 on the cell membrane. Our findings are supported by other reports that show CAV1 interaction with signaling molecules such as epidermal growth factor (EGF)[45,46]. Others have also previously demonstrated that although EGF is a ligand for its cognate receptor—EGFR, EGF treatment promotes the formation of heterodimers between EGFR and HER2, which activates HER2[47]. Further studies are necessary to evaluate the consequences of lovastatin treatment on the dimerization status of HER2.

Indeed, HER2 localization at the cell membrane is the product of a highly dynamic process[23] involving endocytosis, cytoplasmic recycling, and de novo synthesis. Furthermore, the membrane localization of HER2 is heterogeneous within tumors (Fig. 1b, c). Previous studies have reported that even at the single-cell level, individual HER2 molecules do not function in a uniform manner[48], and that this non-uniform behavior contributes to receptor heterogeneity. Equipped with this information, we analyzed patient tumor samples using immunofluorescence to understand how CAV1 expression patterns may relate to the cellular localization of HER2. Not surprisingly, a higher cell surface localization of HER2 was found in human tumor tissues containing low levels of CAV1 (Fig. 1d). Conversely, tumors containing high levels of CAV1 had a low amount of HER2 localized at the cell membrane (Fig. 1d). Of course, a prerequisite for trastuzumab binding to HER2 is the latter's presence on the surface of a cancer cell and not within intracellular compartments. Taken together, these observations led us to hypothesize that CAV1 expression can be leveraged as a complementary biomarker to identify patients who would or would not benefit from HER2-targeted therapy with trastuzumab. Our findings in this study support previous reports that are suggestive of CAV1's role in the therapeutic response to HER2-targeted therapies[35,36,44,49,50]. Our studies clearly establish that downregulation of CAV1 increases HER2 availability at the cell surface.

Receptor-mediated endocytosis of ADCs such as TDM1 is central to the mechanism of action of this class of drugs. Indeed, the internalization of ADCs precedes the release of the cytotoxic drug within the lysosomal compartment of the cell, leading to cell death and manifestation of tumor regression. Others have demonstrated that the addition of nuclear localization sequence (NLS) peptides to trastuzumab labeled with an auger electron-emitter increases the internalization and nuclear localization of the antibody to decrease clonogenic survival of tumor cells[51] as well as to overcome insulin-like growth factor(IGF)-receptor-induced trastuzumab resistance in breast cancer cells[52]. In light of these reports, it would seem counter-productive to prevent HER2 internalization via pharmacological depletion of CAV1, as this might reduce the therapeutic benefit of HER2-directed ADCs. However, our data suggests that the temporal modulation of CAV1 extends the half-life of HER2 at the tumor cell surface to enhance the tumor's avidity for trastuzumab. The presence of such a target-rich sink could ultimately drive the in vivo pharmacokinetics of trastuzumab in favor of target-mediated drug disposition—leading to a significantly enhanced accumulation of trastuzumab in the tumor at early time points. Finally, being a transient and temporally controlled phenomenon that occurs under the influence of a pharmacological modulator of CAV1, normalization of the cellular distribution of HER2 including receptor-mediated internalization of the antibody bound to it would occur once the transient in vivo effect of the CAV1 modulator has worn out. Our finding that CAV1 depletion improves trastuzumab therapy, suggests that temporal modulation of CAV1 by a statin could be a strategy that can be applied in the clinic to improve trastuzumab binding/therapy for the treatment of HER2-positive tumors (Fig. 4). Admittedly, despite the successful in vitro demonstration of an effective trastuzumab-mediated ADCC potentiated by treatment with lovastatin, we realize that ADCC may not be a predominant mechanism of action contributing to the therapeutic efficacy of trastuzumab and/or combination of trastuzumab with lovastatin in our preclinical in vivo studies, since these experiments were performed using immunodeficient mice.

Statins, methyl-β-cyclodextrin, filipin, nystatin, and cholesterol oxidase are well known pharmacological inhibitors of caveolae/lipid-raft mediated endocytosis. Additionally, selective inhibition of lipid-raft/caveolae-mediated endocytosis can be achieved via acute depletion of the plasma membrane cholesterol. Depletion of cholesterol with methyl-β-cyclodextrin has been shown to release EGFR from lipid rafts, which increases the binding of iodine-125 (^{125}I)-labeled EGF[53]. Others have shown that cholesterol contributes to the cellular dynamics of HER2 and EGFR[33]. Here, we demonstrate that the bioavailability of HER2 at the cell membrane can be modulated via temporal depletion of cholesterol by lovastatin in ways that could serve to enhance trastuzumab binding and therapy against HER2-positive tumors (Figs. 3 and 4). For example, a reduction in the in vivo shedding of HER2

from proteolytic cleavage by sheddases might contribute to our observations of increased trastuzumab accumulation in HER2-positive tumors (Fig. 3c). HER2 shedding generates soluble truncated HER2 molecules in the serum[54]. ^{89}Zr-labeled trastuzumab has been proposed to bind the shed extracellular domain of HER2[55], which contains the binding site for trastuzumab. Notably, cholesterol depletion from cell membranes alters the function of enzymes with sheddase activity[56]. Taken together with our findings, it may be plausible that increased trastuzumab accumulation in membrane-bound fractions may also be a result of decreased shedding of HER2.

Despite being an effective modulator of CAV1 in our experiments, lovastatin is a lactone pro-drug that is plagued by poor oral bioavailability (< 5%) owing to its lipophilic nature[57]. After oral administration, lovastatin undergoes extensive first-pass metabolism and is hydrolyzed to the active beta-hydroxyacid form, which competitively inhibits HMGCR. HMGCR is the rate-limiting enzyme of cholesterol synthesis and is deregulated or elevated in several tumor types[58]. The bioavailability of lovastatin in systemic circulation is low and variable. It has a plasma half-life of 1.1–1.7 h, and takes approximately 2 to 4 h to reach maximum concentration in circulation. Only after metabolism and re-entry into systemic circulation, does lovastatin stand a chance to reach the tumor. The maximum human dose of lovastatin is 80 mg per day (1.33 mg kg^{-1} per day for a 60 kg adult). The doses of lovastatin used in our imaging and therapy studies— 8.33 and 4.15 mg kg^{-1}—correspond to human equivalent doses of 0.68 and 0.34 mg kg^{-1}, which are significantly lower than the maximum recommended daily dose in humans. Previous preclinical studies have demonstrated the therapeutic potential of lovastatin per se using doses between 5 to 10 mg kg^{-1} [59]. In our study, lovastatin was able to decrease CAV1 protein levels and increase cell membrane HER2 after 12 h of oral administration (Fig. 3). The low bioavailability of lovastatin and its short half-life suggests that a limited fraction of lovastatin would have reached the tumor after oral administration. It is expected that a more specific and efficient delivery of lovastatin to the tumors might further improve HER2 localization at the cell surface. Indeed, our findings support the surge in the interest for the use of statins for cancer treatment and the potential benefits thereof[41,58,60]. Since many cancer patients use statins, our data provides a rationale to pursue a clinical study combining lovastatin with trastuzumab to evaluate if this combination might positively affect the therapeutic outcomes or imaging strategies using trastuzumab in HER2-positive patients.

From the perspective of immunoPET, our study presents a major advance in the field of molecular imaging. Traditionally, the sluggish in vivo pharmacokinetics of full-length antibodies has necessitated their radiolabeling with long-lived positron-emitting radionuclides such as zirconium-89 ($t_{1/2}$ = 78.2 h) to yield high contrast images between 72–120 h post-injection of the radioimmunoconjugate tracer. However, this manifests as a logistical inconvenience requiring patients to return to the clinic for a PET scan 4–5 days after they have been injected with the tracer[6]. However, we were able to obtain high contrast PET images as early as 4 h post-injection of ^{89}Zr-radiolabeled trastuzumab in HER2-positive tumors wherein CAV1 was pharmacologically modulated by using lovastatin (Fig. 4). Such an accelerated accumulation of ^{89}Zr-labeled trastuzumab is of tremendous clinical relevance from the standpoint of being able to overcome the current pharmacokinetic limitation of full-length antibodies to achieve same- to next-day immunoPET imaging in patients. This aspect further supports the rationale for combining a cholesterol-lowering drug such as a statin with trastuzumab to facilitate a relatively rapid turnaround time for the diagnosis of HER2-positive tumors via molecular imaging with full-length antibodies.

In conclusion, our study establishes the inverse relationship between CAV1 expression and HER2 localization at the cell membrane, and how this relationship can be pharmacologically modulated to augment HER2-targeted therapy of various cancers. Our findings suggest that CAV1 can be a promising biomarker to select patients for trastuzumab therapy. Finally, our preclinical data demonstrate the potential benefit of using statins to improve the therapeutic efficacy of trastuzumab and advance HER2-targeted molecular imaging in the clinic.

Methods

Cell lines and patient samples. Gastric human cancer cell lines NCIN87 and KATOIII, breast cancer cell lines MDA-MB-231, SK-BR-3, MCF-7, and BT474 were purchased from American Type Culture Collection (ATCC). The human bladder cancer cell line, UMUC14, was obtained from Sigma-Aldrich. All cell lines were mycoplasma free and maintained at 37 °C in a humidified atmosphere at 5% CO_2. Cell lines utilized in this work were purchased in 2014–2016, and they were used within passage number of 15. All the cell lines were authenticated at Memorial Sloan-Kettering Cancer Center (MSKCC) integrated genomics operation core using short tandem repeat analysis. Deidentified patient gastric and bladder cancer samples were obtained from Memorial Hospital following IRB approval. PBMCs, obtained from the Immune Monitoring Facility at MSKCC, were separated from the blood of normal volunteers using lymphocyte separation medium (MP Biomedicals). Patients provided informed consent.

Cell culture. NCIN87 cells were grown in Roswell Park Memorial Institute (RPMI)-1640 growth medium supplemented with 10% fetal calf serum (FCS), 2 mM L-glutamine, 10 mM hydroxyethyl piperazineethanesulfonic acid (HEPES), 1 mM sodium pyruvate, 4.5 g L^{-1} glucose and 1.5 g L^{-1} sodium bicarbonate. KATOIII cells were grown in Iscove's Modified Dulbecco Medium (IMDM) growth medium supplemented with 20% FCS and 1.5 g L^{-1} sodium bicarbonate. UMUC14 cells were grown in Minimum Essential Media (MEM) growth medium supplemented with 10% FCS, non-essential amino acids (NEAA), 2 mM L-glutamine, 1 mM sodium pyruvate, and 1.5 g L^{-1} sodium bicarbonate. MDA-MB-231 cells were grown in Dulbecco's Modified Eagle's Medium-high glucose (DMEM-HG) supplemented with 10% FCS. SKBR3 cells were grown in McCoy's medium supplemented with 10% FCS, 1.5 mM glutamine, 2.2 g L^{-1} sodium bicarbonate. MCF-7 cells were grown in Eagle's Minimum Essential Medium (EMEM) supplemented with 0.01 mg mL^{-1} of human recombinant insulin and 10% FCS. BT474 cells were grown in a 1:1 mixture of DMEM:F-12 medium, supplemented with 10% FCS, 2 mM glutamine, NEAA. All cell culture media were supplemented with 100 units mL^{-1} penicillin and streptomycin.

Organotypic cultures of fresh human bladder tissues. Fresh biopsy samples of bladder tissues were obtained immediately after surgical resection by the tissue procurement services at MSKCC. Normal and tumor bladder tissues were kept in organotypic cultures[41]. Tissue specimens were placed in Ham F-12 media supplemented with 20% inactivated FCS, 100 U mL^{-1} penicillin, 100 µg mL^{-1} streptomycin, 2.5 µg mL^{-1} amphoterycin B, and 100 µg mL^{-1} of kanamycin. A Vibratome (Vibratome VT1200; Leica) was used to cut thin slices (300–500 µm) from biopsy specimens. Samples were soaked in ice-cold phosphate-buffered saline buffer (PBS) and immobilized using cyanoacrylate glue on the Vibratome platform. Tissue slices were cultured on organotypic inserts (Millipore) for up to 96 h at 37 °C in a 5% CO_2 humidified incubator. Five tissue slices were harvested at baseline time (T0) and thereafter, at 24 h intervals for viability assays using 1-(4, 5-dimethyltiazol-2-yl)-3, 5-diphenylformazan (MTT, Sigma-Aldrich) and CellTiter-Glo 3D (Promega) assays. For the MTT assay, tissue slices were incubated with 5 mg mL^{-1} of MTT at 37 °C for 4 h, harvested, and the precipitated-salt extracted by incubation with 0.1 M hydrochloric acid (HCl)-isopropyl alcohol at room temperature for 25 min. A viability value was obtained by dividing the optical density of the formazan at 570 nm by the weight of the explants. Tissue viability was expressed as percentage of viability relative to that of samples at T0. For the CellTiter-Glo 3D cell viability assay, tissues were incubated with 100 µL of the CellTiter-Glo 3D reagent on a plate shaker for 5 min, followed by incubation for 30 min at room temperature. A viability value was obtained by dividing the luminescence signal by the weight of the explants.

Transfection assays. CAV1 was depleted using a pool of three target-specific 20–25 nt siRNA (Santa Cruz Biotechnology). Cancer cells were transfected in 6-well culture plates, at 60–80% confluence, with siRNA CAV1. Cells were also transfected with a scr siRNA in parallel as controls. For each transfection, cells were treated for 5 h with 2.4 µM of siRNA in transfection medium (Santa Cruz) containing 0.5 µL cm^{-2} of transfection reagent (Santa Cruz).

CAV1 was amplified in cancer cells using CRISPR activation plasmid (h, Santa Cruz). Cancer cells were transfected in 6-well culture plates, at 60–80% confluence, with CRISPR Activation Plasmid CAV1. For each transfection, cells were treated for 5 h with 0.9 ng μL^{-1} of CRISPR Activation Plasmid CAV1 in transfection medium (Santa Cruz) containing 0.5 $\mu L\ cm^{-2}$ of transfection reagent (Santa Cruz).

After incubation with siRNA CAV1 or CRISPR Activation Plasmid CAV1, complete media was added and the cells were incubated for 48 h. CAV1 downregulation or upregulation was evaluated 48 h post-transfection by western blotting.

Further experiments, to determine the effects of CAV1 depletion or amplification on HER2 stability at the cell membrane, were performed at 48 h post-transfection.

Western blot analysis. Whole-protein extracts from cells or tumors were prepared after cell scrapping or tissue homogenization, respectively, in radioimmunoprecipitation assay buffer [RIPA buffer: 150 mM sodium chloride (NaCl), 50 mM Tris hydrochloride (Tris-HCl), pH 7.5, 5 mM ethylene glycol tetraacetic acid (EGTA), 1% Triton X-100, 0.5% sodium deoxycholate (DOC), 0.1% sodium dodecyl sulfate (SDS), 2 mM phenylmethanesulfonyl (PMSF), 2 mM iodoacetamide (IAD), and 1 × protease inhibitor cocktail (Roche)]. After centrifugation at 16,000×*g* for 10 min at 4 °C, supernatants were used for protein quantification as determined with the Pierce BCA Protein Assay Kit (Thermo Fisher Scientific), followed by denaturation of the sample with Laemmli buffer. Following electrophoresis and transfer to polyvinylidene difluoride (PVDF) membranes (Bio-Rad), the blots were incubated in 5% (m/v) BSA in Tris-buffered saline buffer-Tween (TBS-T, Cell Signaling Technology) and probed with mouse anti β-actin 1:20,000 (Sigma, A1978), rabbit anti-HER2 1:800 (Abcam, ab131490), rabbit anti-HER2 phospho Y1139 1:500 (Abcam, ab53290), and rabbit anti-CAV1 1:500 (Abcam, ab2910) antibodies. After washing, the membranes were incubated with IRDye®800CW anti-Rabbit or anti-Mouse IgG 1:15,000 (LI-COR Biosciences) and imaged on the Odyssey Infrared Imaging System (LI-COR Biosciences) followed by densitometric analysis. Supplementary information contains uncropped scans of the blots shown in the figures.

Biotin pull down of cell-surface proteins. For biotin pull down assays, cells were washed twice with ice-cold PBS buffer containing 0.5 mM magnesium chloride ($MgCl_2$) and 1 mM calcium chloride ($CaCl_2$). Cells were incubated with 0.5 mg mL^{-1} of EZ-LINK Sulfo-Biotin (Thermo Fisher Scientific) for 30 min at 4 °C with gentle rotation. The reaction was stopped by washing twice with 100 mM glycine (Thermo Fisher Scientific) in PBS containing 0.5 mM $MgCl_2$ and 1 mM $CaCl_2$. Cells were scrapped in RIPA buffer, lysates were centrifuged at 16,000×*g* for 10 min at 4 °C, and supernatants were collected and assayed for protein concentration using the Pierce BCA Protein Assay Kit. A volume of 500 µL of RIPA buffer containing equal amount of proteins was incubated with NeutrAvidin Agarose Resins (Thermo Fisher Scientific) for 2 h at 4 °C with gentle rotation and washed three times with RIPA buffer before suspension in Laemmli buffer.

Isolation of caveolae-rich fractions. Isolation of caveolae-rich fractions was done by discontinuous sucrose gradient (5−80% v/v) centrifugation using a caveolae/rafts isolation kit (Sigma-Aldrich). The gradient was centrifuged in a swing bucket rotor TH-641 (Sorvall) at 200,000×*g* for 4 h at 4 °C. Fractions were collected from the top to the bottom of the tube and analyzed by western blot.

Endocytosis of biotinylated cell-surface proteins. Following cell-surface biotinylation, endocytosis was initiated by the addition of pre-warmed cell culture medium in the presence of 1 µM trastuzumab at 37 °C for 15, 30, 60, and 90 min. Endocytosis was stopped by incubation of cells on ice for 10 min. For removal of non-internalized cell-surface biotin, cells were incubated with 50 mM Tris-HCl pH 8.7 [containing 20 mM dithiothreitol (DTT), 100 mM NaCl, 2.5 mM $CaCl_2$] for 20 min at 4 °C. Cells were rinsed with ice-cold PBS and scrapped in RIPA buffer. Biotinylated cell-surface HER2 was collected in NeutrAvidin Agarose Resins as described above.

Protein–protein associations. HER2 protein expression was correlated with CAV1 expression (using data from Cancer Cell Line Encyclopedia[37] or densitometric measurements of Western blot analysis) using a Spearman's rank correlation. Additionally, the STRING database (string-db.org) was used to determine HER2 protein – CAV1 protein interactions. High-confidence associations (score ≥ 0.700) were used to estimate the accuracy of the protein–protein networks.

Immunofluorescence microscopy. For immunocytochemistry, cells grown on coverslips were incubated with 1 µM trastuzumab for 90 min at 37 °C in the presence and absence of the active form of lovastatin. Cells were incubated with 25 µM of lovastatin for 4 h prior and at same time as the addition of trastuzumab. Cells were then permeabilized with 1% Triton X-100 in PBS (pH 7.4) and blocked with 5% bovine serum albumin in PBS buffer, before incubation with the DAPI and secondary fluorescent antibody goat anti-human IgG.

Immunofluorescence staining of HER2 and CAV1 were carried out on formalin-fixed, paraffin-embedded sections (10 µM) sections of human gastric tumors and NCIN87 s.c. tumors. Sections were submitted to MSKCC Molecular Cytology Core Facility for HER2, CAV1, hematoxylin and eosin staining.

Cholesterol enrichment and caveolae depletion. To enrich membrane cholesterol, cancer cells were exposed to methyl-β-cyclodextrin (MβCD, Santa Cruz Biotechnology) solution saturated with cholesterol[61] for 30 min before addition of trastuzumab. To inhibit caveolae-mediated pathways, cells were incubated with 2.5 mM MβCD or 0.5 µg mL^{-1} filipin (Santa Cruz Biotechnology) for 30 min before addition of trastuzumab. For in vitro experiments with lovastatin, cells were incubated with 25 µM of the active form of lovastatin (Millipore) for 4 h prior addition of trastuzumab[40]. To determine whether mevalonic acid treatment rescued the lovastatin effect, the cell lines were treated with 25 µM lovastatin and 200 µM of R-Mevalonic Acid (Santa Cruz Biotechnology) for 4 h[62]. Cells were then treated with 1 µM [^{89}Zr]Zr-DFO-trastuzumab for 1.5 h.

Conjugation and radiolabeling of trastuzumab. Conjugation of trastuzumab with Indocyanine Green (ICG) was performed by incubation of trastuzumab with ICG at a molar ratio of 1:6 in 0.1 M Na_2HPO_4 (pH 8.6) at room temperature for 1.5 h, followed by purification with a size exclusion column (PD-10; GE Healthcare, Piscataway, NJ, USA). The concentration of ICG was calculated by measuring the absorption with the UV–Vis system to confirm the number of fluorophore molecules conjugated with each antibody molecule. The protein concentration was also determined by measuring the absorption at 280 nm with a UV–Vis system. BT474 CT and statin treated cells were incubated with trastuzumab—ICG conjugate and submitted to the Molecular Cytology Core Facility for live cell imaging.

Conjugation and radiolabeling of human IgG (Sigma-Aldrich) or trastuzumab with zirconium-89 (^{89}Zr) was achieved using the bifunctional chelate *p*-isothiocyanatobenzyl-desferrioxamine (DFO-Bz-NCS; Macrocyclics, Inc)[8]. Zirconium-89 was produced via proton beam bombardment of yttrium foil and isolated with high purity as ^{89}Zr-oxalate at MSKCC[63].

Internalization and saturation-binding assays. For the internalization assays with [^{89}Zr]Zr-DFO-trastuzumab, cells were incubated with cell culture medium in the presence of 1 µM [^{89}Zr]Zr-DFO-trastuzumab for 90 min at 37 °C. Media containing non-cell-bound radiotracer was removed and the cells were washed twice with PBS. Cell surface-bound radiotracer was collected by cells incubation at 4 °C for 5 min in 0.2 M glycine buffer containing 0.15 M NaCl, 4 M urea at pH 2.5. Internalized fraction was obtained after cell lysis with 1 M sodium hydroxide (NaOH). Finally, the three fractions were measured for radioactivity on a gamma counter calibrated for ^{89}Zr.

For the saturation-binding assays, cells were incubated with [^{89}Zr]Zr-DFO-trastuzumab (0–128 nM) in PBS (pH 7.5) containing 1% (m/v) human serum albumin (Sigma) and 1% (m/v) sodium azide (Acros Organics) for 3 h at 4 °C. Unbound radioactivity was removed and cells were washed three times with PBS. The cells were solubilized in 100 mM NaOH, recovered, and the total cell-bound radioactivity was measured on a gamma counter calibrated for ^{89}Zr. Total binding was plotted vs. the concentration of [^{89}Zr]Zr-DFO-trastuzumab; the data were fit via non-linear regression with a one-site binding model in GraphPad Prism 7.00 to determine B_{max}, K_D and the non-specific binding component. The non-specific component was subtracted from the total binding to generate specific binding curves (Fig. 2h).

Uptake in organotypic cultures and autoradiography. Slices of normal and tumor bladder tissues ($n = 4$) were harvested after 48 h of ex vivo culture and incubated with 25 µM of the active form of lovastatin for 4 h prior and at the same time as the addition of 1 µM [^{89}Zr]Zr-DFO-trastuzumab. Slices were harvested at 3 h after incubation with [^{89}Zr]Zr-DFO-trastuzumab, washed with PBS (pH 7.5) containing 0.1% (m/v) bovine serum albumin (BSA), air dried, weighed, and counted in a gamma counter calibrated for ^{89}Zr. For autoradiography, slices were mounted in glycergel mounting medium, placed in a film cassette against phosphor imaging plate (Fujifilm BAS-MS2325; Fuji Photo Film) for 10 min at −20 °C. Phosphor imaging plates were read at a pixel resolution of 25 µm with a Typhoon 7000 IP plate reader (GE Healthcare).

In vitro antibody-dependent cellular cytotoxicity (ADCC). Scr or CAV1-depleted NCIN87, UMUC14, BT474, and SK-BR-3 cancer cells (1.7×10^4) were preincubated with trastuzumab (1 µM) for 1.5 h at 37 °C in serum-free cell culture medium supplemented with 0.1% BSA before adding the effector cells in 1:1, 10:1, 25:1, or 50:1 effector (E) to target (T) ratios. PBMCs were used as effectors and cancer cells as targets. The cells were incubated for additional 48 h before determination of cell death using the Cytotoxicity Detection Kit (LDH; Roche). The percentage of cytotoxicity was calculated as follows: % cytotoxicity (experimental lysis−spontaneous effector lysis – spontaneous target lysis)/(maximum target lysis −spontaneous target lysis) × 100. Control Fc gamma receptor (FcγR) blocking studies were performed by pretreating PBMCs with 10 µg mL^{-1} of human isotype IgG for 1 h before adding them to cancer cells in a ratio of 50:1.

Additional ADCC experiments were performed with the ADCC Reporter Bioassay, Core Kit (Promega), according to manufacture instructions. Briefly, Scr or CAV1 depleted NCIN87, UMUC14, BT474 and SK-BR-3 cancer cells were plated at the density of 5,000 cells/well in complete culture medium overnight before bioassay. On the day of the assay, the medium was removed, and then the series of concentrations of trastuzumab (0–10,000 ng mL^{-1}) were added to the cells, followed by addition of ADCC Bioassay Effector Cells (engineered Jurkat cells that stably express the FcγRIIIa receptor). The E:T ratio was 15:1, according to manufacture instructions. After 6 h of induction, luciferase assay reagent was added and luminescence determined using a luminometer. The data were fitted to a 4PL curve using GraphPad Prism software.

Tumor xenografts. All animals were treated according to the guidelines approved by the Research Animal Resource Center and Institutional Animal Care and Use Committee at Memorial Sloan Kettering Cancer Center, NY. Pereira PMR has a Category C accreditation for animal research given from Federation of European Laboratory Animal Science (FELASA). We adhere to the animal research: reporting of in vivo experiments (ARRIVE) guidelines and to the guidelines for the welfare and use of animals in cancer research. Eight- to 10-week-old *nu/nu* female mice (Charles River Laboratories) were injected subcutaneously with 2.5 million UMUC14, 5 million NCIN87 cells, or 5 million BT474 in a 150 µL cell suspension of a 1:1 (v/v) mixture of medium with reconstituted basement membrane (BD Matrigel, BD Biosciences). Drinking water of mice receiving estrogen receptor-positive cells BT474 was supplemented with 0.67 µg mL^{-1} 17β-estradiol (Sigma) from 1 week in advance of inoculation until scarified. Fresh-estradiol supplemented water was provided twice a week. The mice were housed in type II polycarbonate cages, fed with sterilized standard laboratory diet and received sterile water ad libitum. The animals were housed at approximately 22 °C, 60% relative humidity, and a 12 h light, 12 h dark cycle was maintained. After arrival, all mice were allowed to acclimate to the facility's laboratory conditions for 1 week prior to experimentation.

Mice-bearing bilateral tumors were developed by subcutaneous injection of cancer cells on the bilateral dorsal flank regions using a sterile syringe with a 28-gauge needle. For experiments with mice-bearing unilateral tumors, cancer cells were subcutaneously injected on the right shoulder. The tumor volume (V/mm^3) was estimated by external vernier caliper measurements of the longest axis, α/mm, and the axis perpendicular to the longest axis, b/mm. The tumors were assumed to be spheroidal and the volume was calculated in accordance with the equation $V = (4\pi/3)$ x $(\alpha/2)^2$ x $(b/2)$.

An intratumoral injection of the active form of lovastatin (0.44 mg kg^{-1} of mice) was performed in the pilot study with mice-bearing bilateral tumors. In further experiments with mice-bearing unilateral tumors, lovastatin was orally administered (8.3 mg kg^{-1} of mice). The doses of lovastatin used in our study were lower when compared with the human maximum dose (80 mg per day): the 0.44 mg kg^{-1} and 8.3 mg kg^{-1} of mice doses correspond to daily human doses of 2.15 and 40.14 mg assuming an average human body weight of 60 kg. It should be noted that the intratumoral dose 0.44 mg kg^{-1} of lovastatin was defined as 5% of oral dose 8.3 mg kg^{-1} of mice, assuming 5% lovastatin bioavailability after oral administration.

When the volume of xenografts reached approximately 100 mm^3, mice were randomized into groups and treatments initiated. The active form of lovastatin (0.44 mg kg^{-1} of mice) was intratumorally injected into the left-sided tumor of mice-bearing bilateral tumors (four mice per group) 4 h prior and at the same time as the tail vein injection of [^{89}Zr]Zr-DFO-trastuzumab (8.14–10.18 Mbq, 80–100 µg protein). The right-sided tumor was used as the CT and it was intratumorally injected with PBS.

For experiments in mice-bearing unilateral tumors, mice were randomly assigned into the following groups ($n = 4$ mice per group): *Group I*, oral administration of PBS 12 h prior to and at the same time as the tail vein injection of [^{89}Zr]Zr-DFO-trastuzumab (8.14–10.18 Mbq, 80–100 µg protein); *Group II*, oral administration of lovastatin (8.3 mg kg^{-1} of mice) 12 h prior to and at the same time as the tail vein injection of [^{89}Zr]Zr-DFO-IgG (8.14–10.18 Mbq, 80–100 µg protein).

Patient-derived xenograft (PDX) mouse models. PDX models were established, by the Anti-tumor Assessment Core, from tumor specimens collected under an approved institutional review board protocol by the Research Animal Resource Center and Institutional Animal Care and Use Comittee at Memorial Sloan Kettering Cancer Center, NY. Briefly, tumors were minced, mixed with Matrigel, and implanted subcutaneously in 6- to 8-week-old female NSG mice (Jackson Laboratories). Once established, tumors were maintained and expanded by serial subcutaneous transplantation. Tumor samples were evaluated by immunohistochemistry and graded for HER2 and CAV1 expression.

Acute biodistribution studies. Acute biodistribution studies were performed after injection of radiolabeled trastuzumab. Mice were sacrificed and organs were harvested, weighed, and assayed in the gamma counter for biodistribution studies. Radioactivity associated with each organ was expressed as percentage of injected dose per gram of organ (% ID g^{-1})[8].

Small-Animal positron emission tomography (PET) Imaging. PET imaging experiments were conducted on a microPET Focus 120 scanner (Concorde Microsystems). Mice were anesthetized by inhalation of 1.5–2% isofluorane (Baxter Healthcare) in an oxygen gas mixture 10 min before recording PET images. PET data for each group ($n = 4$) was recorded, with mice under isofluorane anesthesia (1.5–2%), in list mode at 4, 8, 24, and 48 h after intravenous injection of [^{89}Zr]Zr-DFO-trastuzumab or [^{89}Zr]Zr-DFO-IgG. Images were analyzed using ASIPro VM software (Concorde Microsystems).

In vivo therapeutic efficacy. When tumor volumes reached 100 to 300 mm^3, mice were randomly grouped into treatment cohorts ($n \geq 8$ per group): vehicle, trastuzumab, lovastatin, or a combination of trastuzumab with lovastatin. Intraperitoneal trastuzumab administration 5 mg kg^{-1} weekly (during 5 weeks) was started at day 0. Lovastatin (4.15 mg kg^{-1} of mice) was orally administrated 12 h prior and at the same time as the intraperitoneal injection of trastuzumab. Tumor volumes were determined twice a week.

Statistical analysis. Data are expressed as mean ± S.E.M. Differences were analyzed by the Student t-test. The non-parametric one-tailed Spearman test was used to determine the correlation coefficient.

Data availability

All data supporting the findings of this study are available in the Article, Supplementary Information, or upon request from the corresponding author. The Source Data underlying Figures in the main text and Supplementary Figures are provided as a Source Data file.

Received: 12 April 2018 Accepted: 13 November 2018
Published online: 03 December 2018

References

1. Slamon, D. J. et al. Studies of the HER-2/neu proto-oncogene in human breast and ovarian cancer. *Science* **244**, 707–712 (1989).
2. Yan, M. et al. HER2 expression status in diverse cancers: review of results from 37,992 patients. *Cancer Metast. Rev.* **34**, 157–164 (2015).
3. Slamon, D. J. et al. Human breast cancer: correlation of relapse and survival with amplification of the HER-2/neu oncogene. *Science* **235**, 177–182 (1987).
4. Baselga, J. & Swain, S. M. Novel anticancer targets: revisiting ERBB2 and discovering ERBB3. *Nat. Rev. Cancer* **9**, 463–475 (2009).
5. Pereira, P. M. R., Abma, L., Henry, K. E. & Lewis, J. Imaging of human epidermal growth factor receptors for patient selection and response monitoring: From PET imaging and beyond. *Cancer Lett.* **419**, 139–151 (2018).
6. O'Donoghue, J. A. et al. Pharmacokinetics, biodistribution, and radiation dosimetry for ^{89}Zr-Trastuzumab in patients with esophagogastric cancer. *J. Nucl. Med.* **59**, 161–166 (2018).
7. Ulaner, G. A. et al. Detection of HER2-positive metastases in patients with HER2-negative primary breast cancer using ^{89}Zr-Trastuzumab PET/CT. *J. Nucl. Med.* **57**, 1523–1528 (2016).
8. Janjigian, Y. Y. et al. Monitoring afatinib treatment in HER2-positive gastric cancer with ^{18}F-FDG and ^{89}Zr-Trastuzumab PET. *J. Nucl. Med.* **54**, 936–943 (2013).
9. Janjigian, Y. Y. et al. Genetic predictors of response to systemic therapy in esophagogastric cancer. *Cancer Discov.* **8**, 49–58 (2018).
10. Jordan, N. V. et al. HER2 expression identifies dynamic functional states within circulating breast cancer cells. *Nature* **537**, 102–106 (2016).
11. Turner, N. H. & Di Leo, A. HER2 discordance between primary and metastatic breast cancer: Assessing the clinical impact. *Cancer Treat. Rev.* **39**, 947–957 (2013).
12. Lindström, L. S. et al. Clinically used breast cancer markers such as estrogen receptor, progesterone receptor, and human epidermal growth factor receptor 2 are unstable throughout tumor progression. *J. Clin. Oncol.* **30**, 2601–2608 (2012).
13. Niikura, N. et al. Loss of human epidermal growth factor receptor 2 (HER2) expression in metastatic sites of HER2-overexpressing primary breast tumors. *J. Clin. Oncol.* **30**, 593–599 (2012).
14. Gebhart, G. et al. Molecular imaging as a tool to investigate heterogeneity of advanced HER2-positive breast cancer and to predict patient outcome under trastuzumab emtansine (T-DM1): the ZEPHIR trial. *Ann. Oncol.* **27**, 619–624 (2016).

15. Moasser, M. M. Targeting the function of the HER2 oncogene in human cancer therapeutics. *Oncogene* **26**, 6577–6592 (2007).
16. Liu, D. et al. 2-AR signaling controls trastuzumab resistance-dependent pathway. *Oncogene* **35**, 47–58 (2016).
17. Gennari, R. et al. Pilot study of the mechanism of action of preoperative trastuzumab in patients with primary operable breast tumors overexpressing HER2. *Clin. Cancer Res.* **10**, 5650–5655 (2004).
18. Wolff, A. C. et al. Recommendations for human epidermal growth factor receptor 2 testing in breast cancer: American society of clinical oncology/ College of american pathologists clinical practice guideline update. *J. Clin. Oncol.* **31**, 3997–4013 (2013).
19. Mosesson, Y., Mills, G. B. & Yarden, Y. Derailed endocytosis: an emerging feature of cancer. *Nat. Rev. Cancer* **8**, 835–850 (2008).
20. Sorkin, A. & Goh, L. K. Endocytosis and intracellular trafficking of ErbBs. *Exp. Cell Res.* **315**, 683–696 (2009).
21. Garrett, T. P. et al. The crystal structure of a truncated ErbB2 ectodomain reveals an active conformation, poised to interact with other ErbB receptors. *Mol. Cell* **11**, 495–505 (2003).
22. Cho, H. S. et al. Structure of the extracellular region of HER2 alone and in complex with the Herceptin Fab. *Nature* **421**, 756–760 (2003).
23. Austin, C. D. et al. Endocytosis and sorting of ErbB2 and the site of action of cancer therapeutics trastuzumab and geldanamycin. *Mol. Biol. Cell* **15**, 5268–5282 (2004).
24. Bertelsen, V. & Stang, E. The mysterious ways of ErbB2/HER2 trafficking. *Membranes (Basel).* **4**, 424–446 (2014).
25. Roepstorff, K., Grøvdal, L., Grandal, M., Lerdrup, M. & van Deurs, B. Endocytic downregulation of ErbB receptors: mechanisms and relevance in cancer. *Histochem. Cell Biol.* **129**, 563–578 (2008).
26. Half, E. et al. HER-2 receptor expression, localization, and activation in colorectal cancer cell lines and human tumors. *Int. J. Cancer* **108**, 540–548 (2004).
27. Wang, Y. -N., Yamaguchi, H., Hsu, J. -M. & Hung, M. -C. Nuclear trafficking of the epidermal growth factor receptor family membrane proteins. *Oncogene* **29**, 3997–4006 (2010).
28. Nagy, P. et al. Lipid rafts and the local density of ErbB proteins influence the biological role of homo- and heteroassociations of ErbB2. *J. Cell Sci.* **115**, 4251–4262 (2002).
29. Shatz, M. & Liscovitch, M. Caveolin-1: A tumor-promoting role in human cancer. *Int. J. Radiat. Biol.* **84**, 177–189 (2008).
30. Bourseau-Guilmain, E. et al. Hypoxia regulates global membrane protein endocytosis through caveolin-1 in cancer cells. *Nat. Commun.* **7**, 11371 (2016).
31. Hommelgaard, A. M., Lerdrup, M. & van Deurs, B. Association with membrane protrusions makes ErbB2 an internalization-resistant receptor. *Mol. Biol. Cell* **15**, 1557–1567 (2004).
32. Raina, D. et al. Targeting the MUC1-C oncoprotein downregulates HER2 activation and abrogates trastuzumab resistance in breast cancer cells. *Oncogene* **33**, 3422–3431 (2014).
33. Orr, G. et al. Cholesterol dictates the freedom of EGF receptors and HER2 in the plane of the membrane. *Biophys. J.* **89**, 1362–1373 (2005).
34. Valabrega, G. et al. TGFα expression impairs trastuzumab-induced HER2 downregulation. *Oncogene* **24**, 3002–3010 (2005).
35. Sung, M. et al. Caveolae-mediated endocytosis as a novel mechanism of resistance to trastuzumab emtansine (T-DM1). *Mol. Cancer Ther.* **17**, 243–253 (2018).
36. Chung, Y. C., et al. Metformin-induced caveolin-1 expression promotes T-DM1 drug efficacy in breast cancer cells. *Sci. Rep.* **8**, article number: 3930 (2018).
37. Barretina, J. et al. The Cancer Cell Line Encyclopedia enables predictive modelling of anticancer drug sensitivity. *Nature* **483**, 603–607 (2012).
38. Keller, S. et al. Effects of trastuzumab and afatinib on kinase activity in gastric cancer cell lines. *Mol. Oncol.* **12**, 441–462 (2018).
39. Marx, C., Held, J. M., Gibson, B. W. & Benz, C. C. ErbB2 trafficking and degradation associated with K48 and K63 polyubiquitination. *Cancer Res.* **70**, 3709–3717 (2010).
40. Guruswamy, S. & Rao, C. V. Synergistic effects of lovastatin and celecoxib on caveolin-1 and its down-stream signaling molecules: Implications for colon cancer prevention. *Int. J. Oncol.* **35**, 1037–1043 (2009).
41. Vaira, V. et al. Preclinical model of organotypic culture for pharmacodynamic profiling of human tumors. *Proc. Natl Acad. Sci. USA* **107**, 8352–8356 (2010).
42. Scaltriti, M. et al. Lapatinib, a HER2 tyrosine kinase inhibitor, induces stabilization and accumulation of HER2 and potentiates trastuzumab-dependent cell cytotoxicity. *Oncogene* **28**, 803–814 (2009).
43. Sukhanova, A. et al. Targeting C4-demethylating genes in the cholesterol pathway sensitizes cancer cells to EGF receptor inhibitors via increased EGF receptor degradation. *Cancer Discov.* **3**, 96–111 (2013).
44. Chung, Y. C., Kuo, J. F., Wei, W. C., Chang, K. J. & Chao, W. T. Caveolin-1 dependent endocytosis enhances the chemosensitivity of HER-2 positive breast cancer cells to trastuzumab emtansine (T-DM1). *PLoS ONE* **10**, e0133072 (2015).
45. Abulrob, A. et al. Interactions of EGFR and caveolin-1 in human glioblastoma cells: evidence that tyrosine phosphorylation regulates EGFR association with caveolae. *Oncogene* **23**, 6967–6979 (2004).
46. Lu, Z. M., Ghosh, S., Wang, Z. Y. & Hunter, T. Downregulation of caveolin-1 function by EGF leads to the loss of E-cadherin, increased transcriptional activity of beta-catenin, and enhanced tumor cell invasion. *Cancer Cell* **4**, 499–515 (2003).
47. Cheng, J. C., Qiu, X., Chang, H. M. & Leung, P. C. K. HER2 mediates epidermal growth factor-induced down-regulation of E-cadherin in human ovarian cancer cells. *Biochem. Bioph. Res. Co.* **434**, 81–86 (2013).
48. Chung, I. et al. High cell-surface density of HER2 deforms cell membranes. *Nat. Commun.* **7**, 12742 (2016).
49. von der Heyde, S. et al. mRNA profiling reveals determinants of trastuzumab efficiency in HER2-positive breast cancer. *PLoS ONE* **10**, e0117818 (2015).
50. Sekhar, S. C. et al. Identification of caveolin-1 as a potential causative factor in the generation of trastuzumab resistance in breast cancer cells. *J. Cancer* **4**, 391–401 (2013).
51. Costantini, D. L., Chan, C., Cai, Z., Vallis, K. A. & Reilly, R. M. ^{111}In-labeled trastuzumab (Herceptin) modified with nuclear localization sequences (NLS): an Auger electron-emitting radiotherapeutic agent for HER2/neu-amplified breast cancer. *J. Nucl. Med.* **48**, 1357–1368 (2007).
52. Costantini, D. L. et al. Antitumor effects and normal-tissue toxicity of ^{111}In-nuclear localization sequence-trastuzumab in athymic mice bearing HER-positive human breast cancer xenografts. *J. Nucl. Med.* **51**, 1084–1091 (2010).
53. Pike, L. J. & Casey, L. Cholesterol levels modulate EGF receptor-mediated signaling by altering receptor function and trafficking. *Biochemistry* **41**, 10315–10322 (2002).
54. Tsé, C., Gauchez, A. -S., Jacot, W. & Lamy, P. -J. HER2 shedding and serum HER2 extracellular domain: Biology and clinical utility in breast cancer. *Cancer Treat. Rev.* **38**, 133–142 (2012).
55. Dijkers, E. C. et al. Biodistribution of ^{89}Zr-Trastuzumab and PET imaging of HER2-positive lesions in patients with metastatic breast cancer. *Clin. Pharmacol. Ther.* **87**, 586–592 (2010).
56. Matthews, V. et al. Cellular cholesterol depletion triggers shedding of the human interleukin-6 receptor by ADAM10 and ADAM17 (TACE). *J. Biol. Chem.* **278**, 38829–38839 (2003).
57. Schachter, M. Chemical, pharmacokinetic and pharmacodynamic properties of statins: an update. *Fundam. Clin. Pharmacol.* **19**, 117–125 (2004).
58. Wong, W. W. L., Dimitroulakos, J., Minden, M. D. & Penn, L. Z. HMG-CoA reductase inhibitors and the malignant cell: the statin family of drugs as triggers of tumor-specific apoptosis. *Leukemia* **16**, 508–519 (2002).
59. Hindler, K., Cleeland, C. S., Rivera, E. & Collard, C. D. The role of statins in cancer therapy. *Oncologist* **11**, 306–315 (2006).
60. Campbell, M. J. et al. Breast cancer growth prevention by statins. *Cancer Res.* **66**, 8707–8714 (2006).
61. Christian, A. E., Haynes, M. P., Phillips, M. C. & Rothblat, G. H. Use of cyclodextrins for manipulating cellular cholesterol content. *J. Lipid Res.* **38**, 2264–2272 (1997).
62. Warita, K. et al. Statin-induced mevalonate pathway inhibition attenuates the growth of mesenchymal-like cancer cells that lack functional E-cadherin mediated cell cohesion. *Sci. Rep.* **4**, 7593 (2014).
63. Holland, J. P., Sheh, Y. C. & Lewis, J. S. Standardized methods for the production of high specific-activity zirconium-89. *Nucl. Med. Biol.* **36**, 729–739 (2009).

Acknowledgements

We acknowledge the MSKCC Small-Animal Imaging Core Facility, the Radiochemistry and Molecular Imaging Probe Core, the Anti-tumor Assessment Core and Molecular Cytology Core Facility and the Immune Monitoring Facility, which were supported by NIH grant P30 CA08748. This study was supported in part by the Geoffrey Beene Cancer Research Center of MSKCC. We gratefully acknowledge Mr. William H. and Mrs. Alice Goodwin and the Commonwealth Foundation for Cancer Research and The Center for Experimental Therapeutics of Memorial Sloan Kettering Cancer Center. We thank Dr. Maurizio Scaltriti for reading the manuscript and providing insightful comments. We would also like to acknowledge Ricardo D'Oliveira Albanus from Department of Computational Medicine & Bioinformatics, University of Michigan for assistance in statistical analysis of the data. L.M.C. acknowledges support from the Ruth L. Kirschstein National Research Service Award postdoctoral fellowship (NIH F32-EB025050). P.M.R.P. and

S.K.S. gratefully acknowledge the Tow Foundation Postdoctoral Fellowships from the MSKCC Center for Molecular Imaging and Nanotechnology.

Author contributions

Conception and design: P.M.R.P., J.S.L. Development of methodology: P.M.R.P., L.C., K.J.E., J.P., A.R. Acquisition of data (provided animals, acquired and managed patients, provided facilities, etc.): P.M.R.P., L.C., J.C.D, Y.Y.J., J.S.L. Analysis and interpretation of data (e.g., statistical analysis, biostatistics, computational analysis): P.M.R.P., L.C., S.K.S., J.S.L. Writing, review, and/or revision of the manuscript: P.M.R.P., L.C., K.J.E., S.K.S., J.C.D., Y.Y.J., J.S.L. Study supervision: J.S.L.

Additional information

Supplementary Information accompanies this paper at https://doi.org/10.1038/s41467-018-07608-w.

Competing interests: The authors declare no competing interests.

Reprints and permission information is available online at http://npg.nature.com/reprintsandpermissions/

Publisher's note: Springer Nature remains neutral with regard to jurisdictional claims in published maps and institutional affiliations.

Open Access This article is licensed under a Creative Commons Attribution 4.0 International License, which permits use, sharing, adaptation, distribution and reproduction in any medium or format, as long as you give appropriate credit to the original author(s) and the source, provide a link to the Creative Commons license, and indicate if changes were made. The images or other third party material in this article are included in the article's Creative Commons license, unless indicated otherwise in a credit line to the material. If material is not included in the article's Creative Commons license and your intended use is not permitted by statutory regulation or exceeds the permitted use, you will need to obtain permission directly from the copyright holder. To view a copy of this license, visit http://creativecommons.org/licenses/by/4.0/.

© The Author(s) 2018

Pharmacokinetics, Biodistribution, and Radiation Dosimetry for ^{89}Zr-Trastuzumab in Patients with Esophagogastric Cancer

Joseph A. O'Donoghue[1], Jason S. Lewis[2–5], Neeta Pandit-Taskar[3,4,6], Stephen E. Fleming[3,4], Heiko Schöder[3,4], Steven M. Larson[3–6], Volkan Beylergil[3], Shutian Ruan[3], Serge K. Lyashchenko[2,3], Pat B. Zanzonico[1], Wolfgang A. Weber[3–5], Jorge A. Carrasquillo[*3–6], and Yelena Y. Janjigian[*7,8]

[1]Department of Medical Physics, Memorial Sloan Kettering Cancer Center, New York, New York; [2]Radiochemistry and Molecular Imaging Probes Core, Memorial Sloan Kettering Cancer Center, New York, New York; [3]Department of Radiology, Memorial Sloan Kettering Cancer Center, New York, New York; [4]Department of Radiology, Weill Cornell Medical Center, New York, New York; [5]Molecular Pharmacology Program, Memorial Sloan Kettering Cancer Center, New York, New York; [6]Center for Targeted Radioimmunotherapy and Diagnosis, Ludwig Center for Cancer Immunotherapy, New York, New York; [7]Department of Medicine, Memorial Sloan Kettering Cancer Center, New York, New York; and [8]Department of Medicine, Weill Cornell Medical Center, New York, New York

Trastuzumab with chemotherapy improves clinical outcomes in patients with human epidermal growth factor receptor 2 (HER2)–positive esophagogastric adenocarcinoma (EGA). Despite the therapeutic benefit, responses are rarely complete, and most patients develop progression. To our knowledge, this is the first report evaluating ^{89}Zr-trastuzumab in HER2-positive EGA; here, we evaluate the safety, pharmacokinetics, biodistribution, and dosimetry ^{89}Zr-trastuzumab. **Methods:** Trastuzumab was conjugated with deferoxamine and radiolabeled with ^{89}Zr. A mean activity of 184 MBq was administered to 10 patients with metastatic HER2-positive EGA. PET imaging, whole-body probe counts, and blood draws were performed to assess pharmacokinetics, biodistribution, and dosimetry. **Results:** No clinically significant toxicities were observed. At the end of infusion, the estimated ^{89}Zr-trastuzumab in plasma volume was a median 102% (range, 78%–113%) of the injected dose. The median biologic half-life $T_{1/2\beta}$ was 111 h (range, 78–193 h). The median biologic whole-body retention half-life was 370 h (range, 257–578 h). PET images showed optimal tumor visualization at 5–8 d after injection. The maximum tumor SUV ranged from no to minimal uptake in 3 patients to a median of 6.8 (range, 2.9–22.7) for 20 lesions in 7 patients. Dosimetry estimates from OLINDA showed that the organs receiving the highest absorbed doses were the liver and heart wall, with median values of 1.37 and 1.12 mGy/MBq, respectively. **Conclusion:** ^{89}Zr-trastuzumab imaging tracer is safe and provides high-quality images in patients with HER2-positive EGA, with an optimal imaging time of 5–8 d after injection.

Key Words: HER2; trastuzumab; ^{89}Zr; esophageal cancer; gastric cancer

J Nucl Med 2018; 59:161–166
DOI: 10.2967/jnumed.117.194555

Gastric cancer is the fifth most common malignancy and among the leading causes of cancer death in the world (*1*). Human epidermal growth factor receptor 2 (HER2) is a transmembrane receptor that is overexpressed in approximately 20% of esophagogastric adenocarcinoma (EGAs) (*2*). Trastuzumab, an anti-HER2 monoclonal antibody, is the first Food and Drug Administration–approved targeted agent to treat patients with EGA that overexpresses HER2 (*3*). However, not all patients with HER2-positive EGA respond to trastuzumab (*4*). Furthermore, duration of response to trastuzumab-containing therapy is only 6.7 mo, and the basis of resistance in EGA is an area of investigation.

In patients with HER2 expression in tumors, the heterogeneity of HER2 expression within primary tumors and metastases as well as loss of HER2 expression while undergoing trastuzumab therapy are some factors that have been shown to contribute to therapeutic resistance (*5*). Furthermore, the extent of disease burden and presence of the primary tumor in the stomach has been shown to affect absorption, pharmacokinetics, and efficacy of trastuzumab and lapatinib (oral anti-HER2 tyrosine kinase inhibitor). An imaging agent that can noninvasively assess HER2 status and reflect functional effects of HER2-targeted agents in the primary tumor and metastases would help to elucidate these factors. Using ^{89}Zr-trastuzumab in gastric cancer xenografts, we demonstrated that ^{89}Zr-trastuzumab PET could delineate HER2-positive tumors and measure the pharmacodynamic effects of anti-HER2 therapy (*6*).

Previous reports with ^{89}Zr-trastuzumab have focused on its ability to detect breast cancer (*7*), determine HER2 tumor heterogeneity (*8*), and identify patients likely to respond to HER2-directed treatments (*9,10*). Limited information is available on the pharmacokinetics and dosimetry of ^{89}Zr-labeled antibodies in general (*9–17*), and no detailed data on the pharmacokinetics of ^{89}Zr-trastuzumab have been published in peer-reviewed literature. Only recently has there been a report of ^{89}Zr-trastuzumab dosimetry in breast cancer (*18*). To our knowledge, this is the first report evaluating ^{89}Zr-trastuzumab in HER2-positive EGA; here, we evaluate the safety, pharmacokinetics, biodistribution, and dosimetry of ^{89}Zr-trastuzumab.

Received Apr. 7, 2017; revision accepted Jun. 8, 2017.
For correspondence contact: Jorge A. Carrasquillo, Memorial Sloan Kettering Cancer Center, 1275 York Ave., New York, NY 10065.
E-mail: carrasj1@mskcc.org
*Contributed equally to this work.
Published online Jun. 21, 2017.
COPYRIGHT © 2018 by the Society of Nuclear Medicine and Molecular Imaging.

MATERIALS AND METHODS

Patients

Eligible patients had a diagnosis of HER2-positive metastatic EGA. Other eligibility criteria included measurable or evaluable disease by RECIST (version 1.1), Karnofsky performance of 60% or greater, and adequate organ function. Exclusion criteria included ejection fraction of less than 50% and known hypersensitivity to trastuzumab. For patients receiving trastuzumab, a washout period of at least 14 d was recommended.

Study Design and Cohorts

This was a single-site, prospective open-label imaging protocol. The study was approved by the institutional review board and ethics committees at Memorial Sloan Kettering Cancer Center (MSK) (ClinicalTrials.gov identifier NCT02023996). All patients provided written informed consent. We report the results from the completed cohort 1, of 10 patients who underwent serial ^{89}Zr-trastuzumab PET imaging (Supplemental Fig. 1; supplemental materials are available at http://jnm.snmjournals.org) to determine safety, biodistribution, pharmacokinetics, and dosimetry.

^{89}Zr-Trastuzumab Drug Product

The ^{89}Zr-trastuzumab was manufactured by the MSK Radiochemistry and Molecular Imaging Probes Core Facility in compliance with a Food and Drug Administration investigational new drug application. Clinical-grade trastuzumab (Herceptin; Genentech) was conjugated with p-SCN-Bn-deferoxamine (Macrocylics) chelator, followed by radiolabeling with ^{89}Zr, a positron emitter with a 78.4-h half-life. The conjugation was performed using methodology previously described (*19*). The chelate-to-trastuzumab ratio was 1.03, as determined by the radioisotopic dilution method, with an antibody concentration of 10.6 mg/mL, determined by ultraviolet-visible spectroscopy, and antibody monomer content of 100%, determined by size-exclusion chromatography high-performance liquid chromatography. ^{89}Zr-oxalate was also prepared in-house as previously described (*20*) and used to radiolabel desferrioxamine-trastuzumab as previously described (*19,20*). The ^{89}Zr-trastuzumab final product had a radiochemical purity of more than 95%, endotoxin content of less than 5 EU/mL, and pH of 5.5–8.0 and was sterile. The median immunoreactivity was 94% (range, 86%–97%) (*21*).

Patient unit doses of approximately 185 MBq/3 mg of ^{89}Zr-trastuzumab were mixed with nonradiolabeled trastuzumab to achieve a total mass of 50 mg. The total antibody mass of 50 mg was selected on the basis of the literature experience (*7*). A mean of 184 MBq (range, 182–189 MBq) was injected intravenously over approximately 5 min. Patients were monitored for 2 h after injection, and any adverse effects were graded using Common Terminology Criteria for Adverse Events (version 4).

Imaging

All patients underwent dedicated CT imaging as a reference standard a median of 9 d before (range, 29 d before or 3 d after) ^{89}Zr-trastuzumab injection. Each patient underwent serial whole-body PET/CT scans from mid skull to proximal thigh. All scans were obtained on a Discovery STE PET/CT scanner (GE Healthcare) in 3-dimensional mode with attenuation, scatter, and other standard corrections applied and using iterative reconstruction. Images were acquired within 4 h of injection and at 1, 2–4, and 5–8 d after injection using 3, 4, 5, and 7–8 min per bed position, respectively. Low-dose CT scans were used for attenuation correction using an x-ray tube current of 10–80 mA.

Images were read by an experienced nuclear medicine physician who was aware of the patient's history and conventional imaging. Localization in the tumor was defined as focal accumulation greater than adjacent background in areas in which physiologic activity was not expected. Volumes of interest were drawn on PET/CT images over normal liver, kidney, spleen, bone marrow, and lung using a dedicated workstation (Hermes Medical Solution or GE Healthcare AW server 2.0) and over selected tumor lesions confirmed on CT or ^{18}F-FDG PET. SUVs normalized to lean body mass (SUV_{LBM}) were determined.

Whole-Body and Serum Clearance Measurements

Whole-body clearance was determined by serial measurements of counting rate using a 12.7-cm-thick NaI(Tl) scintillation detector at a fixed 3 m from the patient. Background-corrected geometric mean counts were obtained after infusion and before first voiding, immediately after first voiding, and subsequently at the times of the PET scans. Counting rates were normalized to the immediate postinfusion value (taken as 100%) to yield relative retained activities (in %).

Blood samples were obtained at approximately 5, 15, 30, and 60 min and 2 h after injection and on subsequent days of each PET scan ($n = 8$). Aliquots of serum were counted using a well-type detector (Wallac Wizard 1480 γ-counter; Perkin Elmer). The measured activity concentrations were converted to percentage injected activity per liter.

The whole-body probe data and the serum activity concentration data were fit with monoexponential or biexponential functions using SAAM software (*22*). These data were used to determine cumulated activity per unit administered activity (i.e., residence time) for whole-body and serum. Serum data were also used to determine pharmacokinetic parameters, including concentration at 0 time, median biologic half-life $T_{1/2\beta}$, volume of distribution of central compartment, area under the curve (AUC), and systemic clearance. The total percentage injected activity initially present in the serum was estimated by multiplying the percentage injected activity per liter in serum at concentration at 0 time by the patient's estimated plasma volume determined from a nomogram (*23*).

Normal-Tissue Dosimetry

Image-derived SUV_{LBM} were converted to activity concentration per unit mass (kBq/g). The AUCs were estimated by trapezoidal integration with the contribution of the terminal portion calculated by extrapolation from the last measured value using the faster of apparent terminal clearance rate or physical decay. Subsequently, whole-organ AUCs were estimated by multiplying the activity concentration AUC by organ mass and residence time derived by dividing the AUC by injected activity. Values of standard male/female organ masses were taken from the OLINDA/EXM software (*24*). If the actual body mass was more than 15% greater than the standard value, organ masses were rescaled. The assigned patient mass was the minimum of actual patient mass or a calculated maximum effective mass as previously described (*25*).

The residence time for cardiac contents was calculated by multiplying the serum value (in h/L) by the standard or patient mass–rescaled value of heart contents volume and by (1−measured hematocrit). The residence time for red marrow was calculated as described by Sgouros et al. (*26*). The residence time for the remainder of the body was derived by subtracting all the individually estimated residence times for normal organs from the whole-body residence time. Absorbed radiation doses to various normal organs were estimated using OLINDA/EXM software.

Statistics

Descriptive statistics include median or mean and SD. Comparison between groups was done using the paired *t* test. Statistical analysis was performed with SigmaStat 3.5 (Systat Software Inc.).

RESULTS

Patients

Ten consecutive patients with histologically documented EGA were imaged (esophageal, $n = 2$; gastroesophageal junction, $n = 7$; and gastric, $n = 1$). Tumors were HER2-positive based on immunohistochemistry 3+ ($n = 8$) or 2+ with fluorescence in situ hybridization (FISH) amplification ($n = 2$). Their median age was

TABLE 1
Pharmacokinetic Parameters for ^{89}Zr-Trastuzumab

Parameter	Median	Minimum	Maximum
Co-measured (% injected activity/L)	31.56	24.5	46.7
Co-fit (% injected activity/L)	31.55	24.4	44.8
Vd (L)	3.17	2.23	4.10
$T_{1/2\alpha}$ (h)	3.1	1.9	15.3
$T_{1/2\beta}$ (h)	111	78	193
Clearance (mL/h)	28.8	12.2	52.5
Estimated amount in plasma volume (%)	102	78	113

Vd = volume of distribution of central compartment.

62 y (age range, 46–80 y); 8 were men and 2 women. Patients either were trastuzumab-naïve (n = 3) or were no longer being treated with trastuzumab for a median of 42 d (range, 35–156 d) with the exception of patient 5, who received trastuzumab within 15 d before ^{89}Zr-trastuzumab.

Adverse Events

Two patients reported grade 1 chills during injection that resolved after diphenhydramine and acetaminophen. One patient had chills that did not require treatment, possibly related to ^{89}Zr-trastuzumab administration. No other related adverse events were reported.

Pharmacokinetics

The pharmacokinetic parameters for ^{89}Zr-trastuzumab are shown in Table 1. At the end of infusion, the estimated total activity in serum was a median of 102% (range, 78%–113%) of the injected dose, determined by multiplying the patients' estimated plasma volume by the concentration in serum at the initial sampling time point. The serum volume of distribution of the central compartment was within a median of 3% (range, −10%–28%) of the estimated plasma volume. The median biologic $T_{1/2\beta}$ was 111 h (range, 78–193 h) (Supplemental Fig. 2A).

Biodistribution

Whole-body retention of activity was prolonged, with a median biologic half-time of 370 h (range, 257–578 h), as shown in Supplemental Figure 2B. Excretion in the urine in the first 1.7 h (range, 1.1–2.5 h) was minimal, with a median of 1.6% (range, −1.0%–7.6%). Whole-body excretion over a median of 120 h (range, 115–191 h) was a median of 21.3% (range, 16.7%–30.0%). In 7 of 10 patients, the gallbladder was visualized in the day-of-injection image but seldom in subsequent images. All patients had bowel visualization that moved over time, consistent with intraluminal content. Exactly how much of the total excretion was urinary versus bowel was not determined; however, bowel appeared to be the predominant route of excretion based on visual inspection.

Optimal tumor visualization was generally obtained at the last imaging time point (5–8 d after injection), when most lesions were observed with the best contrast based on visual assessment by an expert reader and with the highest or near-highest $SUV_{LBM\text{-}max}$ (Fig. 1). The initial image primarily showed blood pool and rarely any tumor lesions. Tumor uptake typically increased over time, with the highest uptake most often seen at the last time point (Fig. 2). The highest tumor $SUV_{LBM\text{-}max}$ observed ranged from no uptake in any lesion in 2 patients to a median $SUV_{LBM\text{-}max}$ of 6.8 (range, 2.9–22.7) for 20 lesions in 7 patients with positive scan results, imaged between 115 and 191 h after administration. The time course of normal-organ uptake is shown in Figure 3A. The uptake in liver was relatively low and stable over time as was kidney (with the exception of the last time point representing a single patient). The uptake decreased continuously in the blood pool, lung, and spleen. A slight increase in organ-to-blood ratio was observed for liver, kidney, and bone marrow (Fig. 3B).

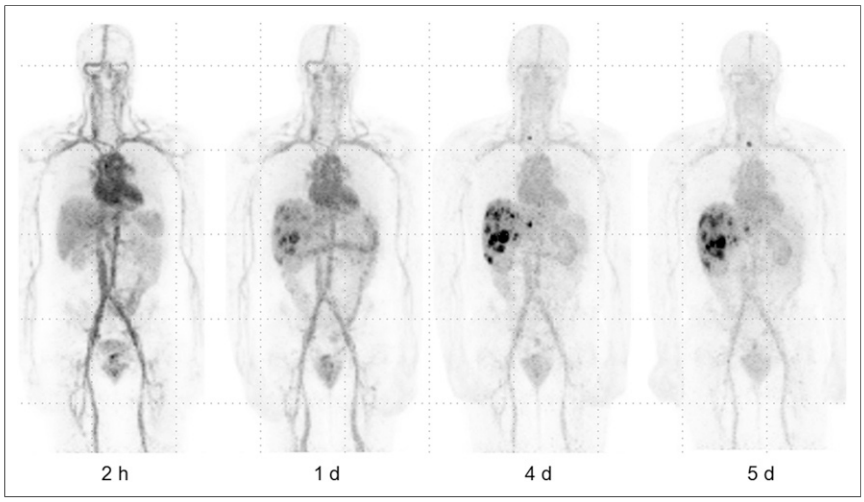


FIGURE 1. Patient 10 with EGA cancer metastatic to liver. Serial maximum-intensity-projection images are shown, after injection of 182.8 MBq of ^{89}Zr-trastuzumab. All images are of good quality up to 5 d after injection (images set to same gray scale). Immediate postinjection images do not show tumor uptake. Images at 1 d after injection show uptake in metastatic liver lesions that increases over time and is well identified at 4 and 5 d after injection with $SUV_{LBM\text{-}max}$ of 22.7. Foci in upper mediastinal nodes are best seen at 5 d after injection. Blood-pool activity decreases over time. Activity in bowel is present at all time points. Minimal or no activity is seen in urinary bladder.

Tumor Imaging

In 80% of imaged patients, accumulation of ^{89}Zr-trastuzumab tracer was noted

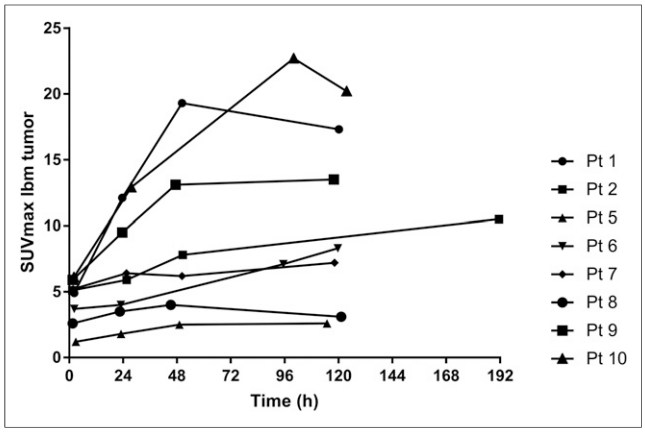


FIGURE 2. Volume of interest drawn over tumor lesions with highest uptake ($SUV_{LBM\text{-}max}$ [8 patients], with ^{89}Zr-trastuzumab uptake usually increasing over time with highest $SUV_{LBM\text{-}max}$ typically at >48 h after injection).

in sites of known disease. Focal areas of ^{89}Zr-trastuzumab uptake were seen within known metastatic sites in the liver, lymph nodes, lung, and bone as well as remaining primary. No uptake was seen in 2 patients on ^{89}Zr-trastuzumab PET. In patient 4, this was likely due to weak HER2 staining (immunohistochemistry 2+/FISH HER2/CEP17 3.4) and focal HER2 expression. In patient 3 with prior gastrectomy, whose primary tumor and biopsy-proven lung metastasis exhibited strong HER2 expression (immunohistochemistry 3+), ^{89}Zr-trastuzumab PET failed to pick up small-volume recurrent disease in a 1.1 × 1.1 cm lung nodule and 1.9 × 1.3 cm retroperitoneal lymph node that were visualized on CT. The retroperitoneal lymph nodes were never biopsied or tested for HER2 overexpression. Patient 8 with very low uptake in bone lesions and no uptake in liver and nodal lesions was receiving chemotherapy at the time of imaging. Heterogeneity of tumor uptake within patients is shown in Supplemental Table 1, along with last trastuzumab therapy since this treatment may compete for tumor uptake.

Absorbed Dose to Normal Organs

The dosimetry estimates from OLINDA are shown in Table 2, indicating that the organs receiving the highest absorbed doses were liver, heart wall, kidney, lung, and spleen with mean values of 1.32, 1.12, 0.9, 0.81, and 0.8 mGy/MBq, respectively. The mean effective dose was 0.48 mSv/MBq.

DISCUSSION

Our data demonstrate for the first time that ^{89}Zr-trastuzumab PET is specific for HER2-positive EGA and visualizes primary tumors and metastases with high contrast. Similar findings have been described previously in patients with breast cancer (*7–10,18*). ^{89}Zr-trastuzumab PET has a potential advantage over single-site biopsies, as it can noninvasively assess variation in level of HER2 and target engagement in both the primary tumor and all sites of metastases simultaneously. ^{89}Zr trastuzumab PET has already been used as a biomarker in the theranostic setting for breast cancer patients treated with trastuzumab emtansine antibody drug conjugate. In that setting, combining ^{89}Zr-trastuzumab and ^{18}F-FDG PET predicted response to treatment with trastuzumab emtansine (*10*). In addition, early changes in ^{89}Zr-trastuzumab uptake in breast cancer metastasis after treatment with heat shock protein 90 inhibitor have correlated with CT changes in the size of lesions (*9*). Last, a preliminary report has suggested that breast cancer patients with prior HER2-negative biopsies may be identified as HER2-positive on imaging and selected for therapeutic intervention that they would not otherwise receive (*8*).

In this study, the biodistribution and imaging of ^{89}Zr-trastuzumab in patients with EGA appeared visually similar to those in patients with metastatic breast cancer (*7,8,18*). Recent analysis of ^{89}Zr-trastuzumab biodistribution in normal organs of women with breast cancer has been expressed as percentage injected dose (*18*), when our data in SUV_{LBM} are converted to percentage injected dose using standard man body weight and organ volumes; we obtained uptake values in the same range (data not shown). A prior study with ^{89}Zr-cmAb-U36 antibody in head and neck cancer (*12*) showed similar biodistribution and percentage injected dose in the liver, spleen, and kidney as previously described in breast cancer patients (*18*). In contrast, some antibodies have higher concentration in organs such as the liver (*15,17,27*) or spleen (*16*), which is probably due to cross-reactivity with antigen in these organs or the mass amount of antibody used. In our study, the uptake in the liver, kidney, and bone marrow showed little increase over time (Fig. 3A). When the ratios of these organs to blood pool was determined, there was evidence of slight accumulation of ^{89}Zr above blood pool in the liver, kidney, and bone marrow (Fig. 3B),

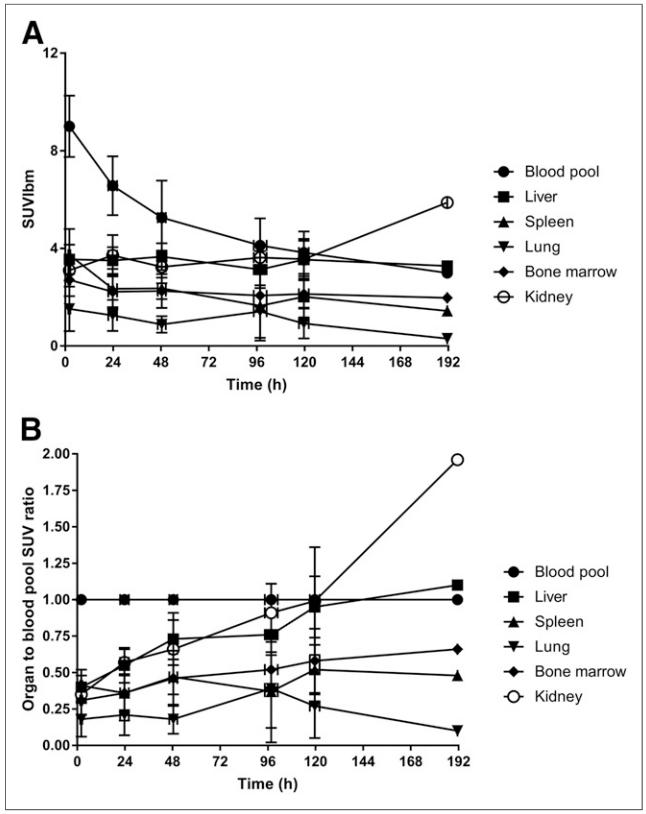


FIGURE 3. (A) SUV_{LBM} was determined by placing volume of interest over various organs and was averaged over all available time points (n = 10 for 2 h and 24 h, n = 9 for 48 h, n = 2 for 96 h, n = 10 for 120 h, and n = 1 for 192 h). SUVs were fairly stable over time for bone marrow, liver, and kidney, except for last time point. Slight decrease in SUV_{LBM} was noted for spleen and lung, as was larger decrease in activity in blood. (B) Organ–to–blood-pool ratios showed fairly stable changes for spleen and lung over time, suggesting no concentration above blood pool. In contrast, liver, kidney, and bone marrow showed slight increase over time, suggesting some ^{89}Zr accumulation in these organs.

TABLE 2
Normal-Organ Absorbed Doses for ^{89}Zr-Trastuzumab

Target organ	Mean	SD	Median	Minimum	Maximum
Adrenals	0.57	0.08	0.57	0.47	0.73
Brain	0.24	0.05	0.25	0.16	0.31
Breasts	0.31	0.05	0.31	0.23	0.38
Gallbladder wall	0.64	0.08	0.65	0.52	0.78
Lower large intestine wall	0.43	0.10	0.42	0.32	0.65
Small intestine	0.40	0.06	0.42	0.30	0.47
Stomach wall	0.43	0.07	0.44	0.32	0.54
Upper large intestine wall	0.44	0.07	0.44	0.35	0.55
Heart wall	1.12	0.18	1.12	0.85	1.46
Kidneys	0.90	0.22	0.78	0.68	1.26
Liver	1.32	0.24	1.37	0.90	1.75
Lungs	0.81	0.18	0.77	0.58	1.17
Muscle	0.33	0.05	0.33	0.23	0.40
Ovaries	0.38	0.07	0.40	0.26	0.47
Pancreas	0.56	0.09	0.56	0.45	0.71
Red marrow	0.45	0.08	0.45	0.32	0.61
Osteogenic cells	0.50	0.11	0.50	0.32	0.69
Skin	0.23	0.04	0.23	0.16	0.29
Spleen	0.80	0.19	0.74	0.59	1.20
Testes	0.26	0.05	0.27	0.17	0.30
Thymus	0.46	0.06	0.47	0.34	0.55
Thyroid	0.31	0.05	0.32	0.21	0.36
Urinary bladder wall	0.33	0.05	0.34	0.23	0.38
Uterus	0.38	0.07	0.39	0.25	0.46
Total body	0.37	0.06	0.37	0.28	0.46
Effective dose equivalent (mSv/MBq)	0.60	0.09	0.60	0.49	0.76
Effective dose (mSv/MBq)	0.48	0.06	0.47	0.38	0.57

Units are mGy/MBq unless otherwise noted.

whereas the ratios in lung and spleen were flat, suggesting no concentration above blood pool (Fig. 3B).

Our dosimetric findings predominantly in men are in line with those described for ^{89}Zr-trastuzumab in women, in whom the maximal absorbed dose was to the liver, kidney, spleen, and lung (*18*). Interestingly, for the few other ^{89}Zr-labeled antibodies, the dosimetry in most normal organs is in the same range as for ^{89}Zr-trastuzumab. The effective dose in our study of 0.48 mGy/MBq was comparable to 0.53, 0.36, 0.41, 0.61, and 0.41 mGy/MBq for cmAB-U36, hJ591, IAB2 M minibody, cetuximab, and rituximab antibodies, respectively (*12,15–17,27*). The major difference in organ dosimetry for these ^{89}Zr-labeled antibodies is in the liver and spleen when antibodies cross-reacted with these tissues (*15,16*). It is possible that changing the mass of antibody administered (or if recent trastuzumab was administered) could result in not only differences in tumor targeting but also differences in biodistribution and dosimetry. This effect of antibody mass in organ dosimetry has been demonstrated with rituximab, where a preinjection of cold antibody will significantly decrease the dose to the spleen by blocking uptake (0.73 vs. 4.1 mSv/MBq).

We have previously reported that while localization can be achieved with shorter-lived positron-labeled ^{68}Ga- or ^{64}Cu-trastuzumab, their targeting is suboptimal (*28,29*), given the biologic half-life of intact antibody in the circulation for ^{89}Zr-trastuzumab in this study (111 h). In our study, we concluded that the 5- to 8-d point offered the best imaging, similar to previous studies (*7,18*). Similar conclusions regarding optimal delayed imaging time with other ^{89}Zr-labeled intact antibodies have been reported (*12,17*). Although studies have shown targeting of ^{111}In-labeled trastuzumab (*30*), the advantage of ^{89}Zr-trastuzumab is its ability to perform quantitative imaging with PET and the higher sensitivity and resolution of PET compared with single-photon emission tomography with ^{111}In.

In this study, we administered approximately 185 MBq, resulting in good images even at 5–8 d after administration. Others have used approximately 37 MBq successfully, although they have pointed out limitations in imaging and defining volume of interest for delayed scans, especially in large patients and delayed times (*7,12,14*). Studies with ^{89}Zr-trastuzumab using 62 MBq showed that delayed imaging could be adequately performed. On the basis of visual data from our images and prior reports, we believe that we will be able to

decrease the administered activity significantly from 185 MBq and still obtain adequate images in patients with EGA (*7,18*).

Adverse events from ^{89}Zr-trastuzumab administration were minor and similar to that observed previously with other ^{89}Zr-labeled antibodies, for which grade 1 infusion reactions have been observed (*9,12,17,27*).

CONCLUSION

The current study demonstrates the feasibility of using ^{89}Zr-trastuzumab to localize HER2-positive gastric cancer, raising the potential of using this reagent to select or identify patients with gastric cancer who are likely to respond to HER2-directed treatment. Additional patient accrual is ongoing to further categorize the heterogeneity of uptake and correlate imaging findings with response to HER2-directed therapies.

DISCLOSURE

Financial support for this study was provided by Mr. William H. and Mrs. Alice Goodwin and the Commonwealth Foundation for Cancer Research, The Center for Experimental Therapeutics of MSK, the Radiochemistry & Molecular Imaging Probes Core (NIH/NCI Cancer Center Support Grant P30 CA008748), the Ludwig Center for Cancer Immunotherapy at MSK, the Conquer Cancer Foundation (Career Development Award, to Yelena Y. Janjigian), the Department of Defense Congressionally Directed Medical Research Program (CA 150646, to Yelena Y. Janjigian, Jason S. Lewis, and Wolfgang A. Weber), and the Geoffrey Beene Cancer Research Center at MSK (to Jason S. Lewis). Yelena Y. Janjigian has received funding, or has pending grants or patents, from Boehringer Ingelheim, Bayer, Genentech, Bristol-Myers Squibb, Eli Lilly, Pfizer, and Merck. No other potential conflict of interest relevant to this article was reported.

ACKNOWLEDGMENTS

We thank Jing Qiao, Ariel Brown, and staff of the MSK Radiochemistry and Molecular Imaging Probe Core for labeling and dispensing the antibody. We also thank Rashid Ghani of the Nuclear Medicine Pharmacy, the Nuclear Medicine nurses Amabelle Lindo and Louise Harris for their help in patient management, RSA Abigail Boswell and CRM Bolorsukh Gansukh for their excellent support with patient flow and protocol management, the nuclear medicine technologists for their excellent technical assistance, and members of the Department of Medicine at MSK for patient referral. We thank Leah Bassity for her helpful suggestions in editing this manuscript and its submission to the journal.

REFERENCES

1. Siegel RL, Miller KD, Jemal A. Cancer statistics, 2016. *CA Cancer J Clin.* 2016;66:7–30.
2. Janjigian YY, Werner D, Pauligk C, et al. Prognosis of metastatic gastric and gastroesophageal junction cancer by HER2 status: a European and USA international collaborative analysis. *Ann Oncol.* 2012;23:2656–2662.
3. Bang YJ, Van Cutsem E, Feyereislova A, et al. Trastuzumab in combination with chemotherapy versus chemotherapy alone for treatment of HER2-positive advanced gastric or gastro-oesophageal junction cancer (ToGA): a phase 3, open-label, randomised controlled trial. *Lancet.* 2010;376:687–697.
4. Ock CY, Lee KW, Kim JW, et al. Optimal patient selection for trastuzumab treatment in HER2-positive advanced gastric cancer. *Clin Cancer Res.* 2015;21:2520–2529.
5. Gajria D, Chandarlapaty S. HER2-amplified breast cancer: mechanisms of trastuzumab resistance and novel targeted therapies. *Expert Rev Anticancer Ther.* 2011;11:263–275.
6. Janjigian YY, Viola-Villegas N, Holland JP, et al. Monitoring afatinib treatment in HER2-positive gastric cancer with ^{18}F-FDG and ^{89}Zr-trastuzumab PET. *J Nucl Med.* 2013;54:936–943.
7. Dijkers EC, Munnink THO, Kosterink JG, et al. Biodistribution of Zr-89-trastuzumab and PET imaging of HER2-positive lesions in patients with metastatic breast cancer. *Clin Pharmacol Ther.* 2010;87:586–592.
8. Ulaner GA, Hyman DM, Ross DS, et al. Detection of HER2-positive metastases in patients with HER2-negative primary breast cancer using ^{89}Zr-trastuzumab PET/CT. *J Nucl Med.* 2016;57:1523–1528.
9. Gaykema SBM, Schroder CP, Vitfell-Rasmussen J, et al. Zr-89-trastuzumab and Zr-89-bevacizumab PET to evaluate the effect of the HSP90 inhibitor NVP-AUY922 in metastatic breast cancer patients. *Clin Cancer Res.* 2014;20:3945–3954.
10. Gebhart G, Lamberts LE, Wimana Z, et al. Molecular imaging as a tool to investigate heterogeneity of advanced HER2-positive breast cancer and to predict patient outcome under trastuzumab emtansine (T-DM1): the ZEPHIR trial. *Ann Oncol.* 2016;27:619–624.
11. Bahce I, Huisman MC, Verwer EE, et al. Pilot study of Zr-89-bevacizumab positron emission tomography in patients with advanced non-small cell lung cancer. *EJNMMI Res.* 2014;4:35.
12. Börjesson PKE, Jauw YWS, de Bree R, et al. Radiation dosimetry of Zr-89-labeled chimeric monoclonal antibody U36 as used for immuno-PET in head and neck cancer patients. *J Nucl Med.* 2009;50:1828–1836.
13. Gaykema SBM, Brouwers AH, Lub-de Hooge MN, et al. Zr-89-bevacizumab PET imaging in primary breast cancer. *J Nucl Med.* 2013;54:1014–1018.
14. Lamberts LE, van Oordt C, ter Weele EJ, et al. ImmunoPET with anti-mesothelin antibody in patients with pancreatic and ovarian cancer before anti-mesothelin antibody-drug conjugate treatment. *Clin Cancer Res.* 2016;22:1642–1652.
15. Makris NE, Boellaard R, van Lingen A, et al. PET/CT-derived whole-body and bone marrow dosimetry of Zr-89-cetuximab. *J Nucl Med.* 2015;56:249–254.
16. Muylle K, Flamen P, Vugts D, et al. Tumour targeting and radiation dose of radioimmunotherapy with Y-90-rituximab in CD20+B-cell lymphoma as predicted by Zr-89-rituximab immuno-PET: impact of preloading with unlabelled rituximab. *Eur J Nucl Med Mol Imaging.* 2015;42:1304–1314.
17. Pandit-Taskar N, O'Donoghue JA, Beylergil V, et al. Zr-89-huJ591 immuno-PET imaging in patients with advanced metastatic prostate cancer. *Eur J Nucl Med Mol Imaging.* 2014;41:2093–2105.
18. Laforest R, Lapi SE, Oyama R, et al. [^{89}Zr]Trastuzumab: evaluation of radiation dosimetry, safety, and optimal imaging parameters in women with HER2-positive breast cancer. *Mol Imaging Biol.* 2016;18:952–959.
19. Vosjan MJ, Perk LR, Visser GWM, et al. Conjugation and radiolabeling of monoclonal antibodies with zirconium-89 for PET imaging using the bifunctional chelate p-isothiocyanatobenzyl-desferrioxamine. *Nat Protoc.* 2010;5:739–743.
20. Holland JP, Sheh YC, Lewis JS. Standardized methods for the production of high specific-activity zirconium-89. *Nucl Med Biol.* 2009;36:729–739.
21. Lindmo T, Boven E, Cuttitta F, Fedorko J, Bunn PA. Determination of the immunoreactive fraction of radiolabeled monoclonal-antibodies by linear extrapolation to binding at infinite antigen excess. *J Immunol Methods.* 1984;72:77–89.
22. Barrett PHR, Bell BM, Cobelli C, et al. SAAM II: stimulation, analysis, and modeling software for tracer and pharmacokinetic studies. *Metabolism.* 1998;47:484–492.
23. Retzlaff JA, Tauxe WN, Kiely JM, Stroebel CF. Erythrocyte volume, plasma volume, and lean body mass in adult men and women. *Blood.* 1969;33:649–661.
24. Stabin MG, Sparks RB, Crowe E. OLINDA/EXM: the second-generation personal computer software for internal dose assessment in nuclear medicine. *J Nucl Med.* 2005;46:1023–1027.
25. Wahl RL, Kroll S, Zasadny KR. Patient-specific whole-body dosimetry: principles and a simplified method for clinical implementation. *J Nucl Med.* 1998;39:14S–20S.
26. Sgouros G, Stabin M, Erdi Y, et al. Red marrow dosimetry for radiolabeled antibodies that bind to marrow, bone, or blood components. *Med Phys.* 2000;27:2150–2164.
27. Pandit-Taskar N, O'Donoghue JA, Ruan ST, et al. First-in-human imaging with Zr-89-Df-IAB2M anti-PSMA minibody in patients with metastatic prostate cancer: pharmacokinetics, biodistribution, dosimetry, and lesion uptake. *J Nucl Med.* 2016;57:1858–1864.
28. Carrasquillo JA, Morris PG, Humm JL, et al. Copper-64 trastuzumab PET imaging: a reproducibility study. *Q J Nucl Med Mol Imaging.* May 12, 2016 [Epub ahead of print].
29. Beylergil V, Morris PG, Smith-Jones PM, et al. Pilot study of ^{68}Ga-DOTA-F(ab') 2-trastuzumab in patients with breast cancer. *Nucl Med Commun.* 2013;34:1157–1165.
30. Perik PJ, Lub-De Hooge MN, Gietema JA, et al. Indium-111-labeled trastuzumab scintigraphy in patients with human epidermal growth factor receptor 2-positive metastatic breast cancer. *J Clin Oncol.* 2006;24:2276–2282.

immunity of trastuzumab. We conducted a phase II trial of pembrolizumab with chemotherapy/trastuzumab.

Methods: Patients (pts) with previously untreated HER2 IHC 3+ or FISH+ tumours irrespective of PD-L1 status received intravenous P 200 mg flat dose, T 6 mg/kg (after 8 mg/kg load), O 130 mg/m2 every 3 weeks and oral C 850 mg/m2 2 weeks on/1 week off. 22 pts received 1 cycle of induction P/T prior to initiation of chemotherapy. The primary endpoint was 6-months PFS; with target accrual of 37 pts. Secondary endpoints included safety, OS, ORR, and biomarker analysis.

Results: Accrual completed and 100% of the 37 evaluable pts had tumour regression (ranging from -4% to -100%). The RECIST 1.1 ORR was 81% (27 PR, 3 CRs), and 12 (52%) of pts that received induction P/T x 1 cycle showed reduction in target lesions. Median PFS was 14.2 months (mo), with 70% 6 mo PFS. Median follow up was only 8 mo. In pts with available material, 14/36 (40%) had PD-L1 CPS >1 and median TMB was 4.4 mut/Mb (0-10.6). There was no correlation between PD-L1 status and PFS or OS. ERBB2 amplification was evident by tissue-NGS in 17/30 (63%) and ctDNA-NGS in 17/30 (58%) pre-treatment, while the remaining pts were ERBB2- by NGS likely due to tumour heterogeneity or low tumour content. CtDNA decreased in 16/24 tested pts after 1 cycle of induction T/P alone. irAEs included interstitial nephritis Gr4 (3%), transaminitis Gr3 (11%), Gr4 (3%), colitis Gr3 (3%).

Conclusions: 40% remain on therapy, and so the primary endpoint should be reached by 9/19. Updated survival, correlative studies and will be presented. These promising preliminary safety and efficacy results led to initiation of a definitive phase III Keynote 811 trial (NCT03615326).

Legal entity responsible for the study: Memorial Sloan Kettering Cancer Center.

Funding: Merck.

Disclosure: Y.Y. Janjigian: Advisory / Consultancy, Research grant / Funding (self): Bristol-Meyers; Advisory / Consultancy, Research grant / Funding (self): Eli Lily; Advisory / Consultancy: Daiichi Sankyo; Advisory / Consultancy: Pfizer; Advisory / Consultancy, Research grant / Funding (self): Merck; Research grant / Funding (self): Amgen; Advisory / Consultancy, Research grant / Funding (self): Bayer; Research grant / Funding (self): Boehringer Ingelhiem; Research grant / Funding (self): Genentech/Roche; Advisory / Consultancy: Merck Serono; Advisory / Consultancy: Imugene. S. Maron: Non-remunerated activity/ies, Research Collaboration Only: Guardant Health; Shareholder / Stockholder / Stock options: Calithera; Travel / Accommodation / Expenses: Merck; Licensing / Royalties, Non-remunerated activity/ies, Research Collaboration Only: Genentech. G.Y. Ku: Advisory / Consultancy, Research Support: Arog; Advisory / Consultancy, Research Support: Bristol-Myers Squibb; Advisory / Consultancy: Eli Lilly; Advisory / Consultancy, Research Support: Merck; Advisory / Consultancy, Research Support: Pieris; Advisory / Consultancy, Research Support: Zymeworks. D.H. Ilson: Advisory / Consultancy: Merck; Advisory / Consultancy: Astellas; Advisory / Consultancy: Bayer; Advisory / Consultancy: Pieris; Advisory / Consultancy: Roche; Advisory / Consultancy: AstraZeneca; Advisory / Consultancy: Eli Lilly; Advisory / Consultancy: Britsol Myers Squibb; Advisory / Consultancy, Contracted Research: Taiho. D. Solit: Advisory / Consultancy: Pfizer; Advisory / Consultancy, Shareholder / Stockholder / Stock options: Loxo Oncology; Advisory / Consultancy: Illumina; Advisory / Consultancy: Vivideon Therapeutics; Honoraria (institution), Speaker Bureau / Expert testimony: Lilly Oncology. J.F. Hechtman: Research grant / Funding (institution): Bayer; Honoraria (institution): Medscape; Advisory / Consultancy: Axiom Healthcare Strategies; Advisory / Consultancy: Cor2Ed. M. Lamendola-Essel: Advisory / Consultancy: Rockefeller University. All other authors have declared no conflicts of interest.

817P First-line pembrolizumab (P), trastuzumab (T), capecitabine (C) and oxaliplatin (O) in HER2-positive metastatic esophagogastric adenocarcinoma

Y.Y. Janjigian[1], S. Maron[2], J.F. Chou[3], A.R. Gabler[2], M.Z. Simmons[4], P. Momtaz[2], M. Shcherba[2], G.Y. Ku[2], E. Won[2], F. Sanchez-Vega[2], H. Gerdes[5], D.P. Kelsen[5], D.H. Ilson[2], D. Solit[6], N. Schultz[3], P.M. Shah[5], M. Capanu[3], J.F. Hechtman[7], M. Lamendola-Essel[8]

[1]Medicine/Gastrointestinal Oncology, Memorial Sloan-Kettering Cancer Center, New York, NY, USA, [2]Medicine, Gastrointestinal Oncology, Memorial Sloan Kettering Cancer Center, New York, NY, USA, [3]Epidemiology-Biostatistics, Memorial Sloan Kettering Cancer Center, New York, NY, USA, [4]Radiology, Memorial Sloan Kettering Cancer Center, New York, NY, USA, [5]Medicine, Gastroenterology, Memorial Sloan Kettering Cancer Center, New York, NY, USA, [6]Office of Physician-In-Chief, Memorial Sloan-Kettering Cancer Center, New York, NY, USA, [7]Pathology, Memorial Sloan Kettering Cancer Center, New York, NY, USA, [8]Medicine, Solid Tumour Division, Memorial Sloan Kettering Cancer Center, New York, NY, USA

Background: Trastuzumab stimulates HER2-specific T cell responses and increases tumour PD-L1 expression, and anti-PD-1 antibody can help enhance T cell-specific

Downloaded from https://academic.oup.com/annonc/article-abstract/30/Supplement_5/mdz247.143/5577576 by guest on 13 December 2019